HOKKAIDO UNIVERSITY

Title	Systematic investigations of transient response of nuclear spins in GaAs under the presence of polarized electron spins
Author(s)	Eldesouky, Mahmoud Rasly Khoudary
Citation	北海道大学. 博士(工学) 甲第13300号
Issue Date	2018-09-25
DOI	10.14943/doctoral.k13300
Doc URL	http://hdl.handle.net/2115/71932
Type	theses (doctoral)
File Information	Mahmoud_Rasly_Khoudary_Eldesouky.pdf

Instructions for use

Hokkaido University Collection of Scholarly and Academic Papers : HUSCAP

Systematic investigations of transient response of nuclear spins in GaAs under the presence of polarized electron spins

Mahmoud Rasly

Laboratory of Nanoscale Electron Devices
Division of Electronics for Informatics,
Graduate School of Information Science and Technology,
Hokkaido University

September, 2018

Copyright (C) 2018 Mahmoud Rasly. All Rights Reserved.

Abstract

Nuclear-spin systems are ideal for the development of quantum computing systems because of their extremely long coherence time. For such computing systems, the nuclear magnetic resonance (NMR) technique enables the control and detection of the nuclear-spin-based quantum bits (qubits), a basic unit of quantum computation. Nevertheless, it is difficult originally to polarize the nuclear spins and to detect the nuclear spin states because of their tiny magnetic moment, leading to a decrease in the signal sensitivity of the NMR system. A possible solution to tackle this problem is to apply the so-called dynamic nuclear polarization (DNP), in which the nuclear spins are polarized by exchanging angular momentum with spin-polarized electrons through the hyperfine interaction. Several DNP-combined NMR systems have been developed by using optically or electrically created electron spins. Electrical spin injection from ferromagnetic electrodes into a semiconductor is the most recent proposal for an electrical DNP, and coherent manipulation of nuclear spins, or the Rabi oscillation, which is a key factor for nuclear-spin-based qubits, has been demonstrated.

Basically, the nuclear spins interact with the lattice through an extremely long time scale of T_1 (typically minutes to hours); called the spin-lattice relaxation time, compared to those of their internal interactions. They also interact with electron spins through the hyperfine interaction with a time scale of T_{1e} (typically seconds to minutes); called the DNP time. Therefore, during the process of DNP, if the change in the external magnetic field is faster than the polarization rate ($1/T_{1e}$) and/or depolarization rate ($1/T_1$), nuclear spins behave in a complicated manner. The quantitative analyses of the DNP, thus, have mostly been limited to steady-state circumstances, where the change in the external magnetic field is relatively slow. For a precise

control of nuclear spin polarization during the DNP, a complete understanding about the dynamics of nuclear spins is indispensable.

The purpose of this research is to provide a quantitative description for the electron-nuclear spin dynamics in semiconductor-based spintronics devices. To do so, we systematically investigated the dependencies of nuclear-spin polarization on the initialization time for the DNP and the sweep rates of the magnetic field through the Hanle signal and spin-valve signal measurements made in an all-electrical lateral spin injection device. In addition, we simulated all the nuclear-spin-related phenomena appearing in the Hanle/spin-valve signals using the time evolution of nuclear field, taking both the rate of polarization ($1/T_{1e}$) and the rate of depolarization ($1/T_1$) into consideration.

This dissertation consists of six chapters and the main content of each chapter is as follows:

Chapter 1 includes a research introduction, a problem statement to be solved, and research goals.

Chapter 2 presents a theoretical framework which we use to analyze our experimental results about electron-nuclear spin dynamics in semiconductor-based spintronics devices.

Chapter 3 states about our experimental techniques and simulation methods.

Chapter 4 focuses on the results and discussion of the DNP made in an all-electrical lateral spin injection device having Co_2MnSi/CoFe/*n*-GaAs Schottky tunnel junctions. At first, we demonstrated clear spin injection from a highly spin-polarized Co_2MnSi source into a GaAs channel through the observation of spin-valve signal and Hanle signal, which are the strong evidences for an electrical spin injection and detection. Then, we described the DNP for Ga and As nuclei with the electron spins injected into GaAs. We

experimentally observed the modulation of Hanle signals arising from the nuclear field produced in the DNP, and showed that the strength of the produced nuclear field was four orders higher than that obtained without polarized electron spins, indicating that the efficient nuclear polarization was successfully achieved by spin injection. Next we systematically investigated the dependencies of nuclear field on the initialization time for the DNP and the sweep rates of the magnetic field through the Hanle signal and spin-valve signal measurements. Moreover, we simulated all the nuclear-spin-related phenomena appearing in the Hanle/spin-valve signals using the time evolution of nuclear field, taking both T_{1e} and T_1 into consideration. The simulation results well reproduced our experimental results, leading to enabling quantitative analysis for the transient response of nuclear spins against the fast change in the magnetic field. We also discussed the DNP in terms of nuclear spin temperature, and showed that the DNP process cooled the nuclear-spin systems. A population inversion of nuclear spins arising from the DNP was also described as a negative spin temperature.

Chapter 5 describes the influence of NMR on the nuclear spin dynamics by both experiment and simulation. Under an irradiation by rf-magnetic field with its frequency of 200 kHz, we observed clear changes in Hanle signal at resonant fields of ^{69}Ga, ^{71}Ga, and ^{75}As nuclei, indicating that the nuclear field was changed by the NMR. By assuming that the nuclear field of each nuclei is vanished at the resonant field, the change of Hanle signal arising from NMR was well reproduced by the simulation, which clarifies the influence of NMR on the nuclear spin polarization. Moreover, we discussed the effect of NMR in terms of the nuclear spin temperature, and showed that the NMR can be treated as a heating of nuclear spin system in contrast to the cooling by DNP.

Chapter 6 summarizes the main results and ends up with a conclusion. In summary, we clarified the transient response of nuclear spins against the change in the magnetic field by both experiment and simulation in an all electrical spin injection device, enabling a precise control of nuclear spin states along with a quantitative analysis under the DNP process with/without NMR. These findings provide a deep understanding of nuclear spin dynamics and offer a promise for multitude of quantum computing applications.

Contents

CHAPTER 3
Experimental methodology and simulation method

CHAPTER 4
Quantification of the transient behaviors of the dynamically polarized nuclear spins in GaAs

List of Figures

List of Tables

Chapter 1

Introduction

1.1. Background

Admittedly, the traditional electronic devices, in which the signal arose due to a move of the electronic charges around, will run out of work one day as the devices scale down to the atomistic scale for many reasons; most significantly is the produced scorching heat. Alternatively, there is an intrinsic quantum property for an electron known as spin, owing to its spin angular motion. In past times, this property was impossible to be experimentally identified. Nowadays, with the great success in the micro and/or nanofabrication, it becomes possible to be recognized and to carry signals instead of charges in the electronic devices. So, those devices are called spin based electronic devices and this research field as a whole is called spintronics.

Similarly, the lattice nuclei for a material, such as GaAs semiconductor, with which we work, possess spin angular momentum and a concomitant magnetic moment. Owing to nuclei having much greater mass than electrons, their magnetic moments are so small compared to that of electrons. This results in a weak coupling to the surrounding environment, specifically the lattice, and so having an extremely long coherence time; a time within which information maintains for signal processing in the quantum computing systems. For such systems, the nuclear magnetic resonance (NMR) technique enables the control and detection of the nuclear-spin-based quantum bits (qubits); a basic unit of quantum computations. For that, a lot of research interests recently have been paid for the development of high-sensitivity NMR technology with high spatial resolution and the precise control of nuclear spins.

The common way to polarize a nuclear spin system is to apply a static magnetic field. However, the continuous need for the scaling of the electronic devices to the atomistic scale leads to lowering the sensitivity of NMR systems. One possible solution to tackle this problem and increase the signal sensitivity is by application of the so called dynamic nuclear polarization (DNP). This method

helps to locally polarize the nuclear spins by the aid of spin-polarized electrons through the hyperfine interaction. The polarized nuclear spins, in turn, affect electron spins through an effective magnetic field or Overhauser field, and the overall interaction dramatically increases the signal intensity available for detection of the nuclear-spin states. Typically, in order to obtain a nuclear spin polarization in the order of only 1% by application of a static magnetic field only, one needs to apply an extremely large magnetic field in the order of 10 T at very low temperature 1 K. On the other hand, by application of DNP at the same conditions of field and temperature, then the nuclear spin polarization can reach up to 3 or 4 orders of magnitude larger than that without DNP, which is a real promise for the future of NMR systems.

The conventional DNP-combined NMR devices has been developed optically in quantum wells [1] and electrically in quantum Hall systems [2]. However, both two systems have some restrictions. The optical systems are restricted in its scalability, controlling the nuclear spin polarization or detection of the spin states, because the spatial resolution of the system is limited by the optical wavelength of the incident light. Meanwhile, for the electrical technique, quantum Hall systems work only while observing the quantum Hall states, which require a relatively strong magnetic field of several tesla and a low temperature below 1 K to be detected. Alternatively, in order to achieve an efficient dynamic nuclear polarization in semiconductors, one can polarize the electron spins in semiconductor by an electrical injection of spin-polarized electrons from a ferromagnetic spin source into a channel of semiconductor [3-11].

On the requirement of achieving high spin injection efficiency and thereby DNP, a highly efficient spin source is indispensable. Searching on literature, Co-based Heusler alloys provide a lot of promises in a multitude of spintronic devices, including magnetic tunnel junctions (MTJs) [12-21], giant magnetoresistance (GMR) devices [22-28], and for spin injection into

semiconductors [43-48], due to its complete spin polarization at the Fermi level [29-31]. Recently, Liu *et al.* achieved high tunneling magnetoresistance (MR) ratios of up to 1995% at 4.2 K and up to 354% at 290 K in MTJs having Co_2MnSi (CMS) electrodes [32]. Remarkably, a world record has been achieved also by the same research group while demonstrating MR ratios of 2610% at 4.2 K and 429% at 290 K using Co_2(Mn,Fe)Si MTJs [33,34], providing a high spin polarization of CMS and CMFS. Moreover, Ebina *et al.* achieved highly efficient spin injection into a GaAs channel by utilizing a CMS as a spin source. Polarization of electron spins in GaAs reached up to 52% at 4.2 K, which expects an efficient DNP [35].

1.2. Problem statement

Recent decades have witnessed an immense expansion in exploring the physics of DNP and controlling the nuclear spin states through the hyperfine interaction [4-11, 36-51]. In particular, the dynamics of nuclear spin in GaAs has been investigated at various measurement conditions such as temperature and magnetic field strength [44], the excitation energy of photons [40,47], and also at different impurity concentrations for GaAs itself [46]. However, the time evolution of dynamically polarized nuclear spins is not fully understood yet, and it is still controversial.

Although the nuclear spins are considered as a well isolated system from the lattice, they interact with the lattice through an extremely long time scale of T_1 (typically minutes to hours), called the spin-lattice relaxation time, compared to their internal interactions, and they also interact with the electron spins through a time scale of T_{1e} (typically seconds to minutes) through the hyperfine mechanisms. A more details about the nuclear spin interactions will be given in details in chapter 2. This interaction leads to a wealth of static and dynamical effects that complicate the overall picture. For Instance, if the sweep rate of the external magnetic field is faster than the polarization rate ($1/T_{1e}$) and/or depolarization rate ($1/T_1$), it causes the nuclear spins to behave in a complicated manner. The quantitative analyses of the DNP, thus, have mostly been limited to steady-state circumstances [6], where the change in the external magnetic field is relatively slow.

Recently, Akiho *et al.* experimentally investigated the behavior of nuclear spins under transient state circumstances, in which the magnetic field was swept faster than the time scale of T_{1e} or T_1, using a typical spin injection device consisting of ferromagnetic CMS as injection and detection contacts and a channel of *n*-GaAs semiconductor [9]. Salis *et al.* also observed some complicated behaviors on the spin-valve like effect signal in an electrical spin

injection device with Fe contacts and a channel of *n*-GaAs semiconductor [7]. Although they correlated their results with the polarized nuclear spins, those results were explained qualitatively. Very recently, Uemura *et al.* demonstrated NMR signal under transient state circumstances [10], which made the situation more complicated. Thus, for the development of a novel NMR device applicable to the quantum computing system, a full understanding about the dynamics of nuclear spins under the presence of spin-polarized electrons with and without NMR are indispensable.

1.3. Goal and scope of the work

The general goal of this research is to address a quantitative description for the electron-nuclear spin dynamics in semiconductor-based spintronics devices. Following four specific goals have to be achieved during the term of study.

1) To fabricate all-electrical nuclear-spin-based devices with high sensitivity and high spatial resolution based on the electrical spin injection into GaAs,
2) To figure out the transient behavior of nuclear spins and NMR signals through the detection of the Hanle effect signal, and investigate other spin-related phenomena appearing on the spin-valve effect signal,
3) To quantify the behaviors of nuclear spins using the time evolution of nuclear field, and
4) To deepen the understanding of the dynamics of nuclear spins using the concept of spin temperature with and without nuclear magnetic resonance.

Chapter 2

Theoretical Aspects

2.1. Overview

This chapter presents a theoretical framework on the physics behinds the electrical spin injection/detection, dynamic nuclear-spin polarization (DNP) by spin-polarized electrons and resultant nuclear field, and the nuclear magnetic resonance (NMR), to be used for analysis of our experimental results. Schematically shown in Fig. 2.1 is a description of a lateral spin transport device to be investigated in this study. The device operation includes (a) creation of a spin-polarized electrons through an electrical spin injection from ferromagnetic contacts into a semiconductor channel, (b) initialization of nuclear spins by the DNP, (c) manipulation of nuclear spins by NMR, and (d) readout of the final nuclear-spin states. The details of the operation are as follows: The nuclear spins in a semiconductor channel are initialized through the DNP process, in which the angular momentum is exchanged between the polarized electron spins and unpolarized nuclear spins through the hyperfine coupling, leading to the nuclear spin polarization. The nuclear spin states are then manipulated through the NMR by irradiation of a radio-frequency (rf) magnetic field. The manipulated nuclear-spin states can be readout through a detection of a nonlocal voltage (V_{NL}) between contact-3 and contact-4, because V_{NL} can measure the strength of nuclear field acting on electron spins through the Larmor precession of electron spins.

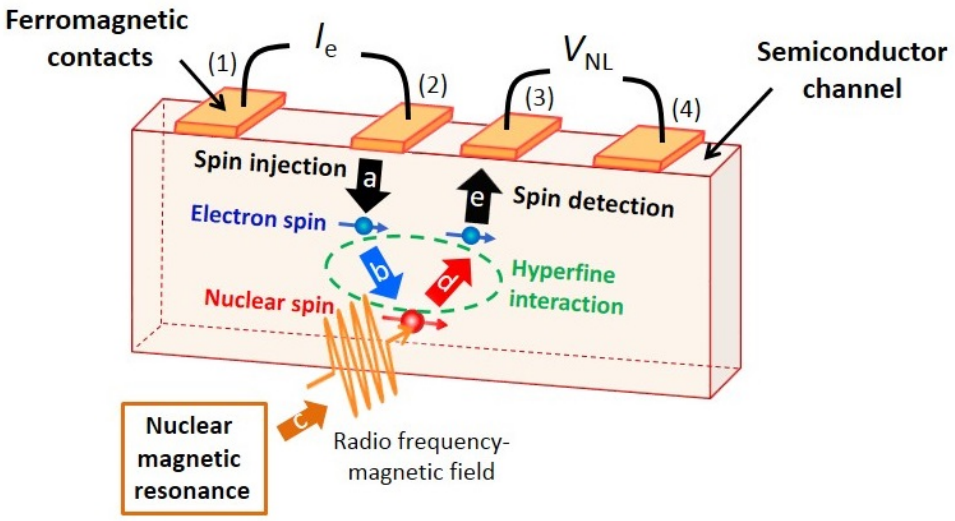

Fig. 2.1: A schematic description of a lateral spin transport device to be used as a novel nuclear magnetic resonance (NMR) system. The device operation includes (a) Electrical spin injection (pass-a), (b) Initialization of nuclear spins by the DNP (pass-b), (c) Manipulation of nuclear spins by NMR (pass-c), and (d) Readout of the final nuclear spin state by detecting the change in the nonlocal voltage (V_{NL}) (pass-d and pass-e).

We overview the sequences by which an electron spin and a nuclear spin interacting through the hyperfine interaction and NMR into one scheme, as shown in Fig. 2.2.

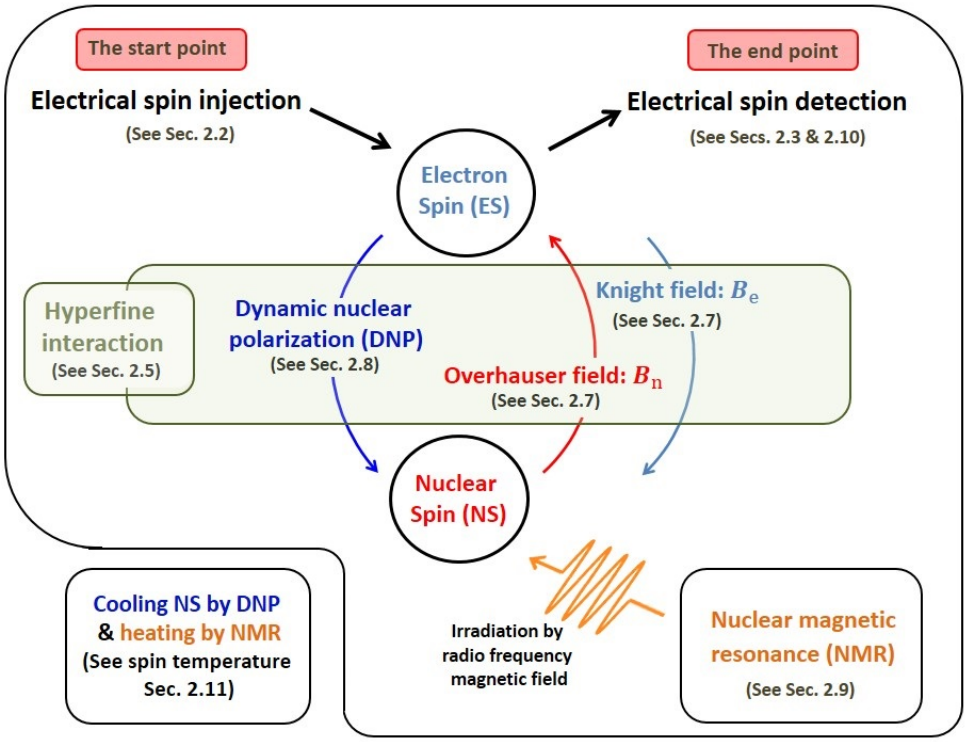

Fig. 2.2: A schematic description of the process of nuclear spin polarization due to interaction with the spin-polarized electrons through the hyperfine interaction. The injected spin-polarized electrons exchange angular momentum with nuclear spins in semiconductor, resulting in producing nuclear spin polarization, called the DNP process. Thus the created nuclear spins affect electron spins as an effective magnetic field, called a nuclear field or the Overhauser field. On the contrary, the polarized electron spins affect the nuclear spins as an effective magnetic field, called the Knight field. The NMR manipulates the nuclear spin states leading to modulating the Overhauser field acting on the electron spins.

→ *We start our chapter by clarifying the essence of creation of a spin-polarized current, concept of the spin polarization along with the theory of the electrical spin injection.*

2.2. Electrical spin injection

Herein, we describe the concept of an electrical spin injection from a ferromagnetic contact into a semiconductor channel; see pass *a* in Fig. 2.1. Following Refs. [52-55], we discuss about the theory of electrical spin injection. By definition, the electrical spin injection is a technique to inject spin-polarized electrons from ferromagnetic (FM) materials into semiconductors (SC) or nonmagnetic materials (NM) generally. We consider a spin injection and detection device with a nonlocal spin transport geometry; simply a detector contact (FM 3) is out of the closed current loop of an injector contact (FM 2) with SC channel, as shown in Fig. 2.1, and detailed in Fig. 2.3. FM 2 and FM 3 are made from the same ferromagnetic material of width W_F, thickness d_F and separated by distance d. A SC channel has a width of W_{sc} and thickness of d_{sc}. The magnetizations of FM 2 and FM 3 can be manipulated between parallel (*see blue arrow*) or antiparallel (*see red arrow*) configuration by an in-plane magnetic field.

In the ferromagnets, the up spin and down spin subbands are shifted in energy due to the strong Stoner exchange interaction favoring the parallel orientation of electron spins. Correspondingly, the density of states (DOS) at the Fermi-energy (E_F) and the Fermi velocities become different between those two spin subbands. Due to the spin dependent DOS, Fermi velocities, and scattering potentials, the flow of usual current has larger proportion of spin up than spin down charge carriers. That is the so called spin-polarized current which can be described by the two different channels model, in which the flow of usual current is treated by flowing of two different current densities $\mathbf{j}^{\uparrow(\downarrow)}$ in two channels, where arrows (↑) and (↓) refers to up and down spin channels, respectively, and is given by

$$\mathbf{j}^{\uparrow(\downarrow)} = \sigma^{\uparrow(\downarrow)}\mathbf{E} - eD^{\uparrow(\downarrow)}\nabla\delta n^{\uparrow(\downarrow)}, \qquad (2.1)$$

where $\sigma^{\uparrow(\downarrow)}$, $D^{\uparrow(\downarrow)}$ and $\delta n^{\uparrow(\downarrow)}$ are the conductivity, diffusion constant, and shift of

carrier density from its equilibrium of the up (down) spin channel, respectively, and e denotes the absolute value of the electron charge. Making use of the Einstein relation $\sigma = e^2 N^{\uparrow(\downarrow)} D^{\uparrow(\downarrow)}$ and $\delta n^{\uparrow(\downarrow)} = N^{\uparrow(\downarrow)} \delta\varepsilon^{\uparrow(\downarrow)}$, where $N^{\uparrow(\downarrow)}$ and $\delta\varepsilon^{\uparrow(\downarrow)}$ are the density of states and the shift in the chemical potential of carrier from its equilibrium value of the up (down) subband, Eq. 2.1 gives

$$\mathbf{j}^{\uparrow(\downarrow)} = \sigma^{\uparrow(\downarrow)} / e \nabla \mu^{\uparrow(\downarrow)}, \tag{2.2}$$

where $\mu^{\uparrow(\downarrow)} = \varepsilon^{\uparrow(\downarrow)} + e\varphi$ is the electrochemical potential and φ is the electric potential.

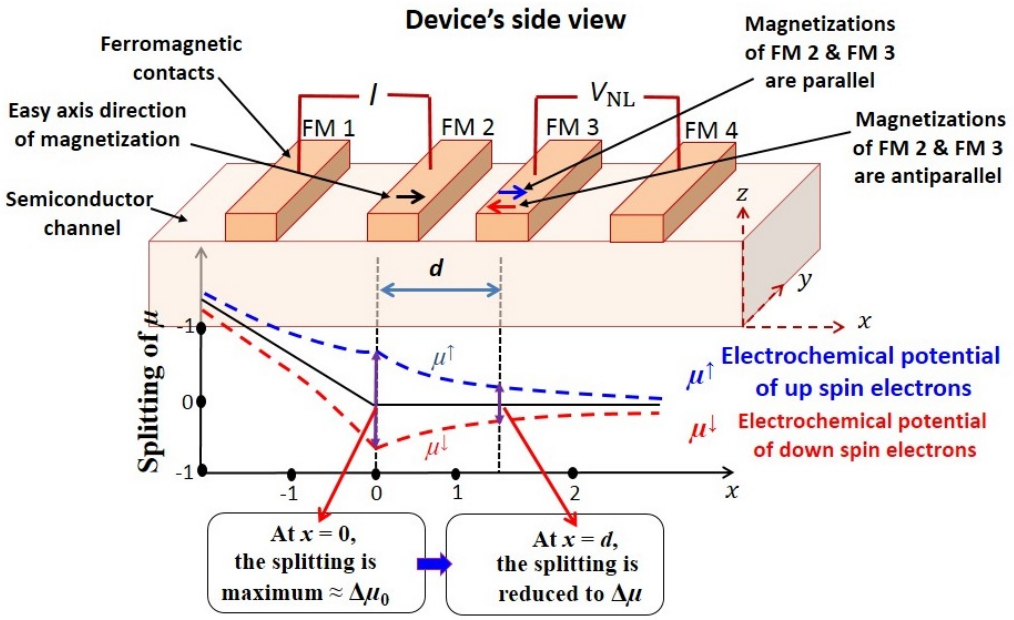

Fig. 2.3. Schematic description of a lateral spin transport device having ferromagnetic/semiconductor heterojunctions and a splitting of the electrochemical potential between up and down spin electrons at their contact interface.

The continuity equations for the charge and spin currents in the steady state are given by

$$\nabla \cdot (\mathbf{j}^{\uparrow} + \mathbf{j}^{\downarrow}) = 0, \tag{2.3}$$

$$\nabla \cdot (\mathbf{j}^{\uparrow} - \mathbf{j}^{\downarrow}) = -e\delta n^{\uparrow} / \tau^{\uparrow\downarrow} + e\delta n^{\downarrow} / \tau^{\downarrow\uparrow}, \tag{2.4}$$

where $\tau^{\uparrow\downarrow}$ and $\tau^{\downarrow\uparrow}$ are the scattering time of an electron from spin up to spin down state and one from spin down to spin up state, respectively. Using these equations and detailed balanced between rate changes of spin up electrons to spin down electrons $N^{\uparrow}/\tau^{\uparrow\downarrow} = N^{\downarrow}/\tau^{\downarrow\uparrow}$, one obtains

$$\nabla^2(\sigma^{\uparrow}\mu^{\uparrow} + \sigma^{\downarrow}\mu^{\downarrow}) = 0, \tag{2.5}$$

$$\nabla^2(\mu^{\uparrow} - \mu^{\downarrow}) = l_{sf}^{-2}(\mu^{\uparrow} - \mu^{\downarrow}), \tag{2.6}$$

where $l_{sf} = \sqrt{D\tau_{sf}}$ is a spin diffusion length with $\tau_{sf}^{-1} = \frac{1}{2}(1/\tau^{\uparrow\downarrow} + 1/\tau^{\downarrow\uparrow})$ and $D^{-1} = (N^{\uparrow}/D^{\downarrow} + N^{\downarrow}/D^{\uparrow})/(N^{\uparrow} + N^{\downarrow})$. By applying the following boundary conditions at FM/SC interface: (1) $\Delta\mu$ must go to zero as one goes far from the interface because of the electron spin scattering and relaxation mechanisms destroying the spin polarization, *i.e.* $\Delta\mu(x = -\infty) = \Delta\mu(x = +\infty) = 0$, and (2) at $x = 0$, there exists continuity in $\mathbf{j}^{\uparrow}$ and $\mathbf{j}^{\downarrow}$ at the interface, *i.e.* $\mathbf{j}^{\uparrow(\downarrow)}(z = 0^{-}) = \mathbf{j}^{\uparrow(\downarrow)}(z = 0^{+})$, then we obtain a spin accumulation or an induced magnetization **M** at FM/SC interface resulting from the difference between $\mu^{\uparrow}$ and $\mu^{\downarrow}$, as shown in Fig. 2.3. More details about derivations can be found in Refs. [52-55]. More importantly, it has proved that $\mu^{\uparrow}$ and $\mu^{\downarrow}$ show a maximum split at FM/SC interface, shown by $\Delta\mu_0$ at $x = 0$ in Fig. 2.3. For a tunnel junction in which the interface resistance is much larger than that of FM elelctrodes, $\Delta\mu_0$ is given by

$$\Delta\mu_0 = P_{\text{inj}} I_e (\rho l_{sf} / S) e, \tag{2.7}$$

where P_{inj} is a spin polarization at FM2/SC interface, I_e is an injection current, ρ is an electrical resistivity of the SC, and S is a cross sectional area of the SC. Far from the interface, the splitting decays exponentially with the inverse of the spin

diffusion length l_{sf} from both sides of interface. So, for instance, the splitting $\Delta\mu$ at $x = d$ is given by

$$\Delta\mu = \Delta\mu_0 \exp(-d / l_{sf}), \tag{2.8}$$

as depicted in Fig. 2.3. In the following section, we will get an expression for detection of a spin dependent voltage associated with those accumulated spins.

2.3. Electrical spin detection

We now turn our discussion to how to detect a spin signal from the accumulated spins, see pass *e* in Fig. 2.1. The direct evidence to detect a spin signal from the accumulated spins is by demonstrating two main effects via nonlocal voltage geometry; the first is called the spin-valve like effect and the second is the Hanle effect. The main difference between each is how the electron spin behaves under an applied magnetic field, either parallel or perpendicular to the direction of spin polarization, respectively. A detailed discussion will be given in the following two sub-sections.

2.3.1 Spin-valve like effect

This effect describes how the accumulated electron spins, diffused between two ferromagnets, behave if the direction of magnetization of two ferromagnets changes or exactly being manipulated by an in-plane magnetic field. Firstly we explain the change in the electrochemical potential of FM 2 along with that of SC because of application of a charge current I_e, and then clarifying how the electrochemical potential of FM 3 responds to this change.

In the absence of a supplied current, as shown in Fig 2.4(a), all Fermi levels of (1) FM 2, (2) SC, (3) FM 3 with parallel magnetization to FM 2, and (4) FM 3 with antiparallel magnetization to FM 2 are aligned at E_F (Hereafter we call electrochemical potential as Fermi level.).

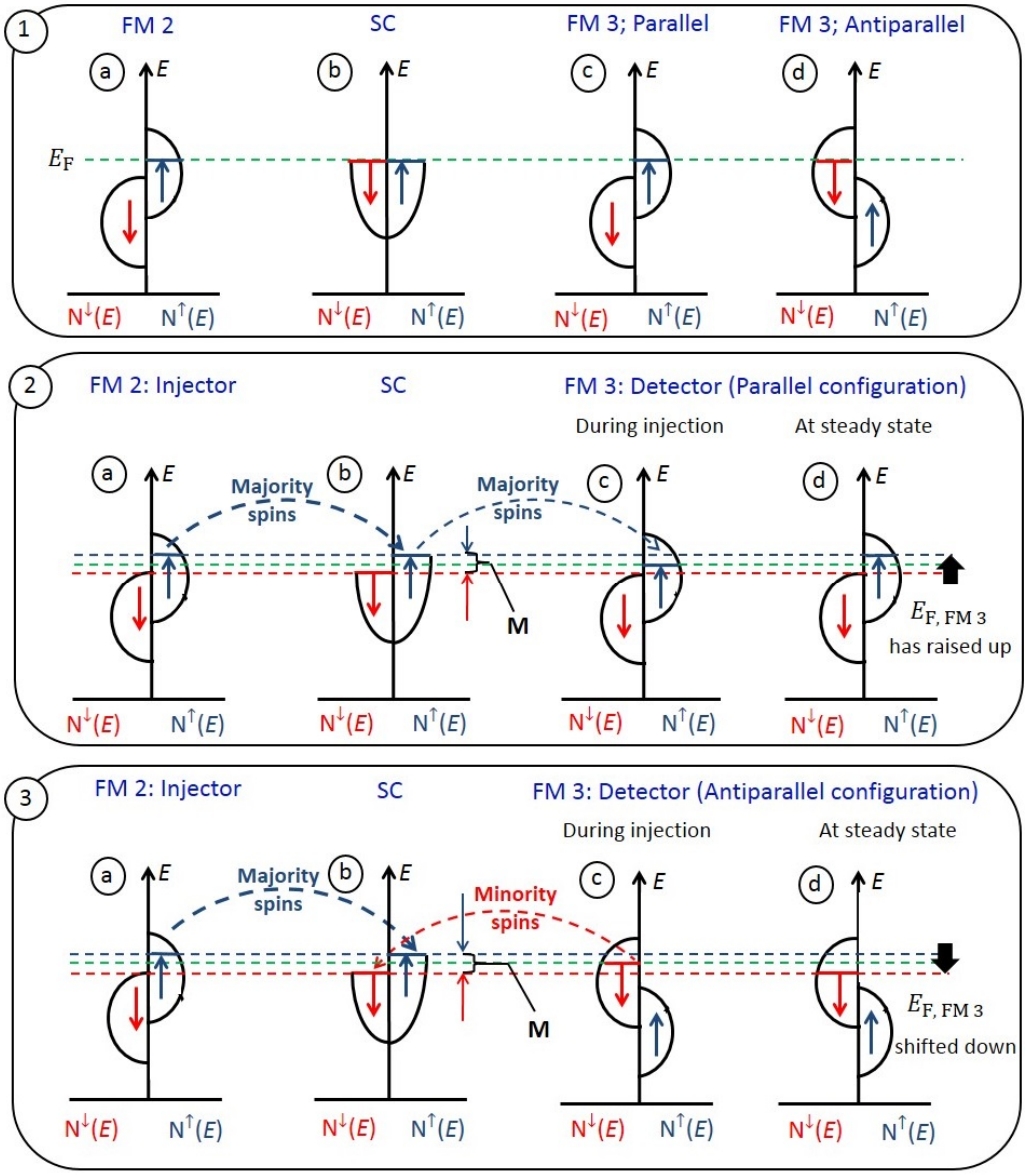

Fig. 2.4. A schematic description of densities of states, N(*E*), as a function of energy, *E*, of a system having ferromagnet (FM 2)/semiconductor (SC)/ferromagnet (FM 3) contacts. In panel (1) the system is under zero-bias current, (2) the system is biased and having FM 2 and FM 3 in a parallel magnetization configurations and (3) the system is biased and having FM 2 and FM 3 in antiparallel magnetization configurations [52].

When electrons were supplied from FM 2 into SC, the Fermi level of up spin and that of down spin split each other, as explained in Sec. 2.2 and illustrated schematically in Fig 2.4.2(b) & Fig 2.4.3(b).

Basically the voltage between FM 3 and FM 4, V_{NL}, is given by the difference of Fermi level of FM 3 and that of FM 4. Now we will consider Fermi level of FM 3 in two cases: parallel configuration (*see* Fig 2.4.2(c & d)) and antiparallel configuration between FM 2 and FM 3 (*see* Fig 2.4.3(c & d)).

Let $E_{\mathrm{F,\,FM3}}^{(\mathrm{P})}$ be the Fermi level of FM 3 for parallel configuration. Since no net current flows between FM 3 and SC, the flow of up spin from SC into FM 3 and the flow of down spin from FM 3 into SC are balanced, and the following

$$\begin{aligned} &\left(\frac{\Delta\mu}{2}-E_{\mathrm{F,\,FM3}}^{(\mathrm{P})}\right)N^{\uparrow}=\left(E_{\mathrm{F,\,FM3}}^{(\mathrm{P})}-\frac{\Delta\mu}{2}\right)N^{\downarrow} \\ &\therefore E_{\mathrm{F,\,FM3}}^{(\mathrm{P})}=\frac{N^{\uparrow}-N^{\downarrow}}{N^{\uparrow}+N^{\downarrow}}\frac{\Delta\mu}{2}=P_{\mathrm{det}}\frac{\Delta\mu}{2} \end{aligned}, \tag{2.9}$$

where P_{det} is a spin polarization at the FM3. On the other hand, the Fermi level of FM 4 is zero, because Fermi level of both up-spin and down-spin in SC is zero. Thus, from Eqs. (2.7), (2.8) and (2.9), V_{NL} for the parallel configuration is given by

$$V_{\mathrm{NL}}^{(\mathrm{P})}=-E_{\mathrm{F,\,FM3}}^{(\mathrm{P})}/e=\frac{1}{2}P_{\mathrm{inj}}P_{\mathrm{det}}I_e\left(\rho\frac{l_{sf}}{S}\right)\exp\left(-\frac{d}{l_{sf}}\right). \tag{2.10}$$

Similarly, V_{NL} for the antiparallel configuration is given by

$$V_{\mathrm{NL}}^{(\mathrm{AP})}=-\frac{1}{2}P_{\mathrm{inj}}P_{\mathrm{det}}I_e\left(\rho\frac{l_{sf}}{S}\right)\exp\left(-\frac{d}{l_{sf}}\right). \tag{2.10b}$$

When the magnetization configuration between FM 2 and FM 3 is switched between parallel and antiparallel by the in-plane magnetic field, the nonlocal voltage changes by ΔV_{NL}, which is given by

$$\Delta V_{\mathrm{NL}}=V_{\mathrm{NL}}^{(\mathrm{P})}-V_{\mathrm{NL}}^{(\mathrm{AP})}=P_{\mathrm{inj}}P_{\mathrm{det}}I_e\left(\rho\frac{l_{sf}}{S}\right)\exp\left(-\frac{d}{l_{sf}}\right). \tag{2.11}$$

2.3.2. Hanle effect

This effect shows how the electron spin polarization can be destroyed by application of a magnetic field **B** perpendicular to the direction of spin polarization, as shown in Fig. 2.5. In order to determine how **M** changes due to application of a magnetic field **B** perpendicular to the direction of spin polarization, we study how the angular momentum of accumulated electron spins changes using the the following expression [4]:

$$\frac{\partial \mathbf{S}(x,t)}{\partial t} = \gamma_e \mathbf{S} \times \mathbf{B} + D\frac{\partial^2 \mathbf{S}}{\partial x^2} + \mu_e E\frac{\partial \mathbf{S}}{\partial x} - \frac{\mathbf{S}}{\tau_{sf}} \tag{2.12}$$

where $\mathbf{S} = (S_x, S_y, S_z)$ is the electron spin, γ_e is the gyromagnetic ratio, μ_e is the electron mobility, and E is applied electric field. The first term on the right-hand side, which is our concern here, refers to a precessional motion of the angular momentum of an electron spin due to a torque induced by **B**. In our case study, we assumed that the injected electrons are polarized along x, and so the detector, whose magnetization is also along x axis direction, will sense the change in x component of the angular momentum, S_x. Since the injected spins rotate by an angle of $\omega_L t$ in an x-y plane for $\mathbf{B} = (0, 0, B_z)$, where $\omega_L = \gamma_e B_z$ is the Larmor precessional frequency, $S_x(x, t)$ is given by $S_x(x, 0)\cos\omega_L t$ [56].

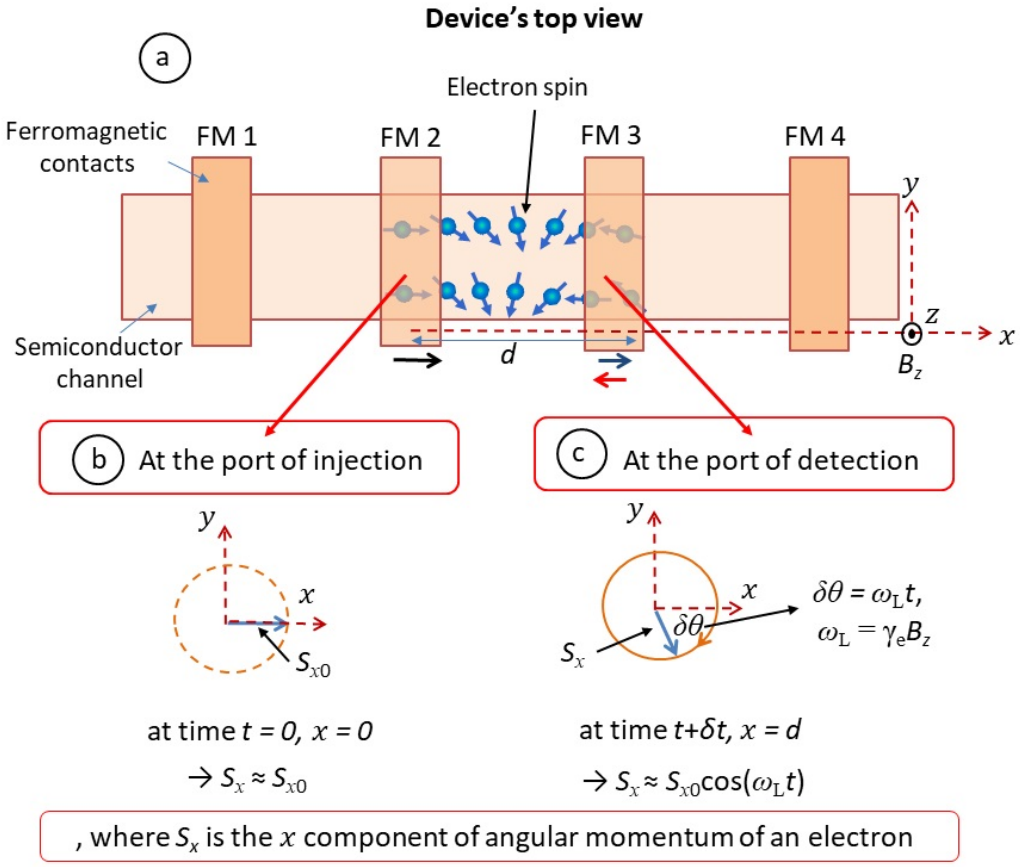

Fig. 2.5: A schematic description for the behavior of an electron spin under a magnetic field B_z perpendicular to the direction of spin polarization (Hanle effect), where x axis is considered the direction of spin polarization, see text.

The second and the third terms of Eq. (2.12) describe the diffusion and the drift of the electrons, respectively. Because no electric field exists at $x > 0$ for non-local configuration, the drift term is ignored, and the diffusion term is the dominant term to drive the spin current. The diffused spins S_x fall off exponentially with a form given by $1/\sqrt{4\pi Dt}\ \exp(-d^2/4Dt)$.

The last term of Eq. (2.12) describes the electron spin relaxation mechanism. The spin-polarized current does not conserve the angular momentum due to multiple relaxation mechanisms, so S_x decays exponentially as a function of time with a relaxation rate $1/\tau_{sf}$, and finally would be relaxed within the limit of the spin diffusion length. The full solution of Eq. (2.12), thus, is given by

$$S_x(x,t) = S_x(0,0)\frac{1}{\sqrt{4\pi Dt}}\exp\left(-\frac{x^2}{4Dt}\right)\cos\omega_L t\exp\left(-\frac{t}{\tau_{sf}}\right) \qquad (2.13)$$

Since all the electrons present at the port of detection, $x = d$, need to be counted, we have to integrate over all time t to obtain the total change of S_x for all injected spins. Then, we obtain

$$S_x(x=d) = S_x(0,0)\int_0^\infty dt\frac{1}{\sqrt{4\pi Dt}}\exp\left(-\frac{d^2}{4Dt}\right)\cos\omega_L t\exp\left(-\frac{t}{\tau_{sf}}\right). \qquad (2.14)$$

V_{NL} is proportional to $S_x(x = d)$ and the proportional constant can be determined by the following condition: V_{NL} should be equal to that given by Eq. 2.10 or Eq. 2.11 when $B_z = 0$. Then, the final expression for the Hanle signal is given by

$$\begin{aligned} V_{NL}(B_z) = \pm\frac{1}{2}P_{inj}P_{det}\left(\rho\frac{l_{sf}}{S}\right)\exp\left(-\frac{d}{l_{sf}}\right) \\ \times\int_0^\infty dt\frac{1}{\sqrt{4\pi Dt}}\exp\left(-\frac{d^2}{4Dt}\right)\cos\omega_L t\exp\left(-\frac{t}{\tau_{sf}}\right) \end{aligned} \qquad (2.15)$$

where +(−) sign corresponds to the parallel (antiparallel) magnetization configuration.

The merit of Hanle effect is that it is sensitive to the precessional motion and/or dephasing of the spins, *i.e.* no relation to the magnetic properties of the ferromagnetic contacts likewise the anisotropic magnetoresistance. This means that the Hanle effect can be measured locally as well as nonlocally. In addition the Hanle effect can be used to measure the spin lifetime directly.

→ *We turn now our description to the nuclear spin polarization, coupling interaction between spin-polarized electrons and nuclear spins through the hyperfine interaction, and the nuclear magnetic resonance.*

2.4. Nuclear spin polarization

Consider an assemble of a set of identical nuclei; each nucleus has an angular momentum $\hbar\mathbf{I}$ and an associated magnetic moment $\boldsymbol{\mu}_n = g_n\mu_N\mathbf{I}$, where $\hbar$ is the reduced Plank's constant, $\mathbf{I}$ is a nuclear spin, g_n is the nuclear g-factor and μ_N is the nuclear magneton. The usual way to polarize a nuclear spin system is by application of an external magnetic field $\mathbf{B}$. The Zeeman Hamiltonian ($\mathcal{H} = -\boldsymbol{\mu}_n\cdot\mathbf{B}$) would therefore split degenerated energy states into $(2I+1)$ states, where I is the spin quantum number. Each state has specified by an energy $E_m = -g_n\mu_N m B_z$, where the magnetic quantum number $m = -I, -I+1, \ldots, +I$ parameterizes each energy level (we have set the direction of applied field and quantization axis to be along z axis direction) [57].

For the purpose of simplicity, let's consider a system of $I = 1/2$ nuclei. According to Boltzmann law of statistical mechanics, the population of the energy state is proportional to $\exp(-E_m/k_B\theta) = \exp(g_n\mu_N m B_z/k_B\theta)$, where θ is the temperature, and the population of our two states system is as shown Fig. 2.6.

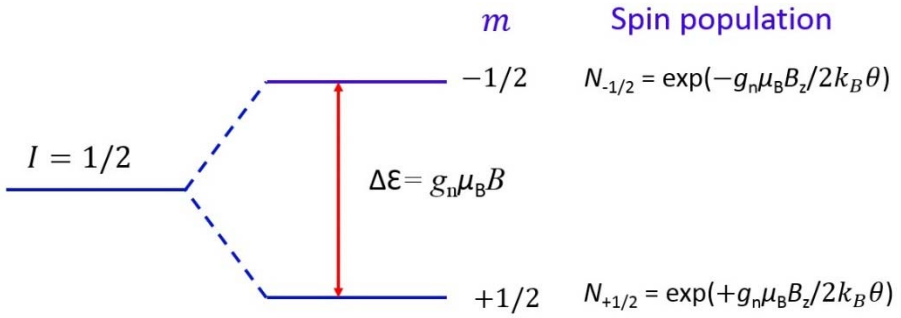

Fig. 2.6: A schematic representation of the population of two energy states of a nuclear spin system with I = 1/2 under an applied magnetic field along z direction and temperature θ.

We can therefore define the nuclear spin polarization P_n by the following expression:

$$P_n = \frac{N_{+1/2} - N_{-1/2}}{N_{+1/2} + N_{-1/2}}, \tag{2.16}$$

where $N_{+1/2}$ and $N_{+1/2}$ are number of nuclei in the state of m = +1/2 and m = −1/2, respectively. Taking $\mu_N = 5.05\times10^{-27}$ J/T, one can obtain

$$P_n = \tanh\left(\frac{g_n\mu_N B_z}{2k_B\theta}\right) \approx 10^{-3}\,\frac{B_z}{\theta}\,\left(\frac{\text{Tesla}}{\text{Kelvin}}\right). \tag{2.17}$$

In order to obtain only a nuclear spin polarization in the order of 1% by this method, one needs to apply an extremely large magnetic field in the order of 10 T at very low temperature 1 K.

In 1953, Overhauser found that the saturation of electron spin resonance of conduction electrons could lead to polarization of the nuclei in metals [58]. This method is first known as the dynamic nuclear polarization (DNP), in which electron spin pumping with a microwave field at a particular frequency induced transition between energy levels of electron-nuclear spin system. These

transitions made simultaneous flipping of electron and nuclear spins, directly by the applied microwave field, and indirectly through relaxation processes, results in a dynamic equilibrium with an enhanced nuclear spin polarization.

Alternatively, in order to achieve an efficient DNP in semiconductors, one can establish a non-equilibrium electron spin polarization through the electrical spin injection as discussed in Sec. 2.2. The angular momentum of an electronic-spin system is therefore transferred to a nuclear-spin system via flip-flop interactions similarly to the spin pumping with microwave assistance. Since the electronic spin accumulation is maintained by the electrical injection, the nuclear spin system can be effectively polarized by DNP. In the following, step by step, we will discuss about the hyperfine interaction, then emphasize on the process of the DNP and the produced nuclear field.

2.5. The hyperfine interaction

Roughly speaking, the hyperfine interaction describes the physics between electron and nuclear spins. Since the nuclei have magnetic moments, even weak, they are sensitive to magnetic fields associated with the spin and orbital angular momentum of the electrons. In the same way, electrons feel magnetic fields originating from nuclear magnetic moments. Coupling interactions of electrons with nuclei through those magnetic fields are defined as the hyperfine interaction.

The most prevalent interactions encountered in the hyperfine interaction are the dipolar interaction and Fermi contact interaction. In most cases, the strength of these interactions mostly depends on the size of nuclei and the distance between electron and nucleus along with the inclined angle in space. For such a case, the more the size of the nuclei increases, the more the strength of interaction increases.

The hyperfine dipolar interaction exists while an electron revolves around a nucleus and keeping a far distance with a magnetic field produced by the nuclei. However, if an electron approaches to a nucleus, the interaction is no longer dipolar; it is called a hyperfine Fermi contact interaction. Through the rest of the chapter, the dipolar interaction will be considered only during the spin-relaxation mechanism, because it is very weak compared to the Fermi contact interaction. However, it becomes a dominant factor for the spin relaxation.

2.6. The Fermi contact hyperfine interaction

Following Refs. [42, 57, 59], the interaction of a single electron of spin **S** with a nucleus of spin **I** is described by the Fermi contact Hamiltonian:

$$H_{\mathrm{HFI}} = \frac{8\pi}{3}\frac{\mu_0}{4\pi} g_e \mu_{\mathrm{B}} \gamma_n \hbar \mathbf{I}\cdot\mathbf{S}\,|\psi(r_i)|^2 \tag{2.18}$$

where **I** and **S** are the nuclear and electron spin operators, respectively, $\psi(r_i)$ is wave function of electron at a distance r_i from a nucleus i, g_e is the electron g-factor, μ_B is the Bohr magneton, $\mu_0 = 4\pi \times 10^{-7}$ $\mathrm{VsA^{-1}m^{-1}}$ is the permeability of the free space in SI unit, γ_n is the nuclear gyromagnetic ratio, $\hbar$ is the reduced Plank's constant. For simplicity, Eq. 2.18 can be written as

$$H_{\mathrm{HFI}} = A\mathbf{I}\cdot\mathbf{S} \tag{2.19}$$

where

$$A = \frac{8\pi}{3}\frac{\mu_0}{4\pi} g_e \mu_{\mathrm{B}} \gamma_n \hbar\,|\psi(r_i)|^2 \tag{2.20}$$

is the hyperfine constant, whose typical values for Ga and As are in the order of 50 μeV [60]. The inner product in Eq. 2.19 can be written as the sum of a static term and a dynamic term as

$$H_{\mathrm{HFI}} = A\mathbf{I}\cdot\mathbf{S} = AI_zS_z + \frac{A}{2}(I_+S_- + I_-S_+) \tag{2.21}$$

where I_z and S_z are the z-component of **I** and **S** along the field direction,

respectively, and $I_{+(-)}$ (= I_x +(−) iI_y) and $S_{+(-)}$ (= S_x +(−) iS_y) are the ladder operators used to raise (lower) the magnetic quantum number m ($\approx I_z$ or S_z) along the quantization direction by unity.

The first term within Eq. 2.21 is called the static term of the Fermi contact hyperfine interaction (effective fields term), and the second is called the dynamic term (or spin exchange term) which results in a DNP. Below we describe each term in details.

2.7. The static term of the Fermi contact hyperfine interaction

The first term of Eq. 2.21, (AI_zS_z), is called the static part of the hyperfine interaction, referring to either a hyperfine magnetic field: Nuclear (Overhauser) field ($\propto AI_z$) experienced by electrons and/or electronic (the Knight) field ($\propto AS_z$) experienced by nuclei. Such double field effects can be clarified as follows. Since the Knight field, B_e, is an effective magnetic field experienced by nuclei, it is given by the magnetic energy divided by the nuclear magnetic moment. Thus, it is given by

$$B_e = \frac{AI_zS_z}{\gamma_n I_z \hbar} = \frac{AS_z}{\gamma_n \hbar} = b_e S_z \tag{2.22}$$

where

$$b_e = \frac{A}{\gamma_n \hbar} = \frac{2}{3}\mu_0 g_e \mu_B |\psi(r_i)|^2 \tag{2.23}$$

In obtaining Eq. (2.23), Eq. (2.20) was used. By the same way, the Overhauser field, B_n, experienced by electrons is given by

$$B_n = \frac{AI_zS_z}{\gamma_e S_z \hbar} = \frac{AI_zS_z}{g_e \mu_B S_z} = \frac{AI_z}{g_e \mu_B} = b_n I_z \tag{2.24}$$

where

$$b_n = \frac{A}{g_e \mu_B} = \frac{2}{3} \mu_0 \gamma_n \hbar |\psi(r_i)|^2 \quad (2.25)$$

Thus the static term of the Fermi contact hyperfine interaction can be written as

$$A I_z S_z \approx B_e \cdot \gamma_n \hbar I_z \approx B_n \cdot g_e \mu_B S_z . \quad (2.26)$$

2.8. The dynamic term of the Fermi contact hyperfine interaction

The second term [$A/2$ ($I_+S_- + I_-S_+$)] of Eq. 2.21 is a spin exchange term, which describes the simultaneous reversal of angular momentum by flip-flop processes through the hyperfine interaction between electron and nuclear spins. Clearly, this interaction conserves the total spin of the electronic-nuclear spin system. The angular momentum can be transferred from electron- to nuclear-spins and vice-versa, providing an effective DNP.

The phonological rate equation of the dynamic nuclear polarization can be constructed from the balance between the rate of nuclear spin polarization ($1/T_{1e}$) due to the simultaneous reversal of flip-flop processes and the rate of depolarization ($1/T_1$) owing to the interaction with lattice environment, where T_{1e} and T_1 are the time scale of nuclear spin polarization and depolarization, respectively. A schematic representation for those rate scales is shown in Fig. 2.7, and the phenomenological rate equation of the nuclear spin polarization is given by [4, 57, 59]

$$\frac{d}{dt}\langle I_z \rangle = -\frac{1}{T_{1e}}\left(\langle I_z \rangle - Q\langle S_z \rangle\right) - \frac{1}{T_1}\langle I_z \rangle . \quad (2.27)$$

where $\langle I_z \rangle$ and $\langle S_z \rangle$ are the average component of the quantized nuclear and electron spin along field direction, and Q defines the momentum conversion coefficient between electron spin to nuclear spin systems, and is given by $f_L I(I+1)/S(S+1)$, where f_L is the leakage factor of nuclear-spin polarization or a quantity referring to the number of un-polarized nuclei. If the nuclear spin system

is relaxed due to electrons only, fully isolated from the other world, then f_L goes to the unity (≈ 1). However, if any other relaxation mechanism is considered, then f_L might reduce than the unity.

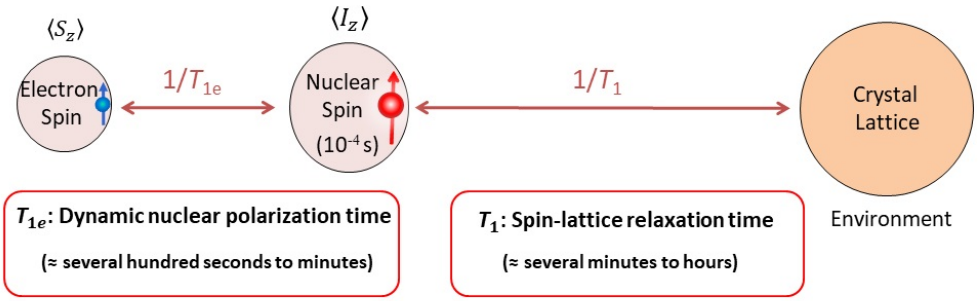

Fig. 2.7: A schematic representation showing the dynamic polarization of nuclear spins due to interaction with the spin-polarized electrons through a polarization rate ≈ $1/T_{1e}$ and the nuclear spin relaxation due to interaction with the lattice (environment) through a spin-lattice relaxation rate ≈ $1/T_1$.

Owing to the large mismatch between electronic and nuclear Zeeman energies, those spin-flip processes are associated with some additional assisting processes, such as an emission or an absorption of photon or phonon seeking for conservation of the energy of the total spin system. Since the dynamic polarization of nuclear spins is almost due to the hyperfine coupling with spin-polarized electrons, the nuclear polarization rate is, therefore, determined by the strength of the hyperfine coupling with electron spin and the rate of the assisting process, and it is expressed as

$$T_{1e}^{-1} = \eta \tau_{1e}^{-1} . \tag{2.28}$$

where η depends on the strength of the hyperfine coupling, and ${\tau_{1e}}^{-1}$ is the transition rate of spin flip-flop assisting process through the hyperfine interaction.

On the other hand, nuclear spins can be depolarized due to a couple of

reasons: depolarization due to their precession about the local dipolar field B_L, resulting from the dipole-diploe interaction between neighboring nuclei, and another precession about the Knight field. The dipole-dipole interactions with neighboring nuclei, B_L, mixes the wave functions of nuclear-spin states on the order of $B_L/|\mathbf{B}|$. The nuclear spin depolarization is led by the transitions between these mixed sates, which is induced by the hyperfine magnetic field of electron spins ($\propto A\langle S_{z'}\rangle$). Then, the rate of nuclear spin depolarization is given by

$$T_1^{-1} = \eta \tau_1^{-1} \left(\frac{B_L^2}{\mathbf{B}^2} \right). \tag{2.29}$$

where τ_1^{-1} is the rate of assisting depolarization process.

If $\langle I \rangle < Q\langle S \rangle$ for an initial condition, which is satisfied in most cases, the first term of Eq. 2.27 describes the nuclear-spin polarization through the flip-flop process. If we ignore the second term, $\langle I \rangle$ increases with a rate of $(1/T_{1e})$ until it reaches to $Q\langle S \rangle$, in which the dynamic process of $I_+S_- + I_-S_+$ are balanced. Multiplying b_n on both side of Eq. 2.27 and using Eq. 2.24, the time evolution of nuclear field is given by

$$\frac{d}{dt} B_n(t) = -\frac{1}{T_{1e}} \left(B_n(t) - b_n Q \langle S_z \rangle \right) - \frac{1}{T_1} B_n(t) . \tag{2.30}$$

The steady-state nuclear field, B_{n0}, is given by solving Eq. 2.30 under the condition of $\frac{d}{dt} B_n(t) = 0$, and we get

$$\begin{aligned} -\frac{1}{T_{1e}} \left(B_{n0} - b_n Q \langle S_z \rangle \right) - \frac{1}{T_1} B_{n0} = 0 \\ \therefore B_{n0} = \frac{b_n Q \langle S_z \rangle}{1 + T_{1e}/T_1} \end{aligned} . \tag{2.31}$$

By substituting Eqs. 2.28 and 2.29 into Eq. 2.31, we get

$$B_{n0} = \frac{b_n Q \langle S_z \rangle}{1 + \xi B_L^2 / \mathbf{B}^2} = f_L b_n \frac{I(I+1)}{S(S+1)} \frac{\langle \mathbf{S} \rangle \cdot \mathbf{B}}{\mathbf{B}^2 + \xi B_L^2} |\mathbf{B}| . \tag{2.32}$$

or

$$\mathbf{B}_{n0} = f_L b_n \frac{I(I+1)}{S(S+1)} \frac{\langle \mathbf{S} \rangle \cdot \mathbf{B}}{\mathbf{B}^2 + \xi B_{\mathrm{L}}^2} \mathbf{B} . \tag{2.33}$$

in a vector form, where $\xi = \tau_{1e} / \tau_1$ is the assisting processes which allow energy to be conserved in mutual spin flips between electrons and nuclei, and

$$\langle S_z \rangle = \frac{\langle \mathbf{S} \rangle \cdot \mathbf{B}}{|\mathbf{B}|} . \tag{2.34}$$

Using the steady-state solution, B_{n0}, given by Eq. 2.32, Eq. 2.31 can be rewritten as

$$\frac{d}{dt} B_n(t) = -\left(\frac{1}{T_{1\mathrm{e}}} + \frac{1}{T_1} \right) \left(B_n(t) - B_{n0} \right) \tag{2.35}$$

Since the direction of nuclear field is along **B**, the nuclear field in a vector form is given by

$$\mathbf{B}_n(t) = B_n(t) \frac{\mathbf{B}}{|\mathbf{B}|} . \tag{2.36}$$

2.9. Nuclear magnetic resonance

In this section, we will clarify the behavior of the polarized nuclear spins while application of a radio-frequency (rf) magnetic field, see pass c in Fig. 2.1. In Sec. 2.8, we discussed about dynamic polarization of the nuclear spins, and derived an expression for the time evolution of nuclear field (the Overhauser field) during DNP. Herein, we discuss about a temporal depolarization of the nuclear spins while irradiated by rf-magnetic field, which is the so-called nuclear magnetic resonance (NMR). Actually, when the Zeeman splitting energy of nuclear spins due to a static magnetic field becomes equal to an energy of irradiated by rf-magnetic field, NMR occur. As a result, transition between the

Zeeman energy states would be enhanced, nuclear spin polarization is destroyed and the nuclear field induced by DNP is suppressed.

On the other hand, if rf-magnetic field is halted, the transitions of the nuclear spins will be hindered. Again, the nuclear spins can be repolarized due to DNP. As we discussed in Sec. 2.4, under application of a static magnetic field along z direction, the Zeeman interaction establishes $2I + 1$ equally-spaced energy states with $E_m = -g_n\mu_n m B_z = -\gamma_n \hbar m B_z$, where m is a quantum number which parameterizes each energy state. For a system of $I = 3/2$ as GaAs semiconductor, we have four states, and their population is as shown in Fig. 2.8. Thus the transition energy between two states is given by

$$\Delta\varepsilon = \gamma_n \hbar B_z . \tag{2.37}$$

where γ_n is the nuclear gyromagnetic ratio. Due to the static magnetic field, the spin magnetic moment make a precessional motion by an angular frequency ω. Therefore, irradiating the system by a wave at an angular frequency ω ($=2\pi f$, where f is the frequency of the applied rf-magnetic field) or an energy $\hbar\omega$ equal to the transition energy leads to enhancing the transition and destroying the polarization of nuclear spins, this is the resonance phenomenon, and the resonance condition is given by

$$\omega = \Delta\varepsilon / \hbar = \gamma_n B_z \tag{2.38}$$

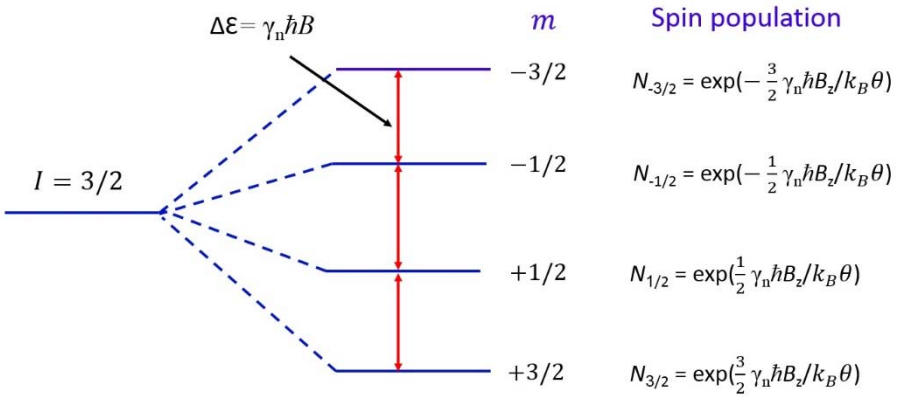

Fig. 2.8: A schematic representation of the population of two energy states of a nuclear spin system with $I = 3/2$ under an applied magnetic field along z direction and temperature θ.

2.10. Detection of the nuclear field by using Hanle effect at an oblique angle

The discussion here is concerning with the detection of the nuclear field acting on the electron spins through the hyperfine coupling, see pass *e* and pass *d* in Fig. 2.1. Simply, we extend our discussion about the Hanle effect, described earlier in Sec.2.3.2. So, briefly, application of an external magnetic field **B** (along z axis with a strength of B_z) perpendicular to the direction of spin polarization (along x axis) leads to that the accumulated spins make a precessional motion about **B**. Such precessional motion is derived by a precessional factor $\cos(\omega_L t)$, where ω_L is the Larmor frequency (= $\gamma_e B_z$, where γ_e is the electronic gyromagnetic ratio). The only difference between the typical Hanle effect and oblique Hanle effect discussed in this section is that the magnetic field is applied

along a direction not orthogonal to **S**, but oblique to **S**, so that the electron spins make a precession about a nuclear field [42, 59].

To explain such effect more clearly, it is better to recall the first term of Eq. 2.12, which describes the change of the angular momentum of electron spin system due to a precessional motion about the magnetic field. However, herein, we have an effective magnetic field ≈ **B** + $\mathbf{B}_n$ about which electron spins precess, *i.e.* the condition to make Hanle precession becomes **S** × (**B** + $\mathbf{B}_n$) ≠ 0. So, if the inclined angle φ between **S** and (**B** + $\mathbf{B}_n$) is 90°, there is no $\mathbf{B}_n$ generated (*see* Eq. 2.32) and we have the typical Hanle precession, as shown in Fig. 1.9(a). If φ is equal 0, on the other hand, there is no precession at all due to a parallel alignment of **S** and (**B** + $\mathbf{B}_n$). So, the only case for **S** to make a precession by generated $\mathbf{B_n}$ is occurring when **B** is applied obliquely to **S**, as shown schematically in Fig. 2. 9(b).

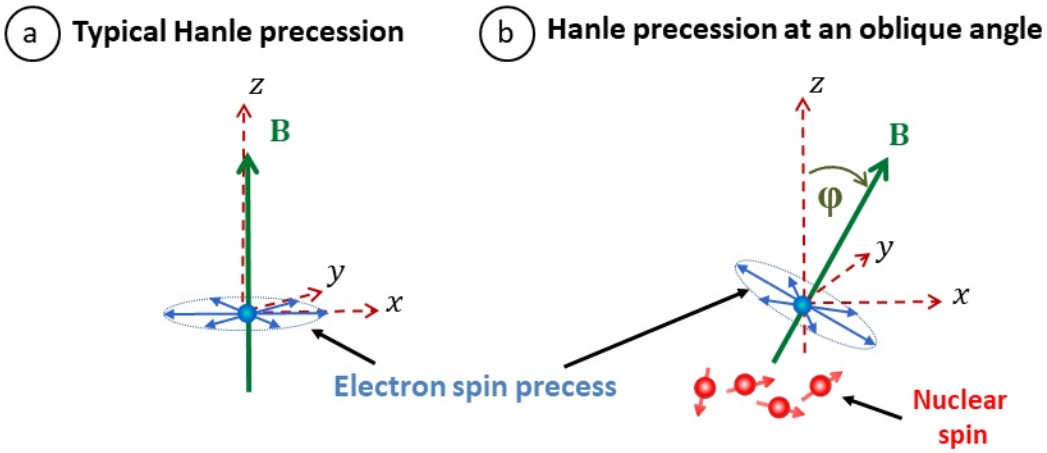

Fig. 2.9: A schematic description of the Hanle spin precession about (a) perpendicular magnetic field and (b) oblique magnetic field to the direction of spin polarization in semiconductor.

Under the presence of nuclear field, the Larmor frequency of the precessional motion changes by $\Delta\omega = \gamma_n B_z$, resulting in changing V_{NL} according to Eq. (2.15).

2.11. Spin temperature

The introduction of nuclear spin temperature is one merit for considering the nuclear system. It is used to describe the state of the nuclear spins, whether in a polarization state or not. So, by knowing the temperature of the nuclear spin system, one can determine the relative orientation of the nuclear spins with respect to magnetic field and electron spin during the dynamic nuclear polarization. As we mentioned in Sec. 2.8, each nucleus experiences a fluctuating local dipolar field (B_L) created by its neighbors. The period of the nuclear spin precession in B_L is defined by a characteristic time scale $T_2 = 1/\gamma_n B_L$, where γ_n is nuclear gyromagnetic ratio for the nuclear spins. Since B_L is on the order of 1 G, the time T_2 is generally on the order of several microseconds. Within such time scale, the nuclear spin system reaches to an internal thermodynamic equilibrium state. This equilibrium has to be described by different temperature than the lattice temperature, which is called the spin temperature (θ). Since the characteristic time of the internal equilibrium of nuclear spin system, T_2, is much shorter than the nuclear polarization time T_{1e} (≈ seconds to several minutes) and the spin-lattice relaxation time T_1 (≈ several minutes to hours), the nuclear spin system is considered an isolated system.

Unlike the spin-spin exchange interaction through the hyperfine coupling, the dipole-dipole interaction is a magnetic interaction, which does not conserve the total nuclear spin. Therefore, the nuclear spins average to zero if the magnetic field is removed. So, only under the magnetic field **B**, nuclear magnetism exists, and following the Curie law of paramagnetism, the average nuclear spins can be given by [57]

$$\langle \mathbf{I}_\alpha \rangle = \frac{(I_\alpha + 1)\mu_{1\alpha}}{3k_B\theta}\mathbf{B} \tag{2.39}$$

where α refers to each nuclei included in a semiconductor, I_α is the value of a nuclear spin, and $\mu_{1\alpha}$ is the nuclear magnetic moment, k_B is the Boltzmann constant, and θ is the nuclear

spin temperature. Under DNP ($\langle\mathbf{S}\rangle\cdot\mathbf{B} \neq 0$) and using Eqs. 2.24, 2.32 and 2.39 with $S = 1/2$, the reciprocal nuclear spin temperature for each nuclei species α at the steady state can be described using the following expression:

$$\frac{1}{k_{\mathrm{B}}\theta_{\alpha 0}} = f_L \frac{4I_\alpha}{\mu_{\mathrm{I}\alpha}} \frac{\langle\mathbf{S}\rangle\cdot\mathbf{B}}{\mathbf{B}^2 + \xi B_L^2}\,. \tag{2.40}$$

Therefore, if we consider that $|\mathbf{S}| = 0.25$ and $|\mathbf{B}| = 5$ mT, then the spin temperature is cooled to 10^{-6} K. Using Eqs. 2.32, 2.39 and 2.40, one can determine the relative orientations of the average nuclear spin $\langle\mathbf{I}\rangle$ and nuclear field $\mathbf{B}_{\mathrm{n}}$ with respect to the average electron spin $\langle\mathbf{S}\rangle$ and the magnetic field $\mathbf{B}$ at a given nuclear spin temperature θ_α, or during the cooling effect of DNP. According to the sign of inner product $\langle\mathbf{S}\rangle\cdot\mathbf{B}$, we can define three states of nuclear spin temperature showing the direction of $\langle\mathbf{I}\rangle$ and/or $\mathbf{B}_{\mathrm{n}}$ relatively to $\langle\mathbf{S}\rangle$. In the following sections, we will see how the temperature of nuclear spins is cooled by DNP or heated up by NMR based on those three states of nuclear spin temperature.

2.11.1. Positive nuclear spin temperature

Shown in Fig. 2.10(a) is a two-level nuclear spin system under only the effect of an external magnetic field $\mathbf{B}$, yielding to a weak nuclear spin polarization. In terms of Eq. 2.32, if $\mathbf{B}$ is applied along a direction parallel to the direction of average electron spin $\langle\mathbf{S}\rangle$, *i.e.* $\langle\mathbf{S}\rangle\cdot\mathbf{B} > 0$, then $\mathbf{B}_{\mathrm{n}}$ would be generated in a direction antiparallel to $\mathbf{B}$, because b_{N} is negative value for all nuclei in GaAs. Then, using Eq. 2. 39, the average nuclear spin $\langle\mathbf{I}\rangle$ is parallel to $\mathbf{B}$ and both of them are antiparallel to $\mathbf{B}_{\mathrm{n}}$. This means that the lower level is populated more spins than the upper level. For such case, one call the nuclear spin system undergoes a positive cooling by DNP or having a positive nuclear spin temperature because of $\langle\mathbf{S}\rangle\cdot\mathbf{B} > 0$, see Eq. 2.40. The distribution of the nuclear spins between states for such case is schematically shown in Fig 2.10(b).

2.11.2. Negative nuclear spin temperature

By the same way, if **B** is applied along an opposite direction to the direction of ⟨**S**⟩, *i.e.* ⟨**S**⟩·**B** < 0, then the higher energy level is populated more spins than the lower energy level (population inversion). For such case, one call the nuclear spin system temperature undergoes a negative cooling by DNP or having a negative nuclear spin temperature. The distribution of the nuclear spin between states for such case is schematically shown in Fig 2.10(c).

2.11.3. Nuclear spin temperature at NMR

As we discussed in Sec. 2.9, NMR produces a temporal depolarization for the nuclear spins under DNP. This means that the nuclear spin system is heated up to an infinite temperature and DNP is suppressed, resulting in ⟨**I**⟩ = 0. The distribution of the nuclear spins at NMR is as shown in Fig. 2.10(d).

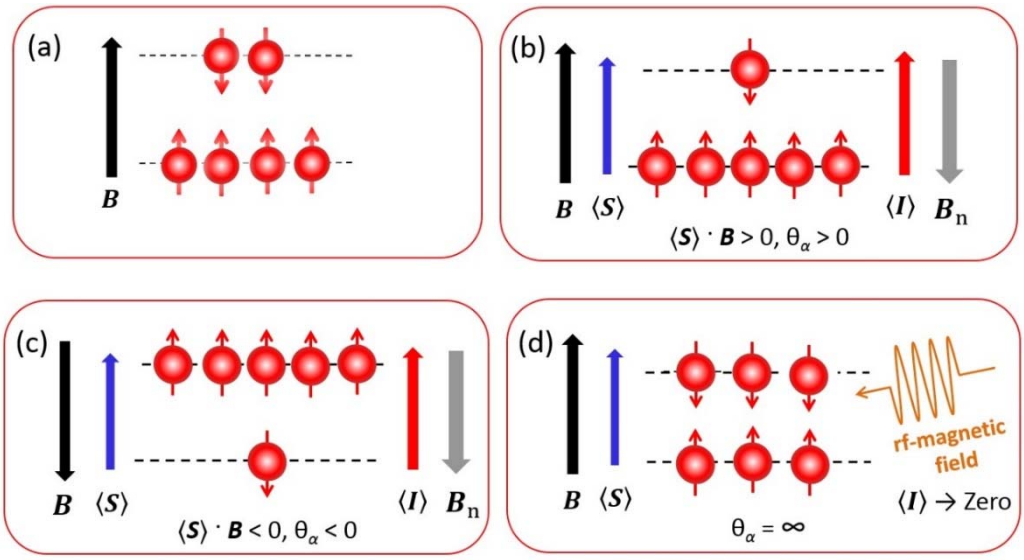

Fig. 2.10. Schematic description for nuclear spin distribution (a) under an external magnetic field, (b) under the DNP process when $\langle \mathbf{S} \rangle \cdot \mathbf{B} > 0$, (c) under the DNP process when $\langle \mathbf{S} \rangle \cdot \mathbf{B} < 0$, and (d) under both DNP and NMR, where $\mathbf{B}$ is an oblique magnetic field to the direction of average electron spin polarization $\langle \mathbf{S} \rangle$.

Chapter 3

Experimental Methods

3.1 Introduction

In this chapter, we overview our experimental methodology and simulation method. The heterostructures of the used device in this study were grown by a molecular beam epitaxy (MBE) and a magnetron sputtering. In addition, using electron beam lithography and Ar ion milling techniques, a novel nuclear magnetic resonance system based on a lateral spin-transport device was fabricated. All measurements were done at 4.2 K using a four probe method.

Following sections we summarize each mentioned process above as follows: In Sec. 3.2 we describe the sample layer structure and the growth conditions of the thin film formation. In Sec. 3.3 we shortly summarize the fabrication process of a novel nuclear magnetic resonance system using a four-terminal lateral spin transport device, having Co_2MnSi/CoFe/GaAs heterojunctions. We describe in details the measurement methodology and conditions required for the spin-valve like signal, Hanle signal, and oblique Hanle signal with and without irradiation by a radio frequency (rf)-magnetic field in Sec. 3.4. Finally, we state about the established simulation model using time evolution of nuclear field to describe the transient behavior of nuclear spins in semiconductors in Sec. 3.5.

3.2 Sample layer structure and growth method

Fig. 3.1 shows a layer structure of a lateral spin-transport device grown in this study. From the substrate side, a 250-nm-thick undoped GaAs buffer layer, followed by a channel layer of n^--GaAs with a Si concentration of 3×10^{16} cm^{-3} and thickness of 2500 nm, then a 15-nm-thick $n^- \rightarrow n^+$-GaAs transition layer, and finally a 15-nm-thick heavily doped n^+-GaAs layer with a Si concentration of a 5×10^{18} cm^{-3} were grown using MBE.

The silicon doping concentration of the n^-- GaAs channel region ($n \approx 3 \times 10^{16}$ cm^{-3}) is selected to be slightly above the metal-insulator transition for

GaAs, as this results in producing the longest spin lifetimes in GaAs [61]. Also, to make the necessary tunnel barrier for spin injection and detection, we used a highly doped interface region ($n \approx 5 \times 10^{18}$ cm^{-3}) to reduce the depletion layer width of the Schottky tunnel barrier [62].

After the GaAs channel is grown, its surface is capped with an As protective layer to prevent the surface oxidation, preparing for a transportation to a separate magnetron sputtering system for the deposition of ferromagnetic layer structures.

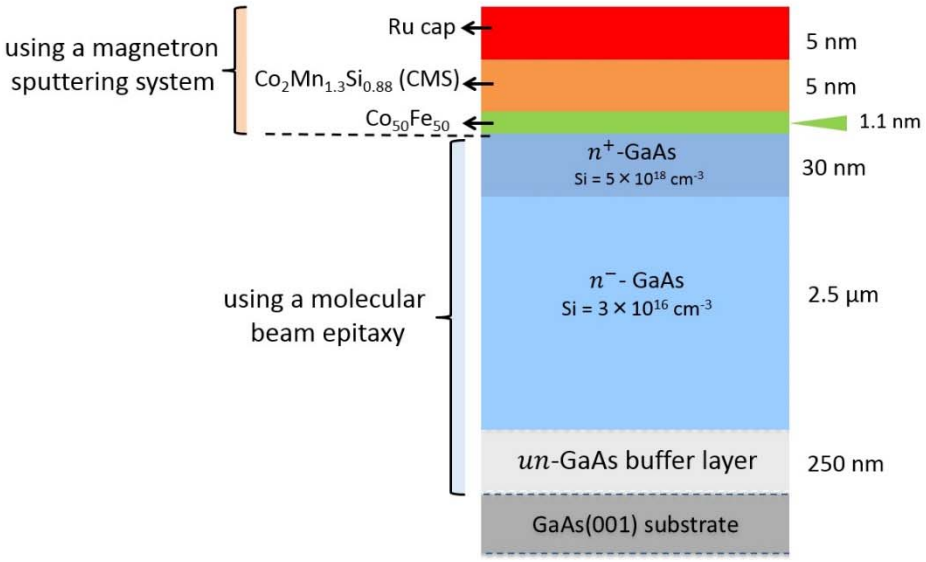

Fig. 3. 1: A schematic description of a layer structure.

Within a heating chamber connected with the main growth chamber of a magnetron sputtering, the protective As layer was removed away by heat treatment up to ≈ 300°C. Before starting deposition of ferromagnetic thin films, the surface of GaAs was checked *in-situ* using reflection high-energy electron diffraction (RHEED), and clear streak patterns for all main crystallographic axes directions of GaAs were observed as shown in Fig. 3.2.

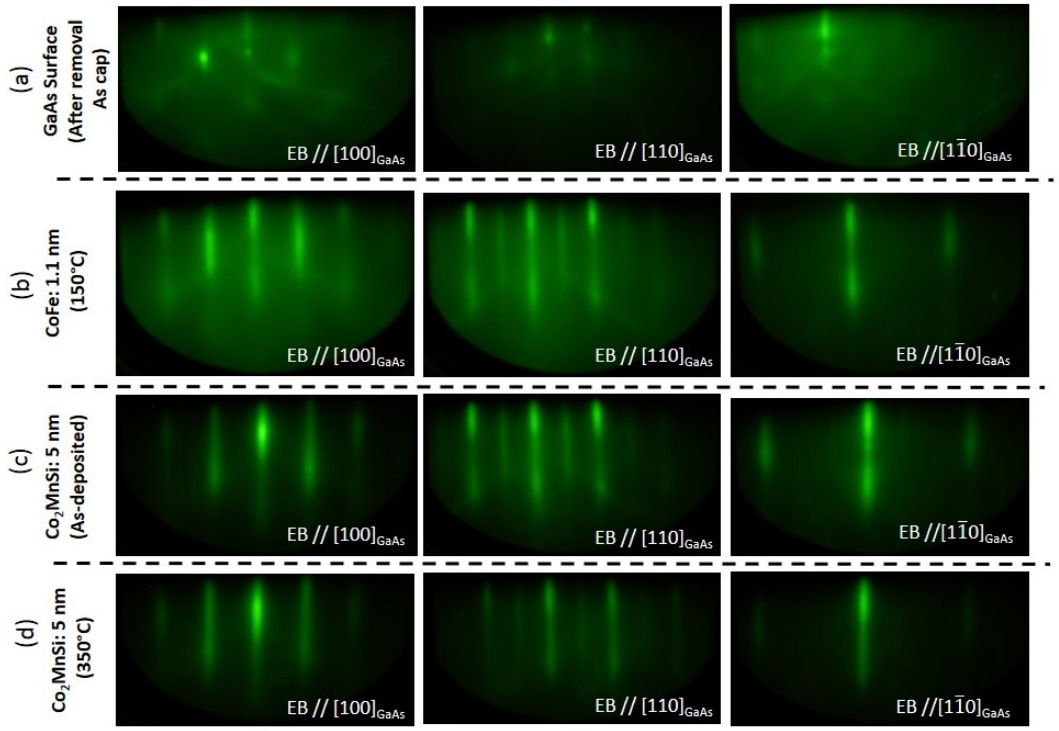

Fig. 3.2: RHEED patterns of (a) the surface of GaAs semiconductor after removing a protective As layer by heat-treatment up to 300°, (b) the surface of a 1.1-nm-thick $Co_{50}Fe_{50}$ layer after thermal annealing at 150°C for 15 min, (c) the surface of the as-deposited 5-nm-thick $Co_2Mn_{1.3}Si_{0.88}$ layer and (d) the surface of a 5-nm-thick $Co_2Mn_{1.3}Si_{0.88}$ layer after thermal annealing at 350°C for 15 min.

After the temperature of the sample cooled to the room temperature (RT), a 1.1-nm-thick $Co_{50}Fe_{50}$ layer was firstly deposited at RT, then annealed at 150° C for 15 min. Again, after the sample was cooled to RT, a 5-nm-thick $Co_2Mn_{1.3}Si_{0.88}$ (CMS) layer was then deposited at RT, followed by annealing at 350°C for 15 min. Finally, the sample was capped with a 5-nm-thick Ru layer.

The thermal annealing process has been attempted for either CoFe or CMS to enhance the surface crystallinity of each layer, which results in improving the magnetic properties of the overall CoFe/CMS ferromagnetic

bilayer.

Remarkably, the main feature of this layer structure is the incorporation of CoFe layer as an insertion layer between CMS and GaAs; it is very beneficial to prevent diffusion of Mn ions from CMS into GaAs semiconductor during the thermal annealing. In general, if some Mn ions are succeeded to diffuse into a GaAs channel, then they work as impurity scatters for the injected spins owing to its magnetic nature, resulting in lowering the spin injection efficiency. Equally important, the thickness of CoFe insertion layer has been selected to be 1.1 nm in order to allow the CMS layer acting as a spin source, not CoFe as it is commonly used through literature. Such layer structure is originally proposed by our research group and more details can be found in Ref. [35].

3.3. Device fabrication

A typical lateral spin transport device can be made in three stages. The first stage is to define and fabricate a channel, the second is to fabricate four terminal electrodes, and the third one is to form contact-pads for the electrical measurements. An insulating layer is put down after each stage for the isolation purpose. A schematic representation for the used device in this study is as shown in Fig. 3.3. In the following we shortly overview each stage.

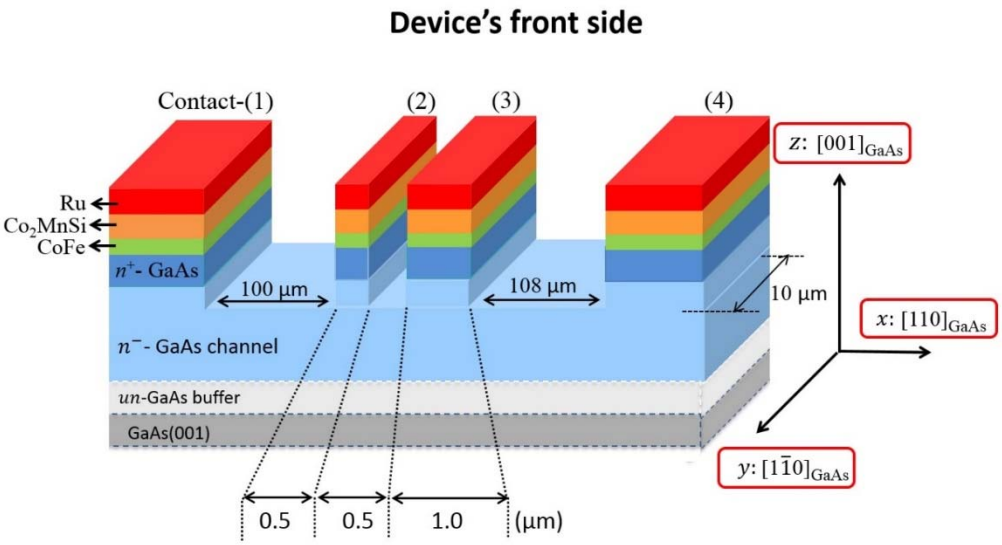

Fig. 3.3: A schematic description of the device's front side showing structures and dimensions.

In the first stage, the channel was firstly defined using an optical photolithography technique, then the channel was etched by an Ar ion milling technique while the milling process was being stopped after passing the n^+-GaAs region, see the 1st milling as shown in Fig.3.4. Afterward, a thin layer of SiO_2 was deposited as an insulation layer, which was then partially removed away from the top surface of the GaAs channel by a simple lift-off process.

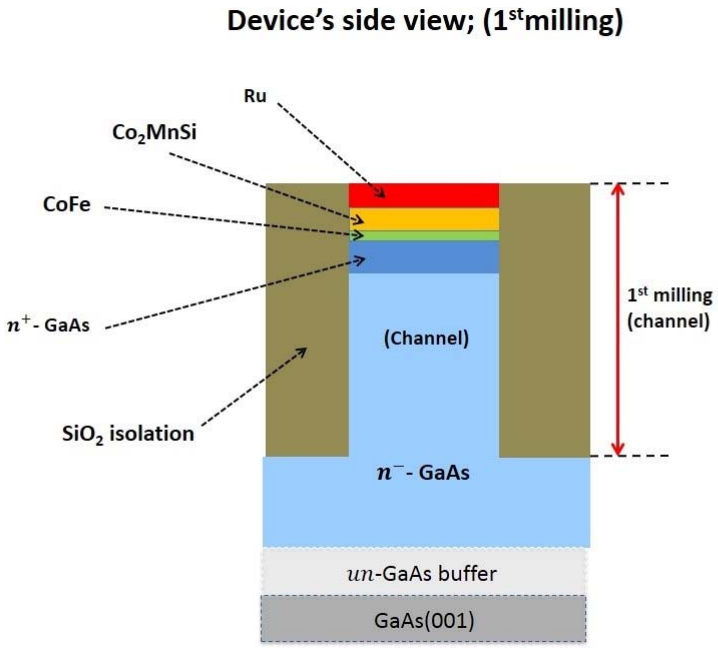

Fig. 3.4: A schematic description of the device's side view showing the 1st milling process, see text.

In the second stage, the four terminal electrodes have been patterned using an electron-beam lithography. Similar to the first stage, the four electrodes were etched using an Ar ion milling technique but firstly the insulation SiO_2 layer was etched away by a reactive ion etching (RIE) technique. Importantly, the Ar ion milling for the four electrodes was being stopped by the time reaching the top of n^--GaAs, see the 2nd milling as shown in Fig 3.4. Thereafter, an insulation layer of SiO_2 was formed, then partially removed away from the top surface of the patterned electrodes by the lift-off process.

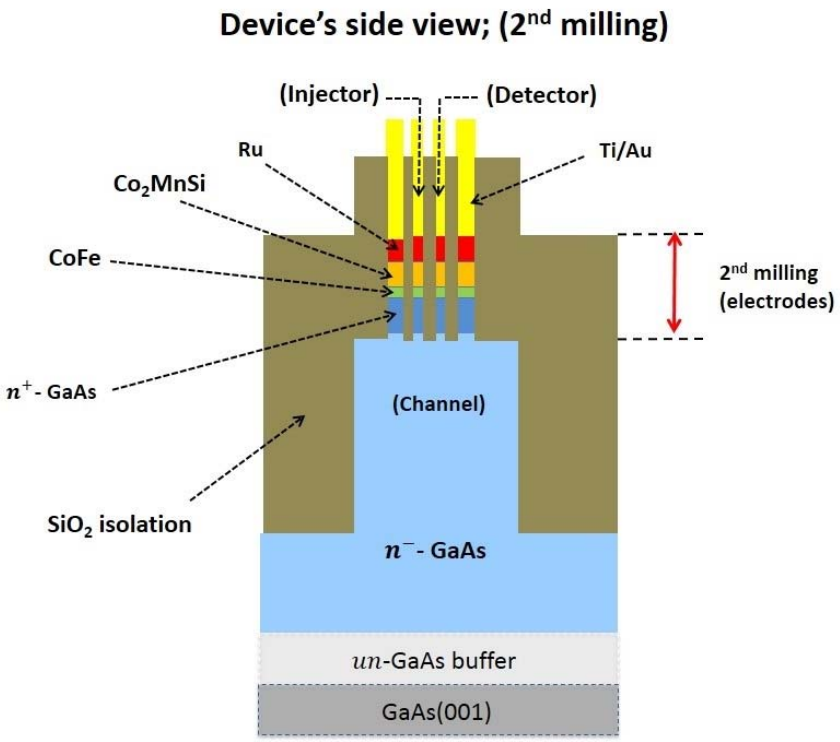

Fig. 3.5: A schematic description of the device's side view illustrating the 2nd milling process together with contact-pads, see text.

Last stage, the third stage, the contact-pads were firstly defined by the optical photolithography, and then a bilayer of Ti/Au is deposited. The reason of introducing Ti is its good adhesion with the surface of SiO_2 compared to the adhesion of Au. Finally, the un-desired portions of Ti/Au bilayer was partially removed away from the contacts by the lift-off processes.

3.4. Measurements

We measured three kinds of signal at 4.2 K, typical Hanle signal, Hanle signal at an oblique angle for the case with and without irradiation by rf-magnetic field, and spin-valve signals. All measurements were conducted using the four-terminal nonlocal geometry, in which the nonlocal voltage (V_{NL}) was measured between contact-3 and contact-4 under a constant bias current I_{bias} supplied between contact-1 and contact-2. As we explained in details in chapter 2 about Hanle effect signals, we study the dephasing mechanism of the accumulated spins in semiconductor due to application of a magnetic field either perpendicular (typical Hanle signal) or making an angle (Hanle signal at an oblique angle) with respect to the direction of spin polarization. Through those signals, we detected the change in V_{NL} which is changed according to the change in the Larmor precession of electron spins about the applied field. On the other hand, in case of the spin-valve like signal measurement, we study the behavior of the accumulated electron spins if the direction of magnetization of ferromagnetic has changed or exactly being manipulated by an in-plane magnetic field.

Figure 3.5 shows (a) electrical spin injection and detection through the nonlocal geometry, (b), (c) and (d) the direction of the applied magnetic field $\mathbf{B_{ap}}$ during measurement of the typical Hanle signal, oblique Hanle signal without and with irradiation by rf-magnetic field and spin-valve like signal, respectively, with respect to the direction of electron spin polarization $\mathbf{S_0}$. In our device, the easy axis of magnetization for the Co_2MnSi/CoFe bilayer is parallel to the *x*-axis – *i.e.* the injected electron spins, $\mathbf{S_0}$, are pointed toward the *x*-axis. We define an angle φ from the *z*-axis in the *x*-*z* plane by which $\mathbf{B_{ap}}$ is applied – *i.e.* $\mathbf{B_{ap}} \equiv B_{ap}(\mathbf{x}\sin\varphi + \mathbf{z}\cos\varphi)$, where B_{ap} is the strength of $\mathbf{B_{ap}}$ (negative B_{ap} means that the direction of $\mathbf{B_{ap}}$ is reversed), φ = 0°, 8°, 6° and 90° for the typical Hanle signal, oblique Hanle signal without and with irradiation by rf-magnetic field, and spin-

valve like signal, respectively, and **x** and **z** are unit vectors along the *x*-axis and *z*-axis directions, respectively.

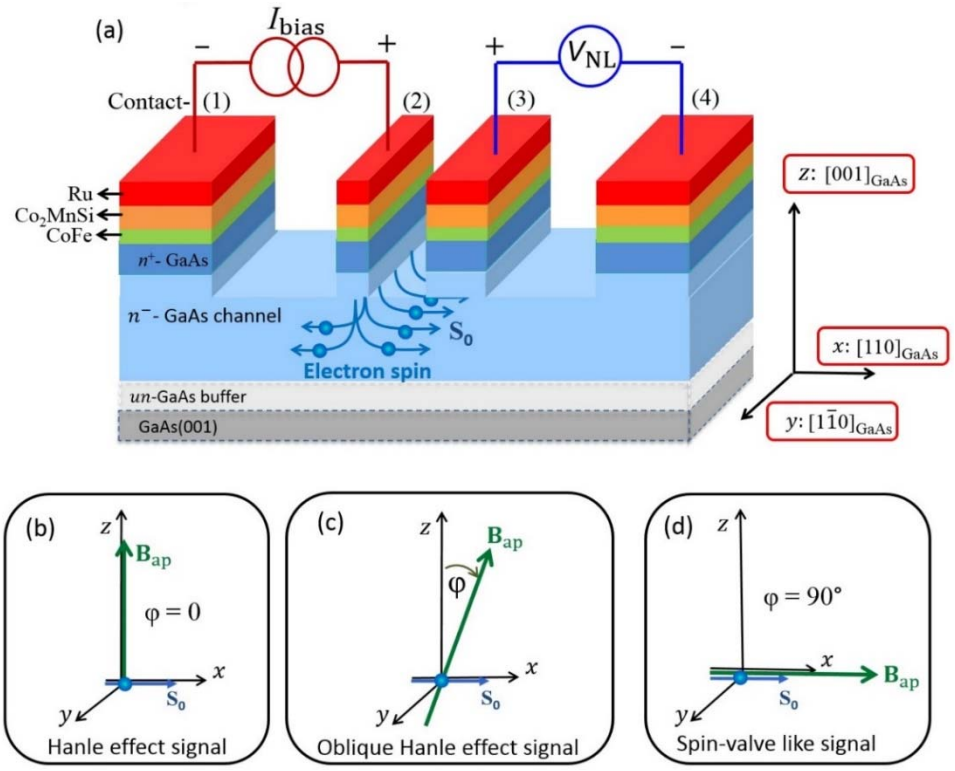

Fig. 3.6: (a) A schematic description of the electrical spin injection along with the nonlocal voltage detection geometry, (b), (c) and (d) the direction of the applied magnetic field $\mathbf{B_{ap}}$ during measurement of the typical Hanle signal, oblique Hanle signal (without and with irradiation by rf-magnetic field), and spin-valve like signal, respectively, with respect to the direction of electron spin polarization $\mathbf{S_0}$.

Simply, in the typical Hanle signal, a fixed bias current $I_{bias} = -40$ μA was supplied, where electron spins were injected from contact-2 into the GaAs. Thereafter, a perpendicular magnetic field was swept from $B_{ap} = +30$ to -30 mT with a sweep rate $r = 0.5$ mT/s. The change in B_{ap} as a function of t can be given

as follows:

$$B_{\mathrm{ap}}(t) = 30 - 0.5t \qquad (0 \le t \le 120) \tag{3.1}$$

For the oblique Hanle signal measurements with and without irradiation by rf-magnetic field, I_{bias} was set to be −70 μA and −60 μA, respectively. The magnetic field $\mathbf{B_{ap}}$ was initially held at B_{ap} = +48 mT for a hold time of t_{hold}, and then it was swept from B_{ap} = +48 to −48 mT at a certain sweep rate (r), which was selected to be faster than the one required to bring the nuclear spins to their equilibrium state. In order to get a complete picture about the transient behaviors of nuclear spins in semiconductors, we systematically changed the initialization-times and the ramp speed of the applied magnetic field. All conditions by which B_{ap} is changed through oblique Hanle signal as a function of t can be given as follows:

$$B_{\mathrm{ap}}(t) = \begin{cases} 48 & (0 \le t \le t_{\mathrm{hold}}) \\ 48 - r(t - t_{\mathrm{hold}}) & (t_{\mathrm{hold}} < t \le t_{\mathrm{hold}} + 96/r) \end{cases} \tag{3.2}$$

where r is a sweep rate and t_{hold} is the initialization time. The conditions f or t_{hold} and r are summarized as follows:

- First, without irradiation by rf-magnetic field:

(a) t_{hold} = 25, 50, 100 and 150 s while fixing the sweep rate r to 0.7 mT/s, &

(b) r = 0.2, 0.35, 0.5 and 0.7 mT/s while fixing t_{hold} at100 s.

- Second, with irradiation by rf-magnetic field:

r was fixed at 0.35 mT/s under application of rf-magnetic field with a frequency of 200 kHz.

For the spin-valve signal measurement, $\mathbf{B}_{\mathrm{ap}}$ was applied exactly along the x axis, parallel to the easy axis direction of magnetization for the Co_2MnSi/CoFe bilayer. This is in order to detect the change of V_{NL} when the magnetization direction of the injector and detector is switched between parallel and antiparallel states. I_{bias} was set −40 μA. We used two different schemes of sweeping B_{ap}.

In the first scheme, similarly to the conventional spin-valve measurement, B_{ap} was swept from 0 to −40 mT; then it was swept back from −40 to +40 mT and finally from +40 mT to zero at a fixed sweep rate r of 0.5 mT/s. So, one can summary the change in B_{ap} as a function of t as follows:

$$B_{ap}(t) = \begin{cases} -0.5t & (0 \le t \le 80) \\ -40 + 0.5(t - 80) & (80 < t \le 240) \\ 40 - 0.5(t - 240) & (240 < t \le 320) \end{cases} \tag{3.3}$$

The second scheme is a special sweep scheme for the change in $\mathbf{B}_{ap}$, in which B_{ap} has been exactly halted at B_{ap}= 0 during the positive sweep, exactly at t = 160 s in order to test the transient response of $\mathbf{B}_n$ at B_{ap} = 0. The corresponding change in B_{ap} as a function of t is given as in following:

$$B_{ap}(t) = \begin{cases} -0.5t & (0 \le t \le 80) \\ -40 + 0.5(t - 80) & (80 < t \le 160) \\ 0 & (160 < t \le 360) \end{cases} \tag{3.4}$$

3.5. Simulation method

First of all, the used equations in establishment of our simulation model are taken from chapter 2. We simulated the oblique Hanle signals and spin-valve signals measured under the above conditions using the time evolution of the nuclear field vector. As we have mentioned that the nuclear-spin system interacts with the electron-spin system through the hyperfine interaction at a polarization rate of $1/T_{1e}$ and also with the lattice at a depolarization rate of $1/T_1$, where T_{1e} and T_1 are the time scale of nuclear spin polarization and depolarization, respectively. T_1 varies with the magnetic field **B** experienced by nuclei, and it is given by (see Eq. 2.29):

$$T_1^{-1} = \eta \tau_1^{-1} \left(\frac{B_L^2}{\mathbf{B}^2} \right). \tag{3.5}$$

where η is a numerical coefficient that depends on the nature of the spin-spin

interactions, and B_{L} is the local dipolar field.

When the direction and strength of **B** changes, the direction of $\mathbf{B_n}$ changes in response quickly because of its adiabatic process, while the strength of $\mathbf{B_n}$ changes slowly on a time scale of $(1/T_{1\mathrm{e}} + 1/T_1)^{-1}$ because of a non-adiabatic process through the interactions with the electron spins or the lattice. Such behavior can be described using a time evolution of the nuclear field $\mathbf{B_n}$ under DNP using the following expressions (see Eq. 2.35 and Eq. 2.36):

$$\begin{aligned} \mathbf{B}_{\mathrm{n}}(t) &= B_{\mathrm{n}}(t)\frac{\mathbf{B}}{|\mathbf{B}|}, \\ \frac{d}{dt}B_{\mathrm{n}}(t) &= -\left(\frac{1}{T_{1e}}+\frac{1}{T_1}\right)\left(B_{\mathrm{n}}(t)-B_{\mathrm{n0}}\right) \end{aligned} \tag{3.6}$$

where B_{n0} is the static solution, which is given by Eq. 2.32 as

$$\mathbf{B}_{n0} = f_L b_n \frac{I(I+1)}{S(S+1)}\frac{\langle \mathbf{S}\rangle \cdot \mathbf{B}}{\mathbf{B}^2+\xi B_{\mathrm{L}}^2}\mathbf{B}\,. \tag{3.7}$$

where f_L (≤ 1) is the leakage factor, ξ is a factor assisting the process, b_{n} is the effective field due to the polarization of all nuclear spins, which takes the negative value of –17 T in GaAs for the theoretical ideal case, and $\langle \mathbf{S} \rangle$ is the average electron spin polarization.

In addition to $\mathbf{B_{ap}}$, we have assumed a constant stray field B_{st} = 1.0 (mT), pointing along the *z*-axis direction as shown schematically in Fig. 3.7(b) and acting as a part of the external magnetic field in our simulation. This field has been intentionally proposed to avoid vanishing the transient nuclear field at B_{ap} = 0. Accordingly, the total external magnetic field **B** can be written as:

$$\mathbf{B} = \mathbf{B_{ap}} + B_{st}\,\mathbf{z} = B_{\mathrm{ap}}(\mathbf{x}\sin\varphi + \mathbf{z}\cos\varphi) + B_{st}\,\mathbf{z} \tag{3.8}$$

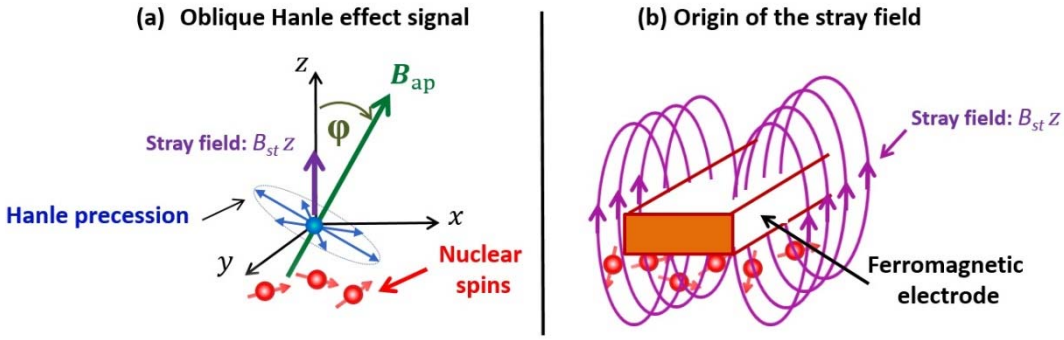

Fig. 3.7: (a) A schematic description of an oblique Hanle signal effect and (b) the influence of the ferromagnetic stray field.

Since electron spins experience $\mathbf{B} + \mathbf{B}_n$, $\langle \mathbf{S} \rangle$ precesses about $\mathbf{B} + \mathbf{B}_n$, whose direction is along $+\mathbf{B}$ or $-\mathbf{B}$, because $\mathbf{B}$ and $\mathbf{B}_n$ are either parallel or antiparallel to each other. This precession changes only the component of $\langle \mathbf{S} \rangle$ perpendicular to $\mathbf{B}$ and conserves the component of $\langle \mathbf{S} \rangle$ parallel to $\mathbf{B}$. Thus, we approximated $\langle \mathbf{S} \rangle \cdot \mathbf{B}$ in Eq. (3.7) by $\mathbf{S_0} \cdot \mathbf{B}$ in our simulation. The precession of the electron spins along the total magnetic field of $\mathbf{B} + \mathbf{B}_n$ results in a change in electron-spin polarization at detector contact-3. As we described in Sec. 2.10, V_{NL} can be given as

$$V_{NL} = \delta \int_0^\infty \frac{1}{\sqrt{4\pi D t}} \exp\left(-\frac{d^2}{4Dt}\right) \cos(\omega_L t) \exp\left(-\frac{t}{\tau_s}\right) dt \,, \qquad (3.9)$$

where δ is a constant, D is the diffusion constant, d is the distance between contact-2 and contact-3, τ_{sf} is the electron spin lifetime, and $\omega_L = g_e \mu_B B_z / \hbar$ is the Larmor frequency, where B_z is the z component of $\mathbf{B} + \mathbf{B}_n$, g_e is an electron g-factor ($g_e = -0.44$ for GaAs), μ_B is the Bohr magneton ($\mu_B = 9.274 \times 10^{-24}$ J/T), and $\hbar$ is the reduced Planck's constant ($\hbar = 1.0546 \times 10^{-34}$ J·s/rad).

The relation between the average nuclear spin for each nuclei species α and the magnetic field **B** can be given by Eq. 2.39, which is rewritten as

$$\langle \mathbf{I}_\alpha \rangle = \frac{(I_\alpha + 1)\mu_{\mathrm{I}\alpha}}{3k_{\mathrm{B}}\theta}\mathbf{B} \tag{3.10}$$

Furthermore, using Eq. 2.40, the reciprocal nuclear spin temperature for each nuclei species α at the steady state can be described using the following expression:

$$\frac{1}{k_{\mathrm{B}}\theta_{\alpha 0}} = f_L \frac{4I_\alpha}{\mu_{\mathrm{I}\alpha}} \frac{\langle \mathbf{S} \rangle \cdot \mathbf{B}}{\mathbf{B}^2 + \xi B_{\mathrm{L}}^2} \tag{3.11}$$

When the nuclear spin system is irradiated by rf-magnetic field, then nuclear magnetic resonance (NMR) might occur if the energy of irradiation by rf-magnetic field is equal to the Zeeman splitting energy of the nuclear spin system. This condition is given as by Eq. 2.38 as:

$$\omega = \gamma_{n\alpha} B_z \tag{3.12}$$

where, $\gamma_{n\alpha}$ is the nuclear gyromagnetic ratio of each nuclei α contained in GaAs and $\omega = 2\pi f$ is the angular frequency of the irradiated rf-magnetic field, where f is the frequency. At the time of resonance; nuclear spins are equally distributed between the energy levels because of the absorbed rf energy, *i.e.* nuclear spin temperature is going to the infinite temperature and hence the average nuclear spins is vanished, see Eq. 310. Hence, in order to include the NMR effect in our simulation, we reset the strength of the nuclear field of each specific nuclei α in GaAs to zero if the resonance condition, Eq. (3.12), would be satisfied.

Using Eqs. (3.5)-(3.9), we simulated the change in V_{NL} as a function of B_{ap} or t. Then using Eq. 3.10, we simulated the effect of the spin temperature. Last, using Eq. 3.12, we introduced the effect of NMR to our simulation model. The parameters used in the simulation are listed in Table 2.1. The values of f_{L} and $T_{1\mathrm{e}}$ were treated as fitting parameters.

Table 3.1. Simulation parameters.

Parameter	Value
$2\lvert\mathbf{S_0}\rvert$	12.8%
l_{sf} (μm)	5
T_{1e} (s)	450
f_{L}	0.023
$\sqrt{\xi}B_{\mathrm{L}}$ (mT)	2.3
d (μm)	0.5
τ_{sf} (ns)	20 ns
b_n of ^{75}As	-3.59 T
b_n of ^{69}Ga	-2.19 T
b_n of ^{71}Ga	-1.99 T
γ_α of ^{75}As	4.581×10^7 rad/T·s
γ_α of ^{69}Ga	6.420×10^7 rad/T·s
γ_α of ^{71}Ga	8.158×10^7 rad/T·s
D (μm)	0.5
f (kHz)	200
I	3/2

Chapter 4

Quantification of the transient behaviors of the dynamically polarized nuclear spins in GaAs

4.1. Introduction

In this chapter, we discuss and analyze the experimental results of the dynamic polarization of nuclear spins due to the hyperfine coupling with spin-polarized electrons (Dynamic nuclear polarization) in an all-electrical lateral spin injection device having Co_2MnSi/CoFe/*n*-GaAs Schottky tunnel junctions.

We start first our discussion by showing a clear evidence of achievement of an electrical spin injection in GaAs (observation of spin valve-like signal and Hanle signal) in Sec. 4.2. Second, in order to visualize the behaviors of the nuclear spins through the process of DNP generally, we describe simply the modulation of Hanle signal due to application of an oblique magnetic field (Oblique Hanle signal) in Sec. 4.3. Thereafter, we discuss about DNP and the overall transient behaviors of nuclear spins in details through the rest of the chapter.

4.2. Spin-valve like signal and Hanle signal

Shown in Fig. 4.1(a) is a schematic representation of a lateral spin transport device with a focus on the injected electron spin **S** in GaAs, (b) experimental result of the measured spin-vale like signal and (c) experimental result of the obtained Hanle signal. A detailed part about measurement methodology can be found in Sec. 3.4. The measurement conditions are summarized shortly on each curve.

As we explained in details in Sec. 2.3.1 and Sec. 2.3.2 about spin-valve like effect and Hanle effect, respectively, we investigate the change in the behaviors of the injected electron spin **S** due to application of an external magnetic field $\mathbf{B}_{ap}$ either parallel (spin-vale like effect signal) or perpendicular (Hanle effect signal) to the direction of electron spin. Such a change in their behaviors results in changing the spin dependent voltage (nonlocal voltage V_{NL}), which we have detected through our measurement and showed the result in

Fig. 4.1(b) for spin-valve like signal and in Fig. 4.1(c) for Hanle signal.

First, regarding to observation of a spin-valve signal in Fig. 4.1(b), the black and blue circles in the figure refer to positive and negative sweeps, respectively. As a normal behavior of the spin-valve signal, we can see clearly that V_{NL} drops to lower values over the magnetic field regions $-29.6 < B_{ap} < -20.7$ and $+29.1 < B_{ap} < +21.9$ mT as well. This behavior can be explained as follows. At first, at state 1 through the negative sweep direction, magnetization directions of FM 2 and FM 3 are parallel (P) to each other, then FM 3 detects the spin dependent voltage associated with the chemical potential of the majority carriers in GaAs, which is given by $V_{(NL)}^{(P)}$ in Eq. 2.10 [52, 63].

Further increasing the magnetic field strength until approaching to $B_{ap} = -19.7$ mT, magnetization configuration is still parallel. Exactly at $B_{ap} = -20.7$ mT, the magnetic field strength comes close to the coercive field of one of the those two electrodes, whatever FM 2 or FM 3, the magnetization direction of such electrode will be reversed. Thus magnetization configurations between two electrodes become antiparallel (AP) to each other, thereby V_{NL} drops to lower values until reaching to $B_{ap} = -29.6$ mT, showing a clear spin valve over the magnetic field region of $-29.6 < B_{ap} < -20.7$ (*see* state 2). Such drop in V_{NL} is due to that reversing the magnetization configurations leads FM 3 to detect a spin dependent voltage associated with the chemical potential of the minority spins in GaAs, which is given by $V_{(NL)}^{(AP)}$ in Eq. 2.10.

At $B_{ap} = -29.6$ mT, the magnetization direction of the second electrode will be also reversed for the same reason. Then, again, at state 3, magnetization configuration changed to P state and thereby V_{NL} returned to its initial value of state 1. A similar situation is happened through the positive sweep direction, we will not repeat our discussion but also the magnetization configurations will be switched between P and AP states over the magnetic field region of $+29.1 < B_{ap} < +21.9$ mT, showing a clear spin valve over there.

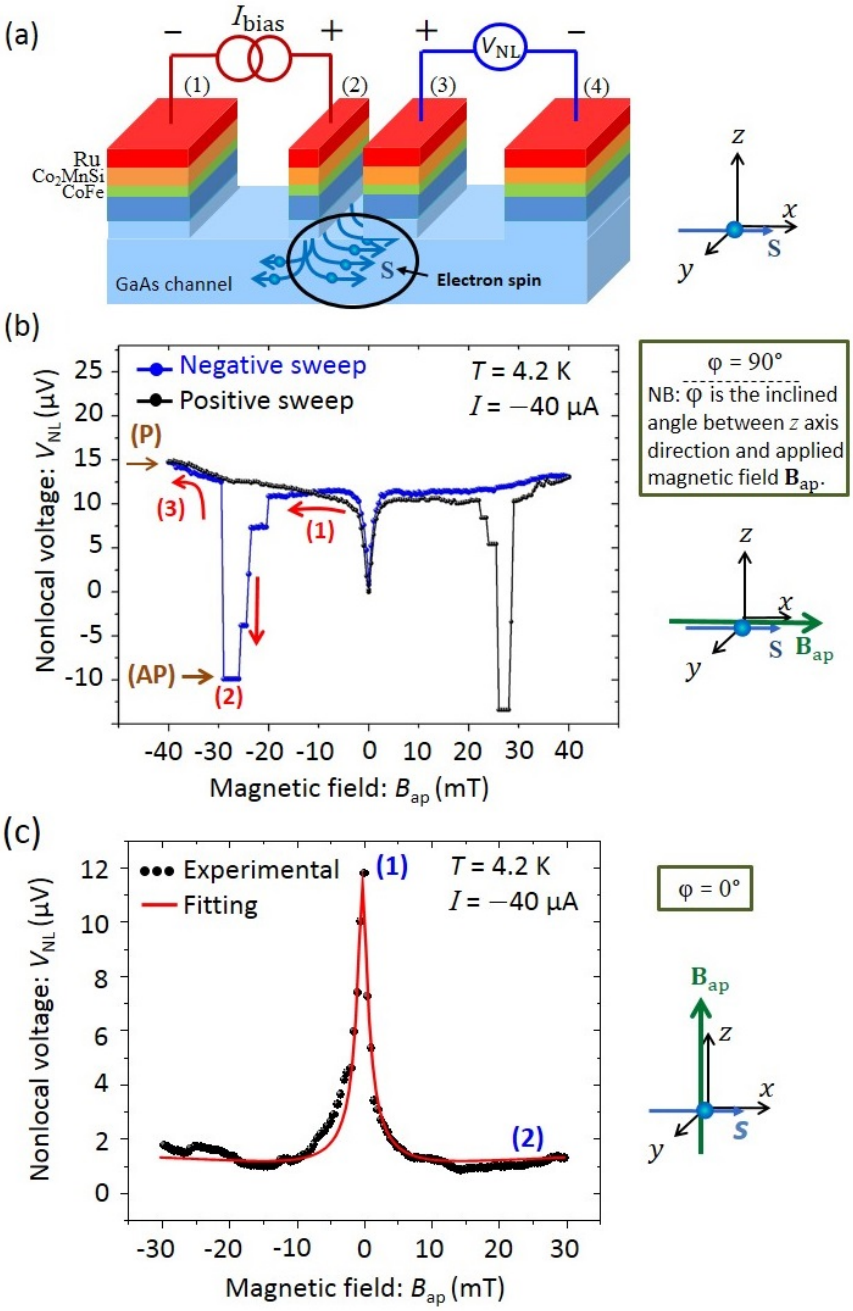

Fig. 4.1: (a) A schematic representation of a lateral spin transport device with a focus on the injected electron spin $\mathbf{S}$ in GaAs channel, (b) an experimental result of spin-vale like signal and (c) an experimental result of Hanle signal for the behaviors of the accumulated electron spin $\mathbf{S}$ in GaAs.

Equally important to shed light here on is that there is a clear dip in V_{NL} at $B_{ap} = 0$. This dip is a nuclear spin related phenomenon [7] and we will give a full explanation about it later in Sec. 4.8.

Second, regarding to observation of a Hanle signal in Fig. 4.1(c), we can see clearly that V_{NL} gives a maximum value at $B_{ap} = 0$ then decreases as the magnetic field strength increase in both sides, positive or negative directions. This behavior can be explained as follows. At first, FM 3 detect the maximum value of V_{NL} arising from the accumulated spins at FM/GaAs interface in the absence of applied field ($B_{ap} = 0$). At this moment, spins seem as they are just transported into GaAs from FM 2, and because of $B_{ap} = 0$ no spin precession or dephase. Thereafter, by increasing the strength of B_{ap} either through the positive side or the negative side, then the accumulated spins start to precess, dephase and completely relax at high magnetic field regions. Correspondingly, V_{NL} gradually decreases and shows its minimum values at high field regions ($\rightarrow B_{ap} = \pm 30$ mT).

All in all, observation of those two signals, spin-valve like signal and Hanle signal, is a clear evidence that spin-polarized electrons are successfully injected into GaAs channel and there is an efficient number of accumulated spins at the interface of FM/GaAs.

By successful fitting of the experimental result of the obtained Hanle signal curve, *see* red curve in Fig. 4.1(c), using Eq. (2.15), we have found that the spin polarization of $P_{inj}(P_{det})$ is 4.4% and the spin lifetime τ_{sf} is in a time scale of 50 ns. Such estimated time scale is comparable to such obtained for GaAs with a doping concentration of 10^{16} cm^{-3} [61]. This means that spin-polarized electrons were injected into the inner deep of GaAs channel and spin-polarized electronic states are extended to the limit of the spin diffusion length $l_{sf} \approx 5$ µm into our device.

4.3. Oblique Hanle effect signal

Last section showed that we have created spin-polarized electronic states in GaAs using electrical spin injection technique. In this section, we will give an evidence for polarization of nuclear spins in GaAs by figuring out their influence on the spin-polarized spins in GaAs through oblique Hanle signal.

To keep the flow of our discussion, we will shortly describe an experimental methodology of measuring an oblique Hanle effect signal. We have applied B_{ap} along a direction making an angle $\approx 8°$ from the z axis in the x-z plane, where the spin polarization in our device is along x direction (see Fig. 4.2(a)). The device was firstly initialized by fixing the strength of $B_{ap} = +48$ mT for a hold time (t_{hold}) of 100 s at an injection current of −70 μA, meaning that electron spins are injected from ferromagnetic contact into the semiconductor and thereby nuclear spins are dynamically polarized. The magnetic field was then swept from +48 to −48 mT, with a sweep rate of 0.35 mT/s.

As we discussed in details about the dynamic nuclear polarization in Sec. 2.8 and detection of the nuclear field in Sec. 2.10, nuclear spin **I** can be effectively polarized due to exchange angular momentum with the electron spin **S** through the hyperfine interaction, dynamic nuclear polarization (DNP). Consequences of that nuclear spins affect back on the electron spin by a nuclear field $\mathbf{B}_n$. This field is able to change the Larmor precession of the electron spin under an oblique magnetic field and thereby changing the corresponding nonlocal voltage (see Eq. 3.9). So, before going to the experimental results, let's have some knowledge about the effect of such nuclear field on the Hanle signal in the steady state circumstances.

Figure 4.2 (a) shows a typical lateral spin transport device with a focus on the injected electron spin **S** interaction with nuclear spin **I** in semiconductor and (b) a simulated V_{NL} as a function of B_{ap}, which is simply given by substituting the static nuclear field solution of Eq. 3.7 into Eq. 3.9. This curve can be

understood as follows. We consider that the easy axis direction of magnetization is along *x* direction, then the direction of the injected electron spin **S** will be along *x* direction.

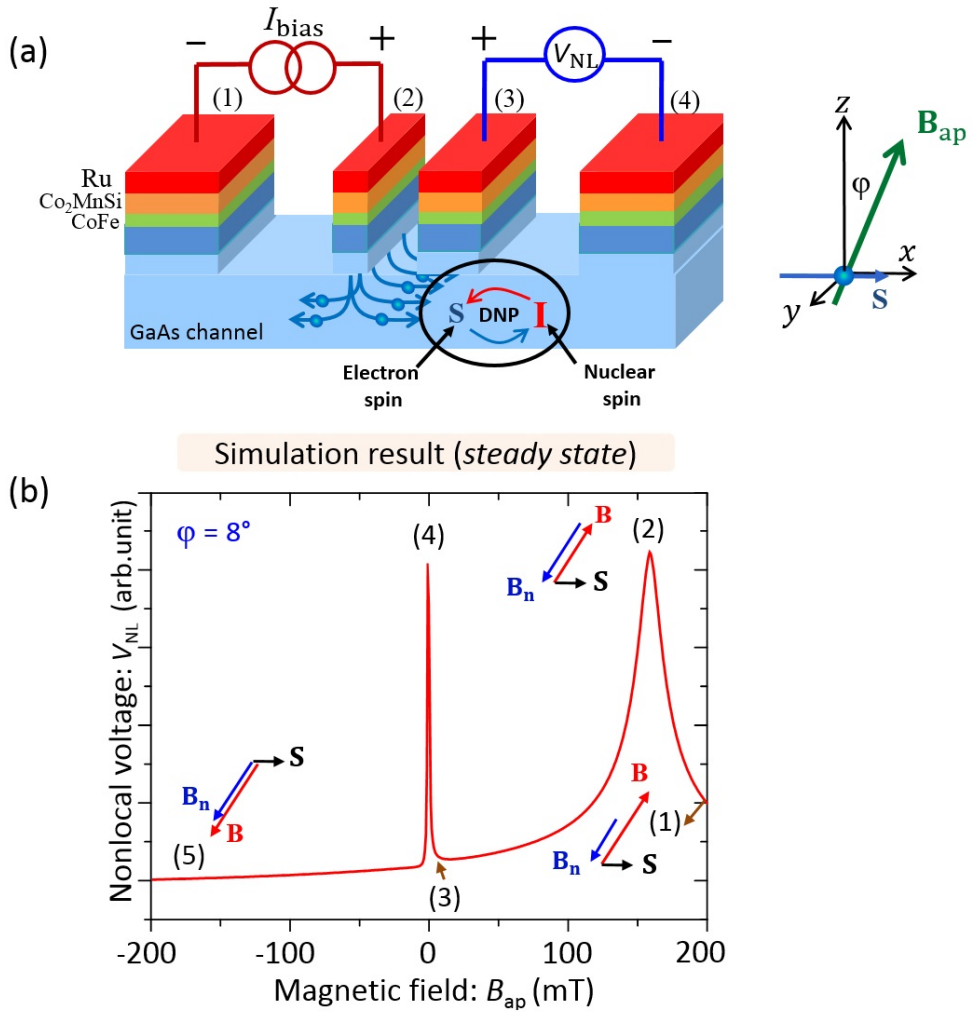

Fig. 4.2: (a) A typical lateral spin transport device with a focus on the injected electron spin **S** interaction with nuclear spin **I** in the semiconductor GaAs channel and (b) a simulation result of steady state oblique Hanle signal.

Under an oblique magnetic field making an angle φ with *z* axis and a continued injection of electron spin **S** (DNP) into semiconductor, then a nuclear

field $\mathbf{B_n}$ is generated. Hence, the electron spin **S** experiences a resultant magnetic field of $\mathbf{B}_{ap} + \mathbf{B_n}$ about which they will make a precessional motion. Of a particular interest in using GaAs as a semiconductor channel, then the direction of such resultant field vector is along + $\mathbf{B}_{ap}$ or – $\mathbf{B}_{ap}$, because $\mathbf{B}_{ap}$ and $\mathbf{B_n}$ are either antiparallel, (if $\mathbf{S}\cdot\mathbf{B}_{ap} > 0$), or parallel, (if $\mathbf{S}\cdot\mathbf{B}_{ap} < 0$), to each other (*see* Eq. 3.7 and notice that b_N is a negative value in GaAs). Thus, the level change in V_{NL} shown in Fig. 4.2(b) can be explained as follows.

At $B_{ap} > 0$, starting with *state*-1, $\mathbf{S}\cdot\mathbf{B}_{ap} > 0$, then $\mathbf{B}_n$ will be generated antiparallel to $\mathbf{B}_{ap}$, and so **S** experiences a smaller effective magnetic field than $|\mathbf{B}_{ap}|$. When $\mathbf{B}_n$ and $\mathbf{B}_{ap}$ cancel each other, precession of **S** about $\mathbf{B}_{ap} + \mathbf{B}_n$ is suppressed and the level of V_{NL} shows a maximum value (see the observed side peak at *state*-2). Afterwards, the strength of $\mathbf{B}_{ap}$ and $\mathbf{B}_n$ are gradually decreased but by different rate. So, **S** experiences $|\mathbf{B}_{ap} + \mathbf{B}_n| \neq 0$ until reaching state-3. Exactly at state-4, the magnitude of $\mathbf{B}_{ap} + \mathbf{B}_n$ become equal to zero because of $B_{ap} = 0$ and the nuclear magnetization is lost, *i.e.* $B_n = 0$, then electron spin precession is suppressed and a central peak, equivalent to the conventional Hanle peak, is observed at state-4. Afterward, by reversing the direction of $\mathbf{B}_{ap}$, $\mathbf{B}_n$ and $\mathbf{B}_{ap}$ become parallel to each other because of $\mathbf{S}\cdot\mathbf{B}_{ap} < 0$, then no cancelation occurs through over all $B_{ap} < 0$, see state-5.

Now, it is the time to discuss about the experimental result of the measured oblique Hanle signal. Figure 4.3 shows an experimental result of the measured oblique Hanle signal. Based on this result, two important and clear observation can be extracted as follows.

● By comparing with the typical Hanle curve, two extra side peaks of V_{NL} through the obtained oblique Hanle signal curve have been observed. Exactly speaking, one side peak has been observed at the right-hand side (centered at B_{ap} = 36.5 mT) and another one has been observed at left-hand side (centered at B_{ap} = −14 mT) of the typical Hanle peak occurring at $B_{ap} = 0$. Such modulation on

the shape of Hanle curve is a strong evidence of the hyperfine coupling interaction between electron **S** and nuclear spin **I**, which results in DNP and generation of $\mathbf{B}_n$.

● By comparing with the steady state oblique Hanle signal shown in Fig. 4.2(b), however, the peak occurring at $B_{ap} < 0$ on the level change in V_{NL} of the obtained oblique Hanle signal curve is different and not appeared on the steady state oblique Hanle signal. Up to current stage, this peak is considered to be due to transient polarization or transient behaviors of nuclear spins in semiconductors. As a consequence, we are unable to explain the obtained result in terms of the steady state solution or steady state model. Motivated by this, we have developed a special simulation model based on the time evolution of the nuclear field, see Sec. 3.5. In the next section, we will show and discuss the results of the transient behaviors of nuclear spins in semiconductors on the basis of the simulation results.

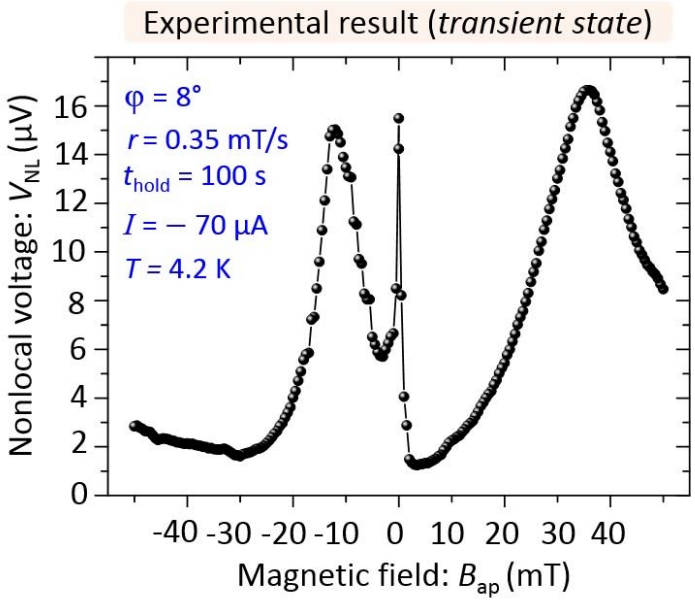

Fig. 4.3: Experimental result of the transient state oblique Hanle signal.

4.4. Quantification of transient behaviors of the dynamically polarized nuclear spins

Herein, we quantify the transient behaviors of the dynamically spin-polarized nuclear spins in semiconductors by analyzing oblique Hanle effect signal.

Shortly, let's recall the experimental curve of oblique Hanle signal, shown in Fig. 4.3 (b). Observation of a side peak at $B_{ap} > 0$ is due to presence of a nuclear field antiparallel to the applied field. This nuclear field is able to cancel the effect of applied field at $B_{ap} > 0$ (electron spin precession), showing a clear side peak. However, existence of a side peak at $B_{ap} < 0$ can't be explained by the same reason. Because the nuclear field would be parallel to the applied field after reversing the direction of applied field, then cancelation is not expected in terms

of steady state nuclear spin polarization. So, as we mentioned in Sec. 4.3, such behavior of nuclear spins is called the *transient behavior* of nuclear spins under DNP.

As we discussed in Sec. 2.8, the nuclear-spin system interacts with the electron-spin system through the hyperfine interaction at a polarization rate of $1/T_{1e}$ and also with the lattice at a depolarization rate of $1/T_1$, where T_{1e} and T_1 are polarization and spin-lattice relaxation time scales. Therefore, sweeping the external magnetic field on a time scale faster than T_{1e} and/or T_1 causes the nuclear spins to be transiently polarized. Such transient polarization can be understood phenomenologically by the balance between the rate of polarization and rate of relaxation which is derived by the solution of the time evolution of nuclear field vector, see Eq. 3.6. Based on this equation, we have simulated the experimental result of the oblique Hanle signal under the transient state circumstances (Hereafter, we call it as the transient state oblique Hanle signal), pre-introduced in Sec. 4.3.

Figure 4.4 shows first a comparison between (a) experimental results of transient state oblique Hanle signal with (b) simulation result. The important simulation parameters are shortly summarized on the curve and more details can be reviewed in Sec. 3.5. We can clearly see that simulation result reproduced the experimental result so precisely, which validates the developed simulation model. On the basis of the simulation results, we have constructed a vector diagram of the relative orientation of the injected electron spin $\mathbf{S_0}$, magnetic field $\mathbf{B}$, and nuclear field $\mathbf{B_n}$, along with the analysis of an oblique Hanle signal, as depicted in Fig. 4.4(c). In the following, we will quantitatively analyze the transient behaviors of nuclear spins using this vector diagram.

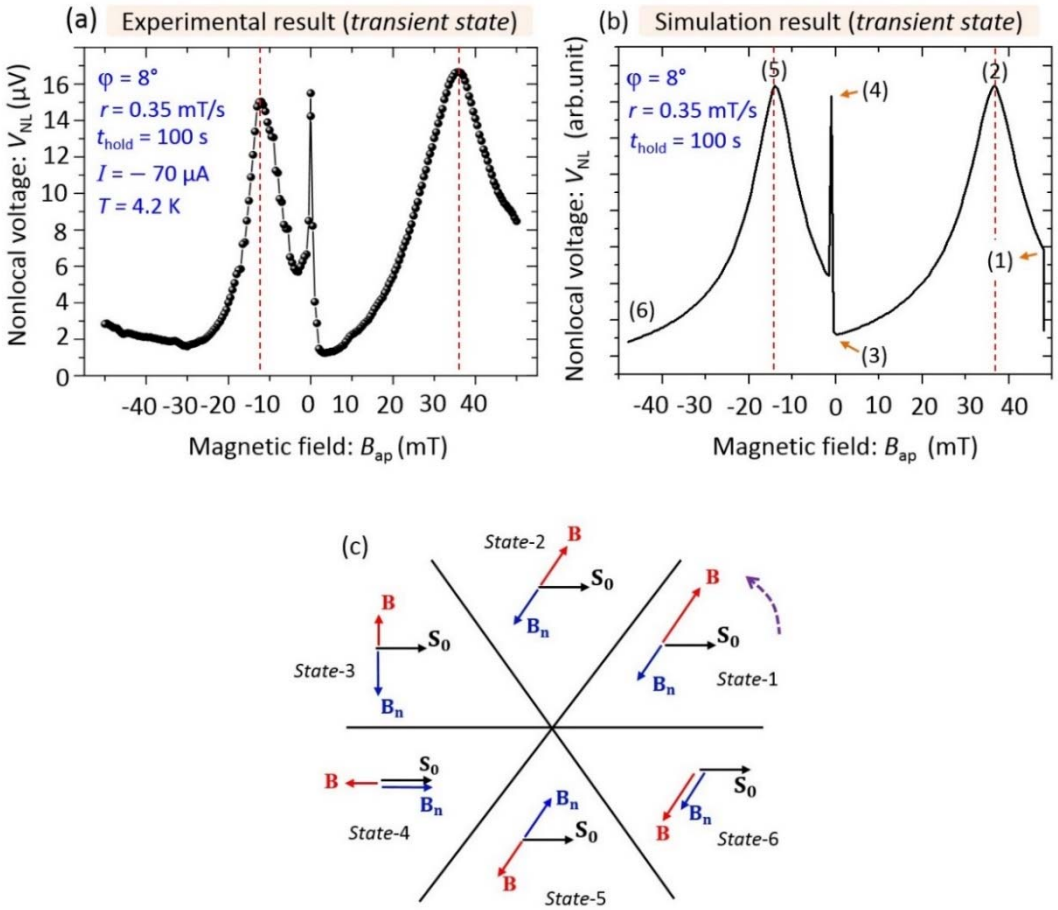

Fig. 4. 4: (a) An experimental result of transient state oblique Hanle signal, (b) the corresponding simulation result of transient state oblique Hanle signal and (c) a corresponding schematic vector diagram for the relative orientation of the injected electron spin $\mathbf{S_0}$, magnetic field $\mathbf{B}$ and nuclear field $\mathbf{B_n}$.

● At first, one has to remember that a constant stray field (B_{st} = 1.0 mT) has been proposed to be pointed along z-axis direction in order to avoid vanishing the transient nuclear field at $B_{ap} = 0$, *see* Eq. 3.8. Accordingly, the total external magnetic field $\mathbf{B}$ is given by

$$\mathbf{B} = \mathbf{B_{ap}} + B_{st}\,\mathbf{z} = B_{ap}(\mathbf{x}\sin\varphi + \mathbf{z}\cos\varphi) + B_{st}\,\mathbf{z}, \qquad (4.1)$$

and the electron spin **S** experiences a resultant magnetic field of $\mathbf{B} + \mathbf{B_n}$ about which they will make a precessional motion. The direction of such resultant field vector is along +**B** or –**B**, because **B** and $\mathbf{B_n}$ are either parallel or antiparallel to each other (*see* Eq. 3.7 and notice that b_N is a negative value in GaAs). This precession changes only the component of average electron spins $\langle \mathbf{S} \rangle$ perpendicular to **B** and conserves the component of $\langle \mathbf{S} \rangle$ parallel to **B**. Thus, we approximated $\langle \mathbf{S} \rangle \cdot \mathbf{B}$ in Eq. 3.7 by $\mathbf{S_0} \cdot \mathbf{B}$ in our simulation, where $\mathbf{S_0}$ is average electron spins at the injection point, injector contact FM 2.

● Second, we divided the oblique Hanle curve into main six regions or correspondingly states as shown in Fig. 4.4(b) and illustrated in Fig. 4.4(c). In the following, we will describe each state in detail.

In *state*-1, where $\mathbf{B_{ap}}$ was constant at B_{ap} = +48 mT for $0 \leq t \leq t_{hold}$, the nuclear spins were dynamically polarized through the hyperfine interaction with the spin-polarized electrons, maintained with the electrical spin injection at a fixed bias current during all the time of the experiment. Since b_n is negative in GaAs and $\mathbf{B} \cdot \mathbf{S}_0 > 0$, $\mathbf{B}_n$ was generated antiparallel to **B** with the strength of $\mathbf{B}_n$ smaller than that of **B**. Although the strength of the total magnetic field ($\mathbf{B} + \mathbf{B_n}$) experienced by the electron spins was smaller than that of **B**, it was still large enough to induce a strong electron spin precession, resulting in a relatively low V_{NL}.

Thereafter, during the sweeping process, $\mathbf{B_{ap}}$ was ramped down from B_{ap} = 48 mT to 0 at a sweep rate r of 0.7 mT/s. This sweep rate was almost 280-times faster than that for the steady-state circumstances in Ref. [6], in which r was on the order of 0.0025 mT/s for the nuclear spins to reach the equilibrium state. Since the time scale for the change in the B_n, which is given by Eq. 3.6 as $(1/T_{1e} + 1/T_1)^{-1}$, was much slower than that of the change in $|\mathbf{B}|$, the effective magnetic field $\mathbf{B} + \mathbf{B_n}$ decreased in strength as the sweeping process of **B** was started. Consequently, V_{NL} increased until it reached to a peak at B_{ap} = 35 mT [*state*-2].

At *state*-2, $\mathbf{B_n}$ and $\mathbf{B}$ completely canceled each other. This means that $\mathbf{B} + \mathbf{B_n} = \mathbf{0}$ and electron-spin precession is suppressed.

From *state*-2 to *state*-3 the strength of $\mathbf{B_n}$ was decreasing until it became a negligible value at $B_{ap} = 0$. Just passing *state*-3, it increased in the negative direction. Across the effective stray field of $B_{st}\mathbf{z}$ at $B_{ap} = 0$, $\mathbf{B}$ reversed direction by rotation in the *z*-*x* plane from *state*-2 to *state*-5 through *state*-3 and *state*-4. When $\mathbf{B}$ changed its direction and strength, the direction of $\mathbf{B_n}$ changed in response quickly because of its adiabatic process, or to conserve the Zeeman energy of the total spin system, while the strength of $\mathbf{B_n}$ changed slowly by a time scale of $(1/T_{1e} + 1/T_1)^{-1}$. Thus, in response to the rotation of $\mathbf{B}$, $\mathbf{B_n}$ also rotated, keeping an antiparallel alignment with $\mathbf{B}$ until reaching *state*-5, showing a clear side peak at $B_{ap} < 0$. As we have mentioned above, this peak can't be explained or observed in terms of the steady-state nuclear spin polarization (slow sweep of the applied magnetic field). Moreover, one has to notice also that $\mathbf{B_n}$ pointed perpendicular to $\mathbf{S_0}$ exactly at state-3 due to existence of $B_{st}\mathbf{z}$, leading to the electron spins experiencing a strong electron-spin precession, and V_{NL} took on a local minimum value.

In *state*-4, $\mathbf{B}$ and $\mathbf{B}_n$ were parallel or antiparallel to $\mathbf{S_0}$. Thus, no Hanle precession occurred, allowing V_{NL} to reach a maximum value or showing a central peak. As B_{ap} decreased (*i.e.*, increases in the negative side), $\mathbf{B}$ and $\mathbf{B_n}$ canceled again in *state*-5, resulting in a side peak of V_{NL} exactly at $B_{ap} = -15$ mT.

Finally, in *state*-6, since sufficient time for the nuclear spins to be negatively polarized had passed, $\mathbf{B}_n$ turned parallel to $\mathbf{B}$, and electron spins experienced a strong magnetic field. After *state*-3, $\mathbf{S_0} \cdot \mathbf{B}$ turned negative, and the steady-state solution of the nuclear field $\mathbf{B_{n0}}$ was parallel to $\mathbf{B}$ (*see* Eq. 4.1). Nevertheless, $\mathbf{B_n}$ and $\mathbf{B}$ remained antiparallel until *state*-5 because the time constant given by $(T_{1e}^{-1} + T_1^{-1})^{-1}$ was approximately 72 s or more, i.e., more than four-times longer than the time taken for $\mathbf{B}$ to change from *state*-3 to *state*-5.

4.5. Analysis of transient behaviors of nuclear spins using the concept of the spin temperature

To get a deeper understanding about the nuclear spin dynamics in semiconductors, we investigate how the nuclear spins behaves as a function of time during the process of dynamic nuclear polarization. To do so, we introduced the concept of spin temperature to analyze the level change in the nonlocal voltage of oblique Hanle signal, which give a direct feedback about the change of nuclear field vector $\mathbf{B}_n$ during DNP.

First of all, there is an important issue to remember before going into deep discussion. We know from Eqs. 2.32, 2.39 and 2.40 that if nuclear spin temperature θ is positive (negative) then the average nuclear spin $\langle \mathbf{I} \rangle$ is parallel (antiparallel) to $\mathbf{B}$, while $\mathbf{B}_n$ is antiparallel (parallel) to $\mathbf{B}$ due to that b_n is negative in GaAs. This means that the lower (upper) level of energy states is populated more spins than the upper (lower) level, *i.e.* a condition that $\mathbf{B}$ and $\mathbf{B}_n$ cancel each other exists only for $\theta > 0$. Figure 4.5 shows the simulation results of time evolution of (a) nonlocal voltage V_{NL}, (b) nuclear spin temperature θ and (c) nuclear field as $-B_n(t)$ along with $B_{ap}(t)$, where $B_n(t)$ is a projection of $\mathbf{B}_n(t)$ on $\mathbf{B}$, and $B_{ap}(t)$ is a projection of $\mathbf{B}_{ap}(t)$ on unit vector $\mathbf{u}$=(sinφ, 0, cosφ), *i.e.* $\mathbf{B}_n(t) = B_n(t)\mathbf{B}/|\mathbf{B}|$, and $\mathbf{B}_{ap}(t) = B_{ap}(t)\mathbf{u}$. Thus, positive (negative) $B_n(t)$ indicates that $\mathbf{B}_n$ is generated parallel (antiparallel) to $\mathbf{B}$, whereas positive (negative) $B_{ap}(t)$ indicates that $\mathbf{B}_{ap}$ is along $+(-)$ $\mathbf{u}$ direction.

Let's start from $t = 0$ s to 100 s (initialization time of the nuclear spin system $\approx t_{hold}$). The inclined angle between the direction of $\mathbf{B}$ and the direction of spin polarization $\mathbf{S_0}$ in GaAs is smaller than 90°, *i.e.* $\mathbf{B}\cdot\mathbf{S_0} > 0$ and so θ is cooled down or nuclear spins undergo a positive cooling. The nuclear spins are gradually polarized and a nuclear field $\mathbf{B_n}$ is generated antiparallel to $\mathbf{B}$ with a strength increasing also gradually with time. Correspondingly, the electron spin

precession about **B** will be gradually decreased, resulting in increasing the level change of the nonlocal voltage V_{NL} [*see state*-1 in Fig. 4.5 representing to (a) the increasing in V_{NL}, (b) cooling effect of the nuclear spin system and (d) the corresponding increase in B_n with time].

Thereafter, during the sweeping process, exactly at t = 149 s, $\mathbf{B}_n$ and **B** became equal in magnitude and antiparallel to each other, *i.e.* B_{ap} = +32 and B_n = − 32. They will cancel each other out and the electron spin precession is suppressed, giving rise to an obvious increasing in the level change in V_{NL} at B_{ap} > 0 [*see state*-2 in Fig. 4.5 (a), (b) and (c)].

Basically, if the applied magnetic field **B** is reversed towards the negative field values, then θ should show negative values because of $\mathbf{B}\cdot\mathbf{S_0} < 0$. This is translated to that **B** and $\mathbf{B_n}$ should be parallel and no cancellation could occur. However, there is a clear peak appeared also over the negative B_{ap}, exactly at B_{ap} = −6 mT, indicating a possible cancellation between **B** and $\mathbf{B}_n$. According to our model, **B** has changed with a sweep rate (r = 0.35 mT/s) faster than that required to bring the nuclear spins to the equilibrium (r = 0.0025 mT/s) as explained in details in Sec. 4.4. Since the time scale for the change in the B_n, which is given by $(1/T_{1e} + 1/T_1)^{-1}$, is slower than that of the change in $|\mathbf{B}|$, the nuclear field is kept as a non-zero value even at B_{ap} = 0 (at t = 273 s) and even after reversing the direction of **B** towards the negative side; B_n is stayed as a non-zero value until t = 315 s, as shown in Fig. 4.5 (c) . Correspondingly, θ is kept positive even after reversing the direction of **B**.

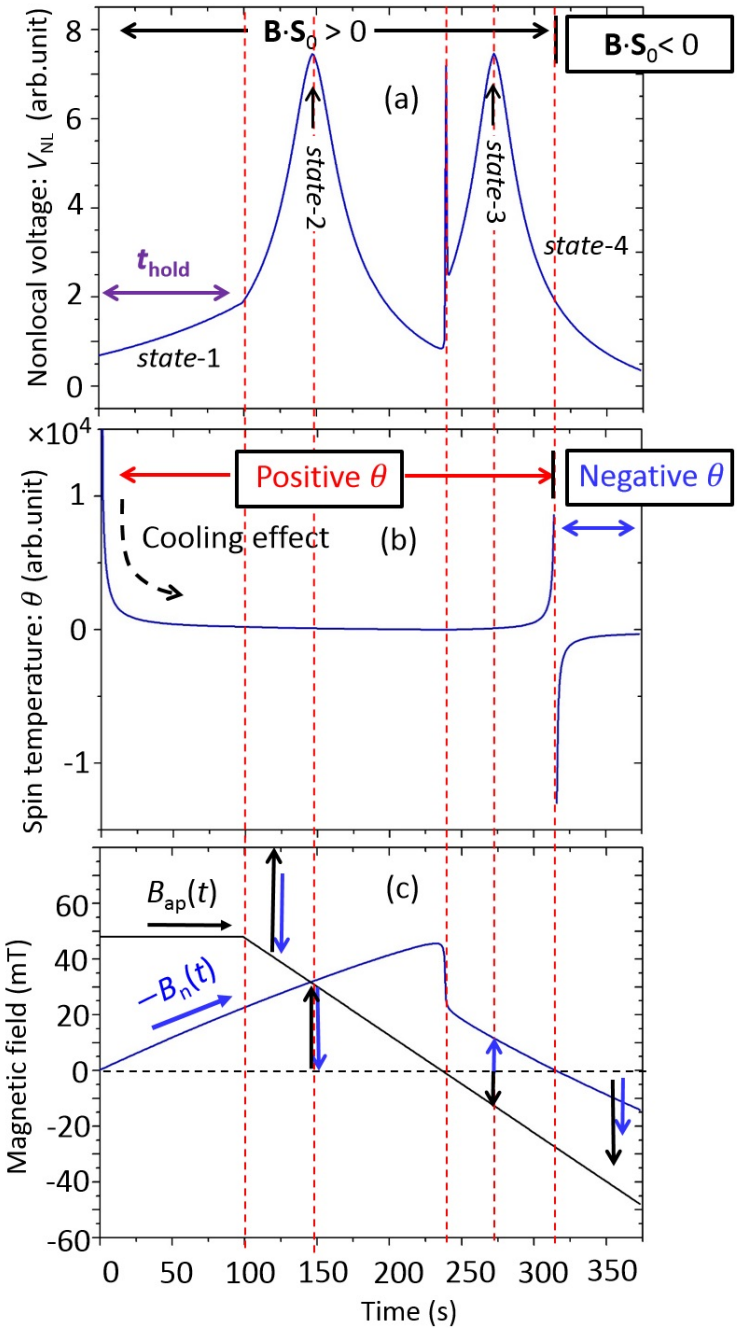

Fig. 4.5: Simulation results of the change in (a) nonlocal voltage V_{NL}, (b) spin temperature θ and (c) transient nuclear field B_{n} along with a magnetic field B_{ap} of an oblique Hanle signal without irradiation by rf-magnetic field.

Exactly speaking, after **B** was reversed, the nuclear spin system changed their spin direction to keep the Zeeman energy in the lower energy state for the negative B_{ap} as for the positive B_{ap}. As a consequence, $\mathbf{B}_n$ is generated antiparallel to **B**. Then, the cancellation condition could be satisfied at $\mathbf{B}\cdot\mathbf{S_0} < 0$. This means that the electron spin precession will be suppressed, giving rise V_{NL} to reach a maximum value or showing a clear side peak at $B = -6$ mT [*see state*-3 in Fig. 4.5 (a), (b) and (c)].

After a sufficient time for the strength of transient B_n is reached to 0, exactly at $t = 315$ s, θ is turned to negative values. Therefore, DNP would result in generating $\mathbf{B_n}$ along a direction parallel to **B** because of $\mathbf{B}\cdot\mathbf{S_0} < 0$, resulting in enhancing the electron spin precession about $\mathbf{B} + \mathbf{B}_n$ and so lowering the level change in V_{NL} [*see state*-4 in Fig. 4.5 (a), (b) & (c)].

4.6. Initialization-time dependence of nuclear spin polarization

According to our analysis in Sec. 4.4 & Sec. 4.5, the resulting nuclear field depends on the vector sum of the fields due to polarization of electron spins in GaAs by maintaining the electrical spin injection continuously running on. So the process of dynamic nuclear polarization is not immediate, which becomes clear by changing the initialization time (t_{hold}) for instance. Such experiment, changing initialization time, is helpful to determine the exact time of DNP and estimate the strength of $\mathbf{B_n}$.

Figure 4.6 shows (a) measured oblique Hanle signals for t_{hold} ranging from 25 to 150 s at a sweep rate of $r = 0.7$ mT/s and (b) the corresponding simulation results. Each single curve represents the changes in V_{NL} while sweeping the magnetic field from $B_{ap} = +48$ to -48 mT. All oblique Hanle curves have three main peaks that appear regardless of the change in t_{hold}, and the side peaks for both the positive and negative B_{ap} region shift to a higher magnetic field as t_{hold} increases.

We can see clearly that the simulation results are well-reproduced all experimental results at different t_{hold}, which confirms the validity of the developed simulation model. On the basis of the simulation results, we have confirmed that the time scale of the dynamic nuclear polarization $T_{1\mathrm{e}}$ is almost 450 s, which is a reasonable one for the dynamic nuclear polarization in a GaAs channel [4, 5, 9]. Second, through the experimental or simulation results, the position of the satellite peak at $B_{\mathrm{ap}} > 0$ shifts to higher strength of **B**. This behavior is reasonable and can be explained as follows. As mentioned in Sec. 4.4, V_{NL} gives the degree of electron-spin precession, and it becomes larger as B_z becomes smaller. Since **B** and $\mathbf{B_n}$ can cancel each other, *i.e.*, $\mathbf{B} + \mathbf{B_n} = \mathbf{0}$, at the side-peak position of V_{NL}. This means that the $|B_{\mathrm{ap}}|$ at the side-peak position gives the strength of $\mathbf{B_n}$, and the results of Figs. 4.6(a) and 4.6(b) suggest that the generated $\mathbf{B_n}$ increases as t_{hold} increases. This can be understood from the analytical solution of Eq. 3.6, when $0 \le t \le t_{\mathrm{hold}}$ or exactly during the stage over which $|\mathbf{B}|$ is constant, which is given as

$$B_{\mathrm{n}}(t_{hold}) = B_{\mathrm{n0}}\left\{1-\exp\left[-t_{hold}\left(\frac{1}{T_{1\mathrm{e}}}+\frac{1}{T_{1}}\right)\right]\right\}. \tag{4.2}$$

According to such equation, (Eq. 4.2), the strength of $\mathbf{B_n}$ increases exponentially as t_{hold} increases and therefore the position of the satellite peak at $B_{\mathrm{ap}} > 0$ is shifted to higher strength of **B**.

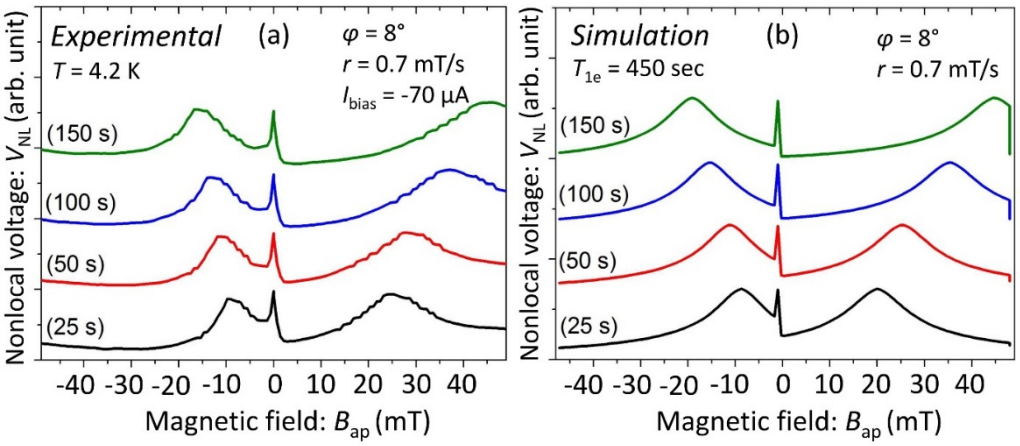

Fig. 4.6: (a) Experimental initialization-time (t_{hold}) dependence of oblique Hanle signals for t_{hold} ranging from 25 to 150 s at a sweep rate of $r = 0.7$ mT/s and (b) corresponding simulation result. Each single curve shows the change in V_{NL} while sweeping the magnetic field from $B_{ap} = +48$ to -48 mT.

Following Sec. 4.4, we have proved that the two side-peaks appearing on the oblique Hanle signal are nuclear-spin-related phenomena in origin, exactly the electron spin precession suppressing owing to $\mathbf{B}_n$ canceling the effect of $\mathbf{B}$ (*state*s-1 and 5). Hence, increasing t_{hold} leads to an exponential increase in B_n, and the magnitude of $\mathbf{B}_{ap}$ required to cancel $\mathbf{B}_n$ also increases. Thus, the cancelation condition or peak point shifts to higher B_{ap}. The shift in the peak on the negative side to a larger $|B_{ap}|$ as t_{hold} increases can be explained similarly. Furthermore, the central peak in *state*-4 does not shift even when changing t_{hold}. As we explained in Sec. 4.4, the central peak in *state*-4 originates from the suppression of electron spin precession due to $\mathbf{B} + \mathbf{B_n}$ being parallel to $\mathbf{S_0}$. This contrasts with the origin of the side peaks, which is the cancelation of $\mathbf{B}$ and $\mathbf{B_n}$. Therefore, in *state*-4, the position of the peak is independent of the initialization process.

4.7. Sweep-rate dependence of nuclear spin polarization

Motivated by the analysis of the initialization-time dependence of nuclear spin polarization in the last section, one expects that changing the ramp speed of the applied magnetic field is also a dominant factor on the process of the dynamic nuclear polarization.

In this section, we study the influence of increasing or decreasing the sweep rare of the magnetic field on the transient behaviors of nuclear spins. This experiment has been attempted to clarify the difference between the transient behavior and the static one for $\mathbf{B}_n$.

Figure 4.7 shows (a) an experimental result of the sweep-rate dependence of oblique Hanle signals and (b) the corresponding simulation result. Each single curve shows a change in V_{NL} when the magnetic field was swept from B_{ap} = +48 to −48 mT at a rate r = 0.2, 0.35, 0.5 and 0.7 mT/s while fixing t_{hold} to 100 s in both the experiment and simulation. Again, we can see clearly that the simulation results are well-reproduced all experimental results at different sweep rates, which provides a further confirmation of the validity of the developed simulation model.

Here, V_{NL} has three main peaks regardless of the change in r. The position of the positive side peaks shifted to higher B_{ap} as the sweep became slower, except for the experimental one with r = 0.7 mT/s. On the other hand, the negative side peaks shifted to smaller $|B_{ap}|$ as the sweep became slower. The position of the central peaks did not change.

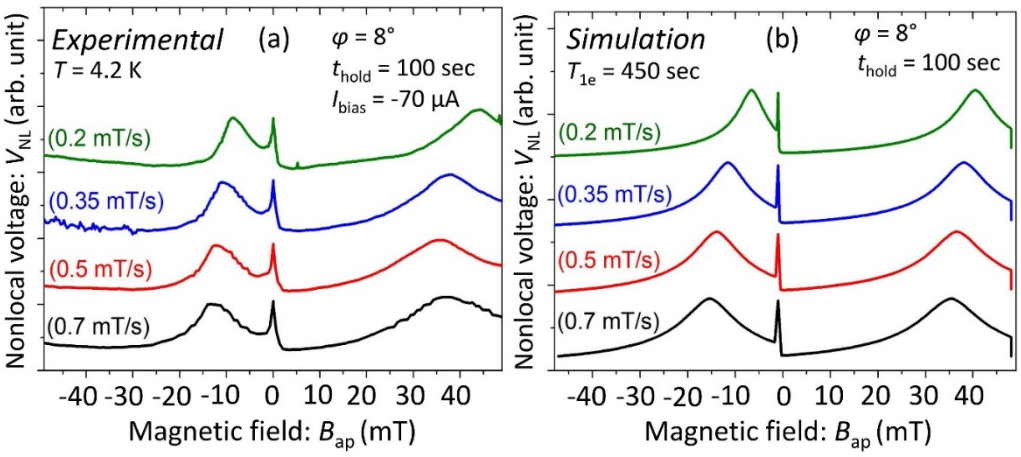

Fig. 4.7: (a) Experimental results of sweep rate (r) dependence of oblique Hanle signals for r ranging from 0.7 to 0.2 mT/s for t_{hold} = 100 s and (b) corresponding simulation result.

The r dependence of the positive side peaks can be understood from the fact that the strength of the generated nuclear field increased as r decreased, as explained in Sec. 4.6. Moving to the r-dependence of the negative side peaks, on the other hand, it is originated mainly from the difference between the transient state and steady state. As r has ramped so slowly such that the solution of Eq. 3.6 is converged to the steady-state one, $\mathbf{B_{n0}}$, which is defined by $B_{n0}\mathbf{B}/|\mathbf{B}|$. Figure 4.8 compares the steady-state solution of V_{NL} and transient solutions for r = 0.1 and 0.3 mT/s. A dramatic transfer between the transient and steady cases appears at *state*-5; the negative side peak disappears in the steady-state case. Since $\mathbf{S_0}\cdot\mathbf{B} < 0$ for the magnetic configuration in *state*-5, $\mathbf{B_{n0}}$ and $\mathbf{B}$ are parallel. This indicates that no cancelation occurs for the steady-state of *state*-5, resulting in the disappearance of the negative side peak. On the other hand, as r increases, $\mathbf{B_n}$ remains antiparallel to $\mathbf{B}$ even in *state*-5, as shown in Fig. 4.4. Thus, the r-dependence of the negative side peaks can be understood by the fact that the behaviors of the nuclear spins get closer to the steady-state as r decreases.

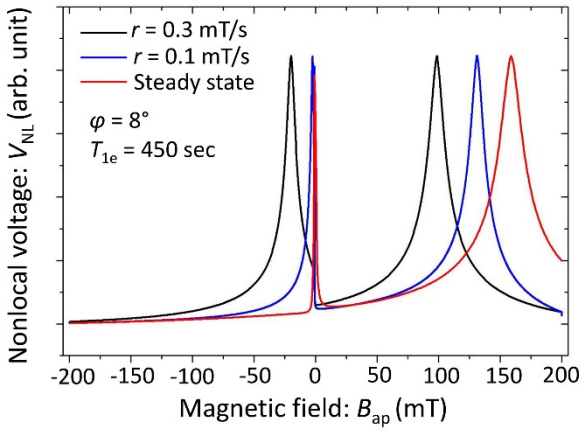

Fig. 4.8: A comparison of a steady-state solution of V_{NL} and transient solutions for r = 0.1 and 0.3 mT/s.

4.8. Nuclear-spin related phenomena appearing in spin-valve signals

Now we are confident from the influence of the transient nuclear field on the electron spins through the hyperfine interaction from last sections. Existence of nuclear field will either enhance or reduce the electron spin precession about the applied magnetic field. Herein, we will discuss about the precession of the electron spins about the nuclear field itself. A transient nuclear field was observed through a spin-valve like effect signal and thereby over attacked the electron spin polarization, as we have mentioned earlier in the beginning of this chapter, see Sec. 4.2. Herein, we will analyze these effects in details.

Figure 4.9(a) shows the experimental results of the spin-valve signal, pre-discussed in Sec. 4.2. However, to keep the flow of discussion here, we describe shortly the curve. The curve shows a change in V_{NL} as a function of an in-plane magnetic field B_{ap}. The closed and open circles in the figure refer to positive and negative sweeps, respectively. As for a normal behavior of the spin-valve signal, V_{NL} drops to a lower value in $-29.6 < B_{ap} < -20.7$ and $+29.1 < B_{ap} < +21.9$ mT owing to switching the magnetization configuration of FM 2 and FM 3 (injector and detector contacts) between parallel and antiparallel states.

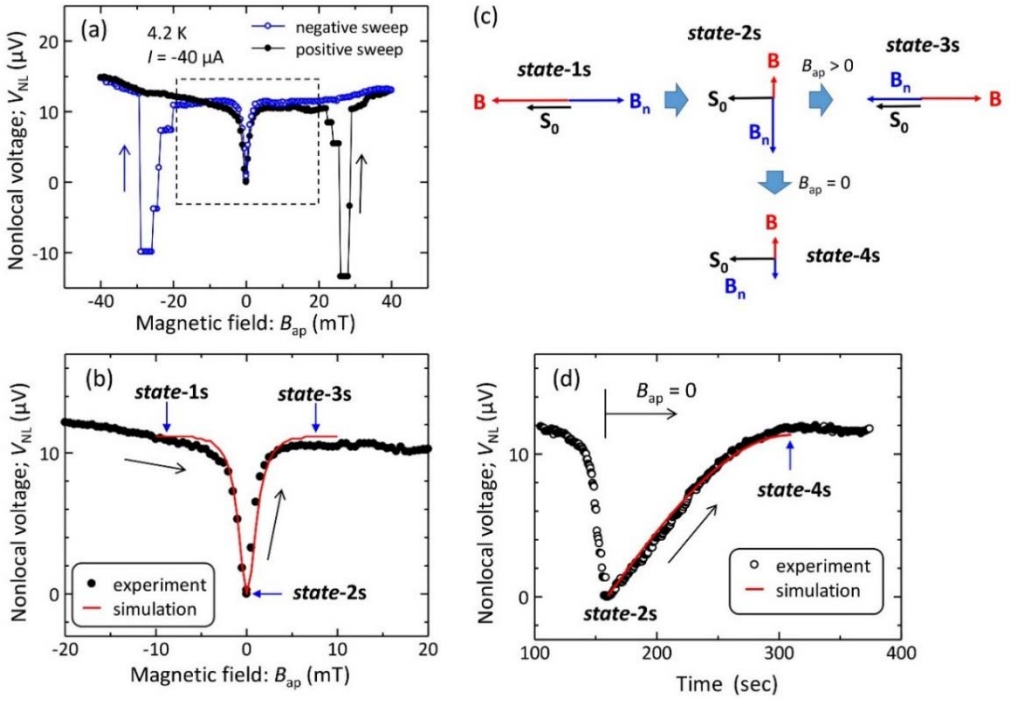

Fig. 4.9: (a) Experimental results of the nonlocal spin-vale signal measured at 4.2 K for a fixed bias current $I_{bias} = -40$ μA, (b) (closed circles) spin-valve signal for positive sweep only along with (red curve) fit with simulation result for parallel configuration, (c) schematic vector diagrams showing relative orientations of $\mathbf{S_0}$, $\mathbf{B}$, and $\mathbf{B_n}$ in the spin-valve measurement, and (d) V_{NL} as a function of time (t). Open circles show the experimental result and the red curve indicates the simulation after $\mathbf{B_{ap}}$ was switched off at $t = 160$ s.

Our focus here is to explore the dip in V_{NL} occurring at $B_{ap} = 0$ during the positive sweep direction, indicating a loss of electron spin polarization under the detector contact as shown in Fig. 4.9(b). We simulated V_{NL} during the positive sweep direction for B_{ap} from −10 to 10 mT under the parallel magnetization configuration between the injector and detector contact. Our model fits the dip in V_{NL} at $B_{ap} = 0$, as shown in Fig. 4.9(b). The analysis evinces that the presence

of this depolarization dip is due to the Hanle precession of electron spins induced by the transiently produced nuclear field.

Figure 4.9(c) shows a vector diagram for the relative orientation of the injected electron spin $\mathbf{S_0}$, magnetic field $\mathbf{B}$, and nuclear field $\mathbf{B_n}$ for such case. The total magnetic field $\mathbf{B}$ rotates in the x-z plane from $-\mathbf{x}$ to $+\mathbf{x}$ through the $+\mathbf{z}$ direction. Since the time scale of the change in the strength of $\mathbf{B_n}$, which is given by $(1/T_{1e} + 1/T_1)^{-1}$, is much slower than that for the change in $\mathbf{B}$, $\mathbf{B_n}$ rotates almost adiabatically as $\mathbf{B}$ rotates. In *state*-1s in Fig. 4.9(c), $\mathbf{B}_n$ is generated antiparallel to $\mathbf{B}$ because of $\mathbf{S_0} \times (\mathbf{B} + \mathbf{B}_n) = 0$, so no electron spin precession occurs, and V_{NL} equals V_{NL}^{P} ($\approx$ equivalent to the original value of V_{NL} in the parallel magnetization configuration). In *state*-2s, $B_{ap} = 0$, however, the transient $\mathbf{B}_n$ still exists and is orthogonal to $\mathbf{S_0}$ because of the presence of the stray field along $\mathbf{z}$ direction. Then, V_{NL} drops from V_{NL}^{P} as a result of an electron spin precession about such transient nuclear field. When B_{ap} turns positive in *state*-3s, V_{NL} recovers to V_{NL}^{P} again, due to $\mathbf{S_0} \times (\mathbf{B} + \mathbf{B}_n) = 0$, and the electron spin precession is suppressed.

To further check that the dip in V_{NL} at $B_{ap} = 0$ originated from the transiently produced nuclear field, we stopped the sweeping of the applied magnetic field exactly at $B_{ap} = 0$ and continuously recorded V_{NL}. The result of the recovery test of V_{NL} as a function of time is shown in Fig. 4.9(d), along with a simulation result. The V_{NL} recovered from its depolarization dip (= 0 V) to V_{NL}^{P} and fitted well with the simulation result. Since the strength of $\mathbf{B_n}$ decreases exponentially after switching off the magnetic field, whose time constant given by $(1/T_{1e} + 1/T_1)^{-1}$ is approximately 72 s for $B_{ap} = 0$, the nuclear field becomes negligibly small after a sufficient time ($t > 300$ s), as shown in *state*-4s in Fig. 4.9(c).

Finally, let us recall and discuss the effect of the proposed stray field in Eq. 3.5. In terms of to this equation, if $B_{st} = 0$, then $T_1 = 0$ at $B_{ap} = 0$. This indicates that the nuclear spins quickly relaxed to their thermal equilibrium at $B_{ap} = 0$, and the nuclear spin polarization disappeared. However, we experimentally found that the nuclear spins kept their polarization state for several hundred seconds after B_{ap} reached to 0, as shown in Fig. 4.9(d). Thus, an effective field which can keep the nuclear spin polarization even at $B_{ap} = 0$ should be present, and we assumed a constant stray field for such an effective field. Another possible origin of the effective field is the Knight field which acts on nuclear spins from polarized electron spins. Further study, however, is required to clarify the origin of such effective field.

Chapter 5

The influence of the nuclear magnetic resonance on the transient behaviors of the dynamically polarized nuclear spins in GaAs

5.1. Introduction

In chapter 4, we studied the behaviors of the electron and nuclear spins through the hyperfine interaction in semiconductors, specifically the dynamic polarization of nuclear spins by exchanging angular momentum with spin-polarized electrons, electrically injected using a ferromagnetic contact with a semiconductor channel. We have constructed a vector diagram showing the relative orientations of the transient nuclear field vector during dynamic nuclear polarization (DNP) with respect to the direction of spin polarization in the GaAs channel. Furthermore, we have introduced the concept of nuclear spin temperature to further explain those behaviors as a function of time.

In this chapter, we investigate the behaviors of the electron and nuclear spins through the hyperfine interaction in semiconductors while irradiating the system by rf-magnetic field; nuclear magnetic resonance (NMR) effects. We shall use the vector diagram developed in chapter 4 to analyze those behaviors. However, our focus here is to explain the differences due to NMR. Moreover, we will use the concept of nuclear spin temperature to quantify the transient behaviors of nuclear spins at resonance with time. In order to recognize transient behaviors of nuclear spins at resonance, we will show first a simple comparison between experimental results of oblique Hanle signals without and with irradiation by rf-magnetic field. Thereafter the chapter moves to the dynamics of the transient behaviors of nuclear spins under NMR.

5.2. Oblique Hanle signal without and with nuclear magnetic resonance

To keep the flow of our discussion through this chapter, we will shortly describe an experimental methodology for detecting NMR signals through oblique Hanle effect signal measurement. Similarly to the oblique Hanle effect

signal measurement, during the initialization time t_{hold} = 100 s, we have supplied a bias current I_{bias} = −60 μA and fixed the strength of the applied magnetic field at B_{ap} = +48 mT making an angle φ ≈ 6° from the z axis in the x-z plane. Thereafter, the magnetic field was swept from +48 to −48 mT (negative sweep direction), with a sweep rate of 0.35 mT/s. To detect NMR signals, we irradiated the system by a radio frequency (rf)-magnetic field with a frequency f of 200 kHz while monitoring the change in nonlocal V_{NL}.

Shown in Fig. 5.1 (a) is a comparison between the experimental results of transient oblique Hanle signal (a) without and (b) with irradiation by rf magnetic field observed in GaAs using a lateral spin injection device having a Co_2MnSi spin source. More details about measurement methodology can be found in chapter 3.

In comparison to the typical curve of the oblique Hanle signal shown in Fig. 5.1 (a) and previously discussed through over chapter 4, we can clearly see that there are three strong step-dips in the change in V_{NL} (at B_{ap} = + 27.9, + 19.7, and + 15.4 mT) along with a clear satellite peak (at B_{ap} = + 3.5 mT) occurring at the positive applied field region and weak two dips (at B_{ap} = −20.1 and −13.4 mT) appearing also in the change in V_{NL} at the negative side of applied magnetic field region in Fig. 5.1 (b). Those behaviors are correlated to the phenomenon of NMR due to irradiation by rf-magnetic field. So, in the following sections, our focus is to quantitatively analyze those behaviors using the time evolution of nuclear field vector and nuclear spin temperature. Again, our focus here is to explain the differences due to NMR.

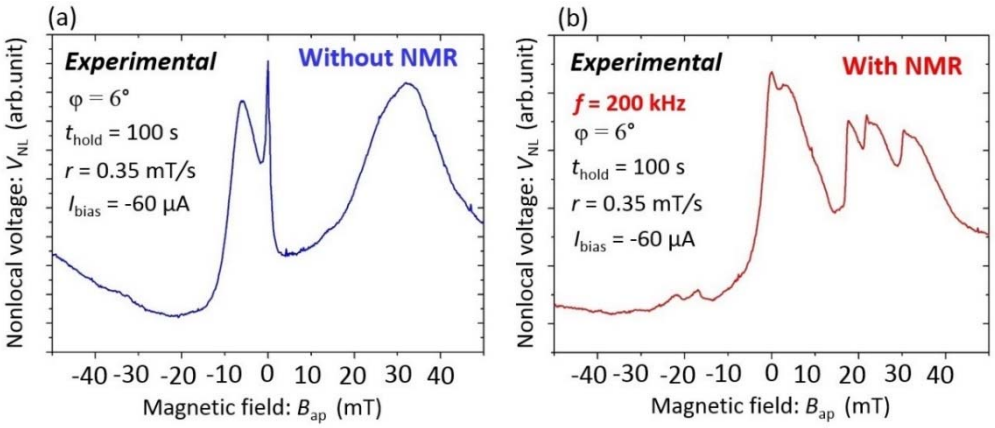

Fig. 5.1: Experimental result of transient oblique Hanle signal (a) without and (b) with irradiation by rf-magnetic field observed in GaAs semiconductor using a lateral spin injection device having a Co_2MnSi spin source.

5.3. Quantification of the transient behaviors of nuclear spins using the time evolution of nuclear field while irradiating the spin system by rf-magnetic field.

Figure 5.2 shows simulation results of oblique Hanle signal (a) without and (b) with irradiation by rf magnetic field. One has to remember firstly that we reset the strength of $\mathbf{B_n}$ to zero if the resonance condition is satisfied. Particularly, by comparing with experimental results given in Fig. 5.1 for the case with NMR (Fig. 5.1(b)), it is clear that simulation result can reproduce experimental result, which gives validity for the simulation model also to analyze transient behaviors of nuclear spins under DNP/NMR conditions. Based on simulation model, we have divided the irradiated oblique Hanle signal with rf-magnetic field (NMR) into seven main states (1n:7n) and plotted a corresponding vector diagram showing the relative orientation of the injected electron spin $\mathbf{S_0}$, magnetic field $\mathbf{B}$, and nuclear field $\mathbf{B_n}$ in Fig. 5.2(c).

In order to emphasize on the influence of irradiation by rf magnetic field or NMR, we will target some states of the change in the nonlocal voltage and explain them before and after the resonances based on the developed simulation model. Those states are 1n, 2n and 6n, and so we have split the resultant nuclear field vector $\mathbf{B_n}$ into sub three vectors particularly at these states. The three vectors are given as $\mathbf{B_n}\_^{75}\mathrm{As}$, $\mathbf{B_n}\_^{71}\mathrm{Ga}$ and $\mathbf{B_n}\_^{69}\mathrm{Ga}$ corresponding to nuclear field vector of $^{75}\mathrm{As}$, $^{71}\mathrm{Ga}$ and $^{69}\mathrm{Ga}$ nuclei, respectively. Now, let's start to explain the behaviors of the nuclear spins for the case without and with NMR.

(a) For the case without NMR:

Roughly speaking, the discussion here is similar to our discussion in Sec. 4.4. So, herein, we will not go through the deep details. After passing the time required for the initialization $t_{\mathrm{hold}} = 100$ s under a fixed bias current $I_{\mathrm{bias}} = -60$ μA, the nuclear spins are dynamically polarized due to DNP and a nuclear field $\mathbf{B}_{\mathrm{n}}$ is generated antiparallel to the direction of $\mathbf{B}$, where $\mathbf{B} = \mathbf{B_{ap}} + B_{st}\,\mathbf{z} = B_{\mathrm{ap}}(\mathbf{x}\sin\varphi + \mathbf{z}\cos\varphi) + B_{st}\,\mathbf{z}$. That is because b_n is a negative in GaAs and $\mathbf{B}\cdot\mathbf{S}_0 > 0$. Therefore, the electron spins make a precessional motion about $\mathbf{B} + \mathbf{B}_{\mathrm{n}}$ [*See state*-1 in Fig. 4.4 is identical with *states*-1n in Fig. 5.2 (a)]. When $\mathbf{B_n}$ become equal in magnitude and exactly opposite in direction to $\mathbf{B}$, they cancel each other completely and so electron-spin precession is suppressed [*See state*-2 in Fig. 4.4 is identical with *states*-2n in Fig. 5.2 (a)]. After that $\mathbf{B_n}$ is decreased in magnitude while decreasing the magnitude of $\mathbf{B_{ap}}$ to 0 mT [*See state*-3n in Fig. 5.2 (a)].

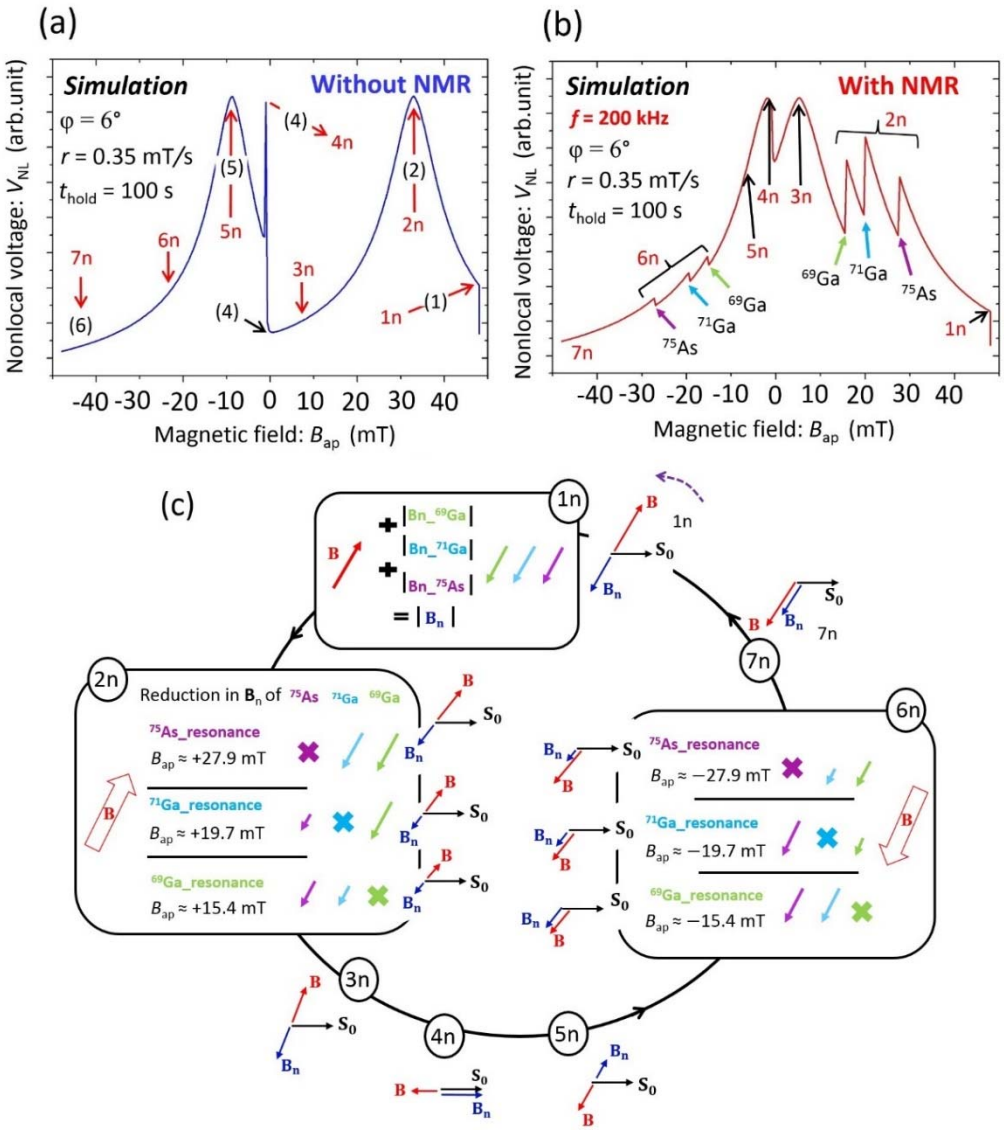

Fig. 5.2: Simulation result of oblique Hanle signal (a) without and (b) with irradiation by rf-magnetic field and a corresponding schematic vector diagram for the relative orientation of the injected electron spin $\mathbf{S_0}$, magnetic field $\mathbf{B}$, and nuclear field $\mathbf{B_n}$ under irradiation by rf-magnetic field.

At *state*-4n shown in Fig. 5.2(a), **B** and transient $\mathbf{B}_n$ are parallel or antiparallel to $\mathbf{S_0}$. Thus, no Hanle precession occurs, allowing V_{NL} to reach a maximum value or showing a central peak. Even after reversing the direction of **B**, the transient $\mathbf{B}_n$ exists and its strength changes in a non-adiabatic process whilst its direction is reversed to an opposite direction to that at the positive field regions. Exactly at state-5n in Fig. 5.2(a), the strength of $\mathbf{B}_n$ becomes equal to the strength of **B**, resulting in suppression of the electron precession, showing a satellite peak in the change of V_{NL} through the negative field values of the applied field at -6 mT.

(b) For the case with NMR:

Partially, the situation here is the same as the case without NMR before passing initialization period (during initialization time t_{hold} = 100 s at a fixed bias current I_{bias} = -60 μA); nuclear spins are dynamically polarized due to DNP and a transient $\mathbf{B}_n$ is generated antiparallel to the field vector **B**. As a consequence, one anticipates that the electron spin precession should be gradually suppressed and the level of V_{NL} should be increased similarly to *state*-2n in Fig. 5.2 (a). However, an irradiation by rf magnetic field with an energy equal to the Zeeman splitting energy leads to the transition of nuclear spins between the ground state and the higher excited states. Therefore, the average nuclear spins is reduced while the resonance condition is satisfied for a given isotope α in GaAs. Consequently, at the time of resonance, the electron spin precession is enhanced and the change in V_{NL} shows three strong dips at $B_{ap} \approx +27.9$, $+19.7$, and $+15.4$ mT, corresponding to the resonance fields of ^{75}As, ^{71}Ga, and ^{69}Ga isotope, respectively [*See state*-2n in Fig. 5.2 (b) & (c)].

After resonances of all of those three isotopes, the nuclear field strength B_n has a chance to be recovered again due to DNP ($\mathbf{B}\cdot\mathbf{S_0} > 0$) and the applied field **B** is not yet reached to zero. The electron spin precession is therefore suppressed again, and the change in the nonlocal voltage shows a clear satellite peak at $B_{ap} \approx +3.5$ mT [*See state*-3n in Fig. 5.2 (b) & (c)].

At *state*-4n, **B** and transient $\mathbf{B}_n$ are parallel or antiparallel to $\mathbf{S_0}$. Thus, no Hanle precession occurs, allowing V_{NL} to reach a maximum value or showing a central peak, as shown in Fig. 5.2(b) & (c). Thereafter, because of resonance and the temporal depolarization of nuclear spins, the strength of the nuclear field is decreased in comparison to case (a) without NMR. Therefore, after reversing the direction of **B**, the precession of the electron spin is stronger than the case (a) without NMR, leading to observation of a continued decrease in the level change of V_{NL} and absence of the satellite peak occurring due to a transient nuclear field at $B_{ap} < 0$ [*See state*-5n before resonance in Fig. 5(a) and after resonance in Fig. 5(b)].

Upon the negative field region, the resonance condition could be satisfied also for $B_{ap} < 0$ at $B_{ap} \approx -27.9$, -19.7, and -15.4 mT [*state*-6n in Fig. 5.2 (b) & (c)]. However, the decrease in the strength of the transient nuclear field along with the absence of the satellite peak at $B_{ap} < 0$ ($\mathbf{B}_n$ is parallel to **B** due to a negative nuclear spin polarization) leads to that the corresponding dips of NMR signals are too small compared with the dips occurring at $B_{ap} > 0$, which is confirmed by simulation results as well. As an overall, such results indicate a high sensitivity of the developed NMR system.

At *state*-7n, nuclear spins are strongly undergoing a negative polarization, resulting in enhancing the electron spin precession and lowering the level change in V_{NL}, as shown in Fig. 5.2(b) & (c).

5.4. Analysis of transient behaviors of nuclear spins at resonances using the concept of spin temperature.

Figure 5.3 shows the simulation results of the time evolution of (a) nonlocal voltage V_{NL}, (b) spin temperature θ, and (c) nuclear field as $-B_n(t)$ along with $B_{ap}(t)$, where $B_n(t)$ is a projection of $\mathbf{B}_n(t)$ on $\mathbf{B}$, and $B_{ap}(t)$ is a projection of $\mathbf{B}_{ap}(t)$ on unit vector $\mathbf{u}$ =(sinφ, 0, cosφ), *i.e.* $\mathbf{B}_n(t) = B_n(t)\mathbf{B}/|\mathbf{B}|$, and $\mathbf{B}_{ap}(t) = B_{ap}(t)\mathbf{u}$. Thus, positive (negative) $B_n(t)$ indicates that $\mathbf{B}_n$ is generated parallel (antiparallel) to $\mathbf{B}$, whereas positive (negative) $B_{ap}(t)$ indicates that $\mathbf{B}_{ap}$ is along $+(-)\mathbf{u}$ direction.

During the initialization time t_{hold}= 100 s, a predicted situation similar to that one without irradiation by rf magnetic field is dominant, Sec. 4.5, *i. e.* θ is a positive value and a transient nuclear field $\mathbf{B}_n$ is generated with a strength increasing antiparallel to $\mathbf{B}_{ap}$ [*See state*-1n in Fig. 5.3 showing (a) the level change in V_{NL}, (b) heating effect of the nuclear spin system by NMR and (d) the change in B_n with time]. Thereafter, as we explained during the last section, irradiating the system by rf magnetic field with an energy equal to Zeeman splitting energy leads to heating the nuclear spins and enhancing the transition of nuclear spins between the ground state and the higher excited states. As a consequence, even under DNP, nuclei of GaAs are temporarily depolarized at the time of resonance of each nuclear isotope existing in GaAs semiconductor. The strength of $\mathbf{B}_n$ is partially reduced and such partial reduction is equal to contributions of each isotope's nuclear field. For instance, at t = 159, 180 and 193 s, we can see clearly that the strength of $\mathbf{B}_n$ is reduced at each resonance fields B_{ab} = + 27.9, + 19.7, and + 15.4 mT, correspondingly to resonant fields of ^{75}As, ^{69}Ga and ^{71}Ga nuclei, respectively. Thus the electron spin precession is enhanced and the level change in V_{NL} is lowered at those resonant fields [*See state*-2n in Fig. 5.3].

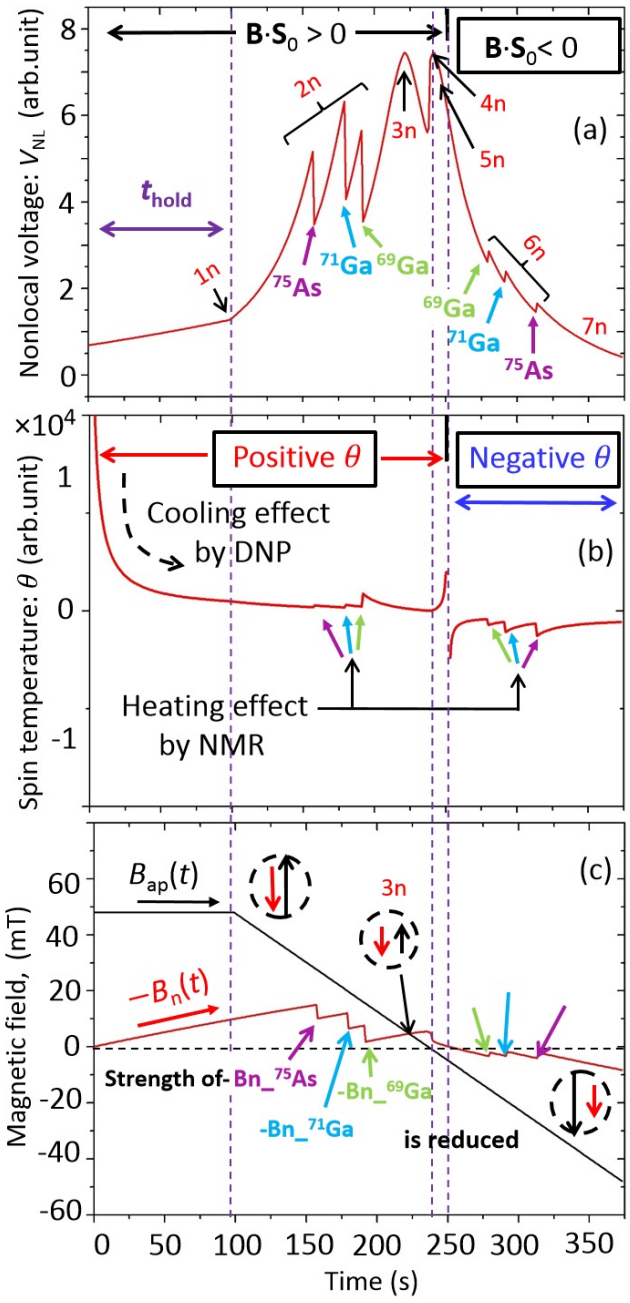

Fig. 5.3: Simulation results of the change in (a) a nonlocal voltage V_{NL}, (b) a spin temperature θ and (c) a transient nuclear field B_n along with a magnetic field B_{ap} of an oblique Hanle signal with irradiation by rf magnetic field.

The clear observation of those resonant fields of different isotopes in the GaAs channel strongly confirms the strong hyperfine coupling between electron and nuclear spins, which indicates a high signal sensitivity of the developed NMR system.

After resonances of all of those mentioned nuclei, θ is still positive and the nuclear field strength $\mathbf{B}_n$ has a chance to be recovered again due to DNP ($\mathbf{B}\cdot\mathbf{S_0} > 0$). Such a recovery comprises from contributions of all nuclear fields arising from each isotope in GaAs. The recovered $\mathbf{B}_n$ can cancel the effect of the low magnetic field values on the electron spins (electron spin precession), resulting in appearance of a clear satellite peak at $t = 224$ s of the change in V_{NL} [*See state*-3n in Fig. 5.3 (a), (b) and (c)]. Such quantitative reproduction for these behaviors is the first among literature.

Remarkably, there is a significant difference between the response of transient nuclear spin θ for the case without NMR and with NMR. This can be explained as follows. Without NMR, the positive θ has maintained as a positive value for an extremely long delay of time even after reversing the direction of $\mathbf{B}_{ap}$ at $t = 237$ s, it is stayed positive until $t = 315$ s (delay of time ≈ 50 s), producing a non-zero value of B_n across this pass (See Sec. 4.5). On the other hand, in this section, due to the effect of NMR and depolarization of nuclear spins, the strength of the nuclear field become weaker compared to the case without NMR. Thus, it will be decayed quickly and dropped to zero after reversing the direction of $\mathbf{B}_{ap}$. Correspondingly, the delay of time response of the transient spin temperature θ is also decreased, e.g. θ turns to negative values at $t = 251$ s (delay of time ≈ 15 s) as shown in Fig. 5.3 (b).

Afterwards, at *state*-4n give in Fig. 5.3, **B** and transient $\mathbf{B}_n$ are parallel or antiparallel to $\mathbf{S_0}$, *i.e.* no Hanle precession is induced and V_{NL} shows such central peak. After the strength of $\mathbf{B}_n$ increase in a parallel direction to $\mathbf{B}_{ap}$, the nuclear spin system is negatively polarized ($\mathbf{B}\cdot\mathbf{S_0} < 0$), resulting in a strong electron spin

precession about $\mathbf{B}_{ap} + \mathbf{B}_n$ and a continuous decrease in the level change in V_{NL} [*See state*-5n in Fig. 5.3 (a)]. Equally important, the resonance condition might be satisfied also for $B_{ap} < 0$ at $B_{ap} \approx -27.9$, -19.7, and -15.4 mT [*See state*-6n in Fig. 5.3 (d)]. However, because a strong electron spin precession about $\mathbf{B}_{ap} + \mathbf{B}_n$ makes it difficult to clearly observe a clear step-dip structures as the case of $B_{ap} > 0$. At *state* -7n, the nuclear spins are completely undergoing a negative polarization, *i.e.* the precession of electron spins is maximized.

Chapter 6

Summary and conclusions

Controlling of the nuclear spins in semiconductors through the nuclear magnetic resonance (NMR) is one of the promising tool for implementation of quantum bits (qubits) for the quantum computation systems, because they possess an extremely longer coherence time than electron spins. However, their smaller magnetic moment compared to those of electrons spins results in lowering the signal sensitivity of NMR systems. One more challenge is that the nuclear spins show complex behaviors, called transient behaviors, against the fast change in the magnetic field. Lack of quantitative analysis about those behaviors results in a difficulty to precisely control the nuclear spin systems.

The main goal of this study is to provide a quantitative description for the electron-nuclear spin dynamics in semiconductor-based spintronics devices. For that we systematically investigated the dependences of the nuclear spin polarization on (1) the initialization times during dynamic nuclear polarization, by injecting spin-polarized electrons in GaAs channel from a highly spin polarized Co_2MnSi source, and (2) sweep rates of the applied magnetic field through Hanle signal and spins valve signal measurement made on an all electrical lateral spin injection devices. Furthermore, to investigate the sensitivity of our device for NMR applications, we investigated the behaviors of nuclear spins by observation of Hanle signals while irradiating the system by rf-magnetic field. In the following we summarized our main results and ending up with conclusions.

The main results are summarized as follows:

1. We have demonstrated an electrical spin injection from a highly spin-polarized Co_2MnSi source into a GaAs channel by observation of spin-valve like signal and Hanle signals. Successful fitting of the measured Hanle curve showed that the spins are transported in our device efficiently, allowing us to determine

the spin lifetime in the GaAs channel.

2. We have achieved an efficient dynamic nuclear polarization (DNP) of nuclear spins by maintaining the electrical injection of spin-polarized electrons into the GaAs channel under application of a magnetic field on the order of few mille-Tesla. The resultant nuclear polarization manifests itself in a hyperfine effective field acting on electron spins, which modulates the shape of the observed Hanle signal and spin valve signal. We have also observed rich applied field dependence of electron spin dynamics as electron spins precess about such effective field.

3. We have developed a simulation model to analyze the modulation of the shape of Hanle signal and spin-valve signal using the time evolution of nuclear field. This simulation accurately reproduced all field dependence of the measured electron spin signals on both Hanle signal and spin valve signal. On the basis of the simulation results, we quantitatively explained all behaviors of nuclear spins in GaAs during DNP and established a vector diagram gathering all relative orientations of the transient nuclear field vector in space during DNP.

○ Particularly, on the observed Hanle signal, we have found that there is a distinct behavior of the transiently polarized nuclear spins on the precession of electron spins at the negative applied field values during DNP. Unlike the steady state nuclear spin polarization, the precession was suppressed. This is due to the fact that the direction of the magnetic field changes adiabatically whereas its strength is not the case. As a consequence, the nuclear field keeps an antiparallel alignment after reversing the direction of applied field with a non-zero value, which results in cancelation of the effect of the applied field on electron spins (spin precession).

○ Moreover, on the spin-valve signal, a clear depolarization of the electron spins at zero magnetic fields had observed because a transient nuclear filed is pointed along a direction perpendicular to the spin exactly while reversing

the direction of the applied magnetic field (zero magnetic fields).

○ Furthermore, we are able also to precisely determine the time required for DNP in GaAs and calculate the strength of the transient nuclear field experienced by the electron spins during DNP.

4. We have also showed that the strength of the transient nuclear field is increased exponentially with increasing the initialization times of DNP and finally saturated at a constant steady state value.

5. Using the concept of spin temperature, we have showed that the cooling of the nuclear spins can be effectively achieved by DNP if we have applied the magnetic field along the direction of the electron spin polarization in GaAs. When this is the case, the lower energy state has more population by nuclear spins than the higher ones and so nuclear spins are polarized positively.

On the other hand, the cooling of the nuclear spins to the negative temperature can be adapted by DNP if we have directed the applied magnetic field in an opposite direction to the electron spin polarization. When this is the case, the nuclear spins show a case of population inversion, the higher energy states has more population by nuclear spins than the lower one, and so nuclear spins are polarized negatively.

6. Moreover, we have proved that the spin temperature of the transiently polarized nuclear spins exhibits a delay of time response with respect to the fast change in the applied magnetic field during DNP. This effect is more observable when the direction of the applied field is reversed. The spin temperature stays a positive value until the effect of the positive cooling is vanished and the nuclear field reset to zero.

7. We have observed clear changes, step-dips, in Hanle signal curve at resonant fields of ^{69}Ga, ^{71}Ga, and ^{75}As nuclei while irradiating the system by rf-magnetic field. Such dips indicates that the precession of the electron spins about the effective field is enhanced due to occurrence of NMR at each resonance field.

8. Last we have found that the delay of time response exhibiting by the spin temperature of the transiently polarized nuclear spins is decreased while the system is irradiated by rf-magnetic field. Such decrease is due to diminishing the strength of the transient nuclear field by NMR in comparison to the case without NMR.

Conclusions

- The study presents a quantitative description for the electron-nuclear spin dynamics in semiconductor-based spintronics devices.
- Whatever NMR happens and regardless to DNP conditions, the behaviors along with strength of the nuclear field can be precisely predicted.
- Our findings provides not only a deep understanding on the electron-nuclear spin dynamics in semiconductors, but also a big step towards the future of the quantum computing systems based on the nuclear spin.

Acknowledgements

Above all, praise to ALLAH, the lord of the world, by whose grace this work has been completed and never leaving me lost.

I would like to thank Prof. Tetsuya Uemura (Lecturer of Spintronics and Head of The Nanoscale Electron Devices Laboratory (NSED), Hokkaido University) who, in 2014, allowed me to join his research group; thankful for his patience, motivation, continued discussion and support over the past 4 years until emerging such an excellent research in science. A special thank for his advices and discussion during writing my publication and this thesis. Uemura is an infinitely generous professor with experiences and times I ever met through my life; he is a good teacher to train one how to think and a good professor to set one on the track of top research. So, again, thank you so much for every single moment I stayed at your Lab or discussed with you.

The deepest gratitude and appreciation should go to Prof. Masafumi Yamamoto (Lecturer of Spintronics and Former Head of NSED) who first recommended me to Prof. Uemura in 2013. For sure, I would like to thank him also for more than one and half year of continuous support and discussion during my study too.

I am also grateful to Prof. Yasuo Takahashi, Prof. Kazuhisa Sueoka, and Prof. Junichi Motohisa for reviewing this dissertation and offering their helpful comments and advices.

I want also to pass my deepest appreciations to former students; Takafumi Akiho for getting me started with the measurement system, Kidist Moges and Hu Bing for assisting me in using a magnetron sputtering professionally. A special thank for Zhichao Lin, whose research has overlapped with mine in the electrical spin injection, exactly speaking sharing long times experiments and measurements (especially during MBE growth). Also, I would like to thank Masaki Inoue and Shin Toyoshima for delivering their experiences on fabrication

of magnetic tunnel junctions and help in using EB lithography. I also want to thank all members of the Laboratory of Nanoscale Electron Devices for sharing experiences and enjoyable times, which will always be one of the best memories in my life.

I would like to convey my deepest gratitude to the ministry of Education, Culture, Sports, Science and Technology in Japan for financially supporting me throughout my doctoral course study.

Great thanks must be given to my mother who is the main power of pushing me forward. Deep thanks to my dear brothers and sisters, my beloved wife and finally to my lovely daughter, Jana, and son, Fahd, for their patient about being me far from home long time and always busy. Thank you all for your supports and kind wishes.

References

[1] H. Sanada, Y. Kondo, S. Matsuzaka, K. Morita, C. Y. Hu, Y. Ohno, and H. Ohno, PRL **96**, 067602 (2006)

[2] H. Takahashi, M. Kawamura, S. Masubuchi, K. Hamaya, and T. Machida, APL **91**, 092120 (2007).

[3] J. Strand, B. D. Schultz, A. F. Isakovic, C. J. Palmstrøm, and P. A. Crowell, Phys. Rev. Lett. **91**, 036602 (2003).

[4] J. Strand, X. Lou, C. Adelmann, B. D. Schultz, A. F. Isakovic, C. J. Palmstrøm, and P. A. Crowell, Phys. Rev. B **72**, 155308 (2005).

[5] P. Van Dorpe, W. Van Roy, J. De Boeck, and G. Borghs, Phys. Rev. B **72**, 035315 (2005).

[6] M. K. Chan, Q. O. Hu, J. Zhang, T. Kondo, C. J. Palmstrøm, and P. A. Crowell, Phys. Rev. B **80**, 161206(R) (2009).

[7] G. Salis, A. Fuhrer, and S. F. Alvarado, Phys. Rev. B **80**, 115332(R) (2009).

[8] J. Shiogai, M. Ciorga, M. Utz, D. Schuh, T. Arakawa, M. Kohda, K. Kobayashi, T. Ono, W. Wegscheider, D. Weiss, and J. Nitta, Appl. Phys. Lett. **101**, 212402 (2012).

[9] T. Akiho, J. Shan, H.-x. Liu, K.-i. Matsuda, M. Yamamoto, and T. Uemura, Phys. Rev. B **87**, 235205 (2013).

[10] T. Uemura, T. Akiho, Y. Ebina, M. Yamamoto, Phys. Rev. B. **91**, 140410 (R) (2015).

[11] Z. Lin, M. Rasly, and T. Uemura, Appl. Phys. Lett. **110**, 232404 (2017).

[12] K. Inomata, S. Okamura, R. Goto, and N. Tezuka, Jpn. J. Appl. Phys. **42**, L419 (2003).

[13] Y. Sakuraba, M. Hattori, M. Oogane, Y. Ando, H. Kato, A. Sakuma, T. Miyazaki, and H. Kubota, Appl. Phys. Lett. **88**, 192508 (2006).

[14] T. Ishikawa, H.-x. Liu, T. Taira, K.-i. Matsuda, T. Uemura, and M. Yamamoto, Appl. Phys. Lett. **95**, 232512 (2009).

[15] N. Tezuka, N. Ikeda, F. Mitsuhashi, and S. Sugimoto, Appl. Phys. Lett. **94**, 162504 (2009).

[16] W. Wang, E. Liu, M. Kodzuka, H. Sukegawa, M. Wojcik, E. Jedryka, G. H. Wu, K. Inomata, S. Mitani, and K. Hono, Phys. Rev. B **81**, 140402(R) (2010).

[17] M. Yamamoto, T. Ishikawa, T. Taira, G.-f. Li, K.-i. Matsuda, and T. Uemura, J. Phys.: Condens. Matter. **22**, 164212 (2010).

[18] H.-x. Liu, Y. Honda, T. Taira, K.-i. Matsuda, M. Arita, T. Uemura, and M. Yamamoto, Appl. Phys. Lett. **101**, 132418 (2012).

[19] H.-x. Liu, T. Kawami, K. Moges, T. Uemura, M. Yamamoto, F. Shi, and P. M. Voyles, J. Phys. D: Appl. Phys. **48**, 164001 (2015).

[20] K. Moges, Y. Honda, H.-x. Liu, T. Uemura, M. Yamamoto, Y. Miura and M.Shirai, Phys. Rev. B **93**, 134403 (2016).

[21] B. Hu, K. Moges, Y. Honda, H.-x. Liu, T. Uemura, and M. Yamamoto, Phys. Rev. B **94**, 094428 (2016).

[22] K. Yakushiji, K. Saito, S. Mitani, K. Takanashi, Y. K. Takahashi, and K. Hono, Appl. Phys. Lett. **88**, 222504 (2006).

[23] T. Furubayashi, K. Kodama, H. Sukegawa, Y. K. Takahashi, K. Inomata, and K. Hono, Appl. Phys. Lett. **93**, 122507 (2008).

[24] Y. Sakuraba, K. Izumi, T. Iwase, S. Bosu, K. Saito, K. Takanashi, Y. Miura, K. Futatsukawa, K. Abe, and M. Shirai, Phys. Rev. B **82**, 094444 (2010).

[25] Y. K. Takahasi, A. Srinivasan, B. Varaprasad, A. Rajanikanth, N. Hase, T. M. Nakatani, S. Kasai, T. Furubayashi, and K. Hono, Appl. Phys. Lett. **98**, 152501 (2011).

[26] H. Narisawa, T. Kubota, and K. Takanashi, Appl. Phys. Express **8**, 063008 (2015).

[27] Y. Du, T. Furubayashi, T. T. Sasaki, Y. Sakuraba, Y. K. Takahashi, and K. Hono, Appl. Phys. Lett. **107**, 112405 (2015).

[28] J. W. Jung, Y. Sakuraba T. T. Sasaki, Y. Miura, and K. Hono Appl. Phys. Lett. **108**, 102408 (2016).

[29] J. Kübler, A. R. Williams, and C. B. Sommers, Phys. Rev. B **28**, 1745 (1983).

[30] S. Ishida, S. Fujii, S. Kashiwagi, and S. Asano, J. Phys. Soc. Jpn. **64**, 2152 (1995).

[31] S. Picozzi, A. Continenza, and A. J. Freeman, Phys. Rev. B **66**, 094421 (2002).

[32] H.-x. Liu, Y. Honda, T. Taira, K.-i. Matsuda, M. Arita, T. Uemura, and M. Yamamoto, Appl. Phys. Lett. **101**, 132418 (2012).

[33] H.-x. Liu, T. Kawami, K. Moges, T. Uemura, M. Yamamoto, F. Shi, and P. M. Voyles, J. Phys. D: Appl. Phys. **48**, 164001 (2015).

[34] K. Moges, Y. Honda, H.-x. Liu, T. Uemura, M. Yamamoto, Y. Miura and M.Shirai,

Phys. Rev. B **93**, 134403 (2016).
[35] Y. Ebina, T. Akiho, H.-x. Liu, M. Yamamoto, and T. Uemura, Appl. Phys. Lett. **104**, 172405 (2014).
[36] G. Lampel, Phys. Rev. B **20**, 491 (1968).
[37] A. I. Ekimov and V. I. Safarov, Pis'ma Zh. Eksp. Teor. Fiz. **15**, 453 (1972) [JETP Lett. 15, 319 (1972)].
[38] M. I. D'yakonov, V. I. Perel', V. L. Berkovits, and V. I. Safarov, Sov. Phys. - JETP **40**, 950 (1975).
[39] D. Paget, G. Lampel, B. Sapoval, and V. I. Safarov, Phys. Rev. B **15**, 5780 (1977).
[40] S. E. Barrett, R. Tycko, L. N. Pfeiffer, and K.W. West, Phys. Rev. B **72**, 1368 (1994).
[41] D. Gammon, Al. L. Efros, T. A. Kennedy, M. Rosen, D. S. Katzer, D. Park, S. W. Brown, V. L. Korenev and I. A. Merkulov, Phys. Rev. Lett. **86,** 5176 (2001).
[42] G. Salis, D. T. Fuchs, J. M. Kikkawa, and D. D. Awschalom, Phys. Rev. Lett. **86**, 2677 (2001).
[43] M. Poggio, G. M. Steeves, R. C. Myers, Y. Kato, A. C. Gossard, and D. D. Awschalom, Phys. Rev. Lett. **91**, 207602 (2003).
[44] P. L. Kuhns, A. Kleinhammes, T. Schmiedel, and W. G. Moulton, Phys. Rev. B **55**, 1997-II (2006).
[45] H. Sanada, Y. Kondo, S. Matsuzaka, K. Morita, C. Y. Hu, and H. Ohno, Phys. Rev. Lett. **96**, 067602 (2006).
[46] J. Lu, M. J. R. Hoch, P. L. Kuhns, W. G. Moulton, Z. Gan, and A. P. Reyes, Phys. Rev. B **74**, 125208 (2006).
[47] S. Mui, K. Ramaswamy, and S. E. Hayes, Phys. Rev. B **75**, 195207 (2007).
[48] R. Matsusaki, R. Kaji, S. Yamamoto, H. Sasakura, and S. Adachi, arXiv:1703.06046 (2017).
[49] T. Machida, T. Yamazaki, and S. Komiyama, Appl. Phys. Lett. **80**, 4178 (2002).
[50] K. Hashimoto, K. Muraki, T. Saku, and Y. Hirayama, Phys. Rev. Lett. **88**, 176601 (2002).
[51] K. Ono and S. Tarucha, Phys. Rev. Lett. **92**, 256803 (2004).
[52] M. Johnson, Phys. Rev. Lett. **70**, 2142 (1993).
[53] A. Fert and H. Jaffrès, Phys. Rev. B **64**, 184420 (2001).

[54] S. Takahashi and S. Maekawa, Phys. Rev. B **67**, 052409 (2003).
[55] J. Fabian, A. Matos-Abiague, C. Ertler, P. Stano, and I. Žutić, Acta Phys. Slov. **57**, 565 (2007).
[56] M. Johnson and R. H. Silsbee, Phys. Rev. Lett. **55**, 1790 (1985).
[57] A. Abragam, Principles of Nuclear Magnetism (Cambridge Univ. Press, London, 1961).
[58] A. Overhauser, Phys. Rev., **92**, 411 (1953).
[59] M. I. Dyakonov and V. I. Perel, Optical Orientation edited by F. Meier and B. P. Zakharchenya (North-Holland, 1984).
[60] C. Testelin, F. Bernardot, B. Eble and M. Chamarro, Phys. Rev. B **79**, 195440 (2009).
[61] R. I. Dzhioev, K. V. Kavokin, V. L. Korenev, M. V. Lazarev, B. Y. Melter, M. N. Stepanova, B. P. Zakharchenya, D. Gammon and D. S. Katzer, Phys. Rev. B. **66**, 245204 (2002).
[62] B. T. Jonker, E. M. Kneedler, P. Thibado, O. J. Glembocki, L. J. Whitman, and B. R. Bennett, Journal of Applied Physics **81**, 4362 (1997).
[63] M. Johnson, Mater. Sci. Eng. **B31**, 199-205(1995).
[64] R. Stratton, J. Phys. Chem. Solids **23**, 1177 (1962).
[65] J. G. Simmons, J. Appl. Phys. **34**, 1793 (1963).
[66] T. Marukame, T. Ishikawa, W. Sekine, K. Matsuda, T. Uemura, and M. Yamamoto, IEEE Trans. Magn. **42**, 2652 (2006).
[67] S. Yuasa, T. Nagahama, A. Fukushima, Y. Suzuki, and K. Ando, Nat. Mater. **3**, 868 (2004).
[68] W. H. Butler, X.-G. Zhang, T. C. Schulthess, and J. M. MacLaren, Phys. Rev. B **63**, 054416 (2001).
[69] Y. Miura, H. Uchida, Y. Oba, K. Nagao, and M. Shirai, J. Phys.: Condens. Matter **19**, 365228 (2007).
[70] S. Trudel, O. Gaier, J. Hamrle, and B. Hillebrands, J. Phys. D: Appl. Phys. **43**, 193001 (2010).

Appendix

Publication list

1. Publication related to this dissertation

1.1. Peer-reviewed Articles

[1] **M. Rasly**, Z. Lin, and T. Uemura, Systematic investigations of transient response of nuclear spins in the presence of polarized electrons, Physical Review B, Vol. 96, No. 18, 184415(8pp), November, 2017.
[2] **M. Rasly**, Z. Lin, M. Yamamoto, T. Uemura, Analysis of the transient response of nuclear spins in GaAs with/without nuclear magnetic resonance, AIP Advances, Vol. 6, No 5, 056305(8pp), March, 2016.

1.2. International Conference Series

[1] **M. Rasly**, Z. Lin, M. Yamamoto and T. Uemura, Electrical control of nuclear spin polarization: Experimental and quantitative modeling, IEEE Int'l Magnetics Conf. 2018 (INTERMAG 2017), Digests (USB Memory), GO-12, Bublin Convention Centre, Dublin, Ireland, April 24−28, 2017. (*Poster presentation*)

[2] **M. Rasly**, Z. Lin, M. Yamamoto, and T. Uemura, Analysis of transient response of nuclear spins in GaAs with/without nuclear magnetic resonance, 13th Joint MMM-Intermag Conference, Abstracts, pp. 278-279, CB-07, San Diego, CA, USA, Jan. 11-15, 2016. (*Oral presentation*)

1.3. Domestic Conferences

[1] **Mahmoud Rasly**, Zhichao Lin, Tetsuya Uemura, "Investigating initialization-time dependence of nuclear spin polarization", The 64th Japan Society of Applied Physics Spring Meeting 2017, 16a-501-5, Pacifico Yokohama, Mar. 14-17, 2017. (*Oral presentation)*

[2] **Mahmoud Rasly**, Zhichao Lin, and Tetsuya Uemura, "Clarification for the transient response of nuclear spins using the time dependent spin temperature", The 21st Symposium on the Physics and Application of Spin-Related Phenomena in Semiconductors (PASPS-21), P-14, Hokkaido Univ., Sapporo-shi, December, 12–13, 2016. (*Poster presentation)*

[3] **Mahmoud Rasly**, Zhichao Lin, Masafumi Yamamoto, and Tetsuya Uemura, "Quantitative analysis of the nuclear spin dynamics in GaAs with irradiation by RF magnetic field", The 63rd Japan Society of Applied Physics Spring Meeting 2016, 21p-W241-11, Tokyo, (March 2016). (*Oral presentation)*

2. Publication related to other researches

2.1. Peer-reviewed Articles

[1] Z. Lin, **M. Rasly**, T. Uemura, Electrical detection of nuclear spin-echo signals in an electron spin injection system, Applied Physics Letter, Vol. 110, No 23, pp. 232404(4pp), Jun., 2017.

[2] **M. Rasly**, M. Afifi, A. E. Shalan, M. M. Rashad, A quantitative model based on an experimental study for the magnetoelectric coupling at the interface of cobalt ferrite–barium titanate nanocomposites, Applied Physics A, Vol. 123, No 5, pp. 331(9pp), April, 2017.

[3] A. E. Shalan, A. M. Elseman, **M. Rasly**, M. M. Moharam, M. Lira-Cantu, M. M. Rashad, Concordantly fabricated heterojunction ZnO–TiO_2 nanocomposite electrodes via a co-precipitation method for efficient stable quasi-solid-state dye-sensitized solar cells, RSC Advances, Vol. 5, No 125, pp. 103095-103104, November, 2015.

[4] A.E. Shalan, **M. Rasly**, M. M. Rashad, Organic acid precursor synthesis and environmental photocatalysis applications of mesoporous anatase TiO_2 doped with different transition metal ions, Journal of Materials Science: Materials in Electronics, Vol. 25, No 7, pp. 3141-3146, May, 2014.

[5] A. E. Shalan, **M. Rasly**, I. Osama, M. M. Rashad, I. A. Ibrahim, Photocurrent enhancement by Ni^{2+} and Zn^{2+} ion doped in SnO_2 nanoparticles in highly porous dye-sensitized solar cells, Ceramics International, Vol. 40, No 8, pp. 11619-11626, 2014.

[6] L. M. Salah, M. M. Rashad, M. Haroun, **M. Rasly**, M. A. Soliman, Magnetically roll-oriented $LaFeO_3$ nanospheres prepared using oxalic acid precursor method, Journal of Materials Science: Materials in Electronics, Vol. 26, No 2, pp. 1045-1052, November, (2015).

[7] M. M. Rashad, **M. Rasly**, H. M. El-sayed, A.A. Sattar, I. A. Ibrahim, Magnetic properties of La^{3+}-ion-doped polycrystalline Z-type hexaferrite powders synthesized via co-precipitation method, Journal of the Korean Physical Society, Vol. 63, No 3, pp. 821-825, August, 2013.

[8] M. M. Rashad, M. Bahgat, **M. Rasly**, S. I. Ahmed, Magnetic, oxidation and reduction behavior of spinel Ni-Cu manganite $Ni_xCu_{1-x}Mn_2O_4$ powders, Materials Science and Engineering: B, Vol. 178, No 16, pp. 1076-1080, September, (2013).

[9] **M. Rasly**, M. M. Rashad, Structural and magnetic properties of Sn-Zn doped $BaCo_2$Z-type hexaferrite powders prepared by citrate precursor method, Journal of Magnetism and Magnetic Materials, Vol. 337, No 8, pp. 58-64, March, 2013.

[10] M. M. Rashad, H. M. El-Sayed, **M. Rasly**, A. A. Sattar, I. A. Ibrahim, Magnetic and dielectric properties of polycrystalline La doped barium Z-type hexaferrite for hyper-frequency applications, Journal of Materials Science: Materials in Electronics, Vol. 24, No 1, pp. 282-289, January, 2013.

[11] M. M. Rashad, **M. Rasly**, H. M. El-Sayed, A. A. Sattar, I. A. Ibrahim, Controlling the composition and magnetic properties of hexagonal Co_2Z ferrite powders prepared using two different methods, Applied Physics A, Vol 112, No 4, pp. 963-973, September, 2013.

[12] H. Hirano, **M. Rasly**, N. Kaushik, M. Esashi, S. Tanaka, Particulate contamination control without causing damage to fragile MEMS structures, IEEJ Transactions on Sensors and Micromachines, Vol 133, No 5, pp. 157-163, November, 2013.

[13] M. M. Rashad, H. M. El-Sayed, **M. Rasly**, M. I. Nasr, Induction heating studies of magnetite nanospheres synthesized at room temperature for magnetic hyperthermia, Journal of Magnetism and Magnetic Materials, Vol 324, No 23, pp. 4019-4023, November 2012.

2.2. International Conferences

[1] Z. Lin, D. Pan, **M. Rasly** and T. Uemura, Electrical spin injection into an AlGaAs/GaAs-based high mobility two-dimensional electron system, IEEE Int'l Magnetics Conf. 2018 (INTERMAG 2018), Digests (USB Memory), HD-11, Marina Bay Sands Convention center, Singapore, April 23－27, 2018. (*Oral presentation*)

[2] Z. Lin, **M. Rasly**, and T. Uemura, Electrical Detection of Nuclear Spin-Echo Signals in an Electron Spin Injection System, the 9th International School and Conference on Spintronics and Quantum Information Technology, Abstract Book, p. 177, B-38, Fukuoka, Japan, June 4－8, 2017. (*Oral presentation*)

[3] M. M. Rashad, **M. Rasly**, H. M. El-sayed, A.A. Sattar, I. A. Ibrahim, Magnetic properties of La doped nanocrystalline Z-type ferrite nanopowders synthesized via co-precipitation method, The 19th International conference on Magnetism (ICM 2012), Buscan, Korea, July 8 － 13, 2012. (*Poster presentation*)

[4] **M. Rasly**, M. M. Rashad, I. A. Ibrahim, Structural, "Microstructure and magnetic properties of $SrCo_2W$-type ferrite synthesized using organic acid precursor method", Joint European Magnetism symposia (JEMS 2012), Parma, Italy, September 9－14, 2012. (*Poster presentation*)

2.3. Domestic Conferences

[1] Da Pan, Zhichao Lin, **Mahmoud Rasly**, Tetsuya Uemura "Electrical spin injection and detection in an AlGaAs/GaAs-based high-mobility two-dimensional electron system", The 53rd Conference of Hokkaido Chapter, The Japan Society of Applied Physics, Collected Abstracts, p. 14, A-14, Hokkaido University, Sapporo-shi, Hokkaido, Japan, January 6-7, 2018. (*Oral presentation*)

[2] Zhichao Lin, **Mahmoud Rasly**, Tetsuya Uemura, "Electrical detection of nuclear spin-echo signals in an electron spin injection system.", The 64th Japan Society of Applied Physics Spring Meeting 2017, 15a-501-8, Pacifico Yokohama, Yokohama, Japan, Mar. 14-17, 2017. (*Oral presentation*)

[3] Zhichao Lin, **Mahmoud Rasly**, Masafumi Yamamoto, and Tetsuya Uemura "Analysis of transient response of nuclear spins to a change in the magnetic field based on a time evolution of nuclear spin temperature", The 51st Conference of Hokkaido Chapter, The Japan Society of Applied Physics, Collected Abstracts, p. 27, A-24, Hokkaido University, Sapporo-shi, Hokkaido, Japan, January 9-10, 2016. (*Oral presentation*)

[4] Zhichao Lin, **Mahmoud Rasly**, Masafumi Yamamoto, and Tetsuya Uemura,"Transient analysis of oblique Hanle signals observed in GaAs based on a time evolution of nuclear spin temperature", The 20th Symposium on the Physics and Application of Spin-Related Phenomena in Semiconductors (PASPS-20), Program and Abstracts, F-2, Laboratory for Nanoelectronics and Spintronics, Research Institute of Electrical Communication, Tohoku University, Sendai-shi, Tohoku, Japan, December 3-4, 2015. (*Oral presentation*)

[5] **M. Rasly**, "Formation of complex magnetic $GdFeO_3$ ortho- and $Gd_3Fe_5O_{12}$ garnet-ferrite nanostructures at relatively low temperature using polyol method", The 1st International Conference on Polyol Mediated Synthesis, Paris-Diderot University, Paris, France, July 22-25, 2014. (*Poster presentation*)

[9] M. M. Rashad, **M. Rasly**, H. M. El-sayed, A.A. Sattar, I. A. Ibrahim "Structural and magnetic properties of La doped nanocrystalline Z-type ferrite nanopowders synthesized via co-precipitation method", International Conference on Nanoscale Magnetism, Istanbul, Turkey, September 2-6, 2013. (*Oral presentation*)

[7] M. M. Rashad, M. Bahgat and **M. Rasly** "Synthesis and reduction behavior of spinel (Ni, Cu) magnetite", 1st international conference on Advanced Basic Applied Sciences (ABAS) including Egyptian-Sweden Workshop on Advanced Materials, Hurghada, Egypt, November 6-9, 2012. (*Poster presentation*)

[8] M. M. Rashad, H. M. El-Sayed, **M. Rasly**, M. I. Nasr, "Induction heating studies of magnetite nanospheres synthesized at room temperature for magnetic

hyperthermia", 1st international conference on Advanced Basic and Applied Sciences (ABAS) including Egyptian-Sweden Workshop on Advanced Materials, Hurghada, Egypt, November 6-9, 2012. (*Poster presentation*)

[6] M. M. Rashad, **M. Rasly**, I. A. Ibrahim "Magnetic properties of BaCo2W-type ferrite synthesized via modified co-precipitation method", International Conference on Nanomaterials and Nanotechnology, University of Dehli, Dehli, India, December 18-21, 2011. (*Oral presentation*)

3. Social Articles

[1] **Mahmhmoud Rasly**, My experience between originality and modernity in Japan, Hokko-kai Magazine, Hokkaido University Engineering Association, Graduate School of Engineering, Hokkaido University, Vol 80, No 10, pp. 19-20, March, 2017.

[2] **Mahmhmoud Rasly**, The era of spin based electronics and quantum computation systems, Student column, Education activities, Graduate School of Information Science and Technology, Hokkaido University, February, 2018. (http://www.ist.hokudai.ac.jp/eng/lounge/lng51.html).